



**Politecnico  
di Torino**

**Politecnico di Torino**

MASTER OF SCIENCE IN CIVIL ENGINEERING

Academic Year 2021-2022

**A STUDY ON FATIGUE CHARACTERIZATION OF  
BITUMINOUS MIXTURES USING THE FOUR-POINT  
BENDING TEST**

Supervisors:

Prof. Ezio Santagata

Prof. Davide Dalmazzo

Prof. Lucia Tsantilis

Candidate:

Vangaveeti Charan Sai - S274175

## ACKNOWLEDGEMENT

Before proceeding with this thesis argument, I would like to thank all the people who have been close to me in this professional growth stage.

Firstly, I would like to thank my chairman, Professor Ezio Santagata, and my supervisors, Professor Davide Dalmazzo and Doctor Lucia Tsantilis, for their excellent mentoring, support, and wise advice. I thank them for their knowledge and the time they took to make me understand the different concepts and processes that helped me develop this thesis. I am deeply grateful to the laboratory engineer, Eng. Riccardo Rabezzana, for technical support, and guidance in the laboratory.

Secondly, I would like to thank my friends, who supported and cared for me in the most challenging moments as if they were my family.

The most significant and special thanks to my family, who were my primary support and never doubted my ability to achieve all my goals. They are my most valuable treasure, and I will thank them all my life.

Thank you all; I would never have made it without you.

## ABSTRACT

This thesis focuses on the characterization of the fatigue resistance of bituminous mixtures following the European standards, by means of the four-point bending test. The effects of material type and test temperature on fatigue properties were investigated. The effects of material type were taken into account by considering two different bituminous mixtures, one mixture prepared for a base layer and the other mixture for a binder layer, compacted at a reference air void content. The effect of temperature was investigated by performing tests on the binder course material at two test temperatures, 10 °C and 20 °C.

As indicated in the European standard, three strain levels (140  $\mu\text{m/m}$ , 200  $\mu\text{m/m}$ , 300  $\mu\text{m/m}$ ) and a minimum of six replicates at each strain level were considered.

Five fatigue failure criteria were selected from the literature to analyse the fatigue resistance of the mixtures: 50 % reduction in the initial modulus taken at the 100<sup>th</sup> cycle (50% $E_0$ ); 50 % reduction in the extrapolated modulus (from the phase of linear decrease) that is based on the modulus reduction (50 %  $E_{00}$ ); the Peak in the Phase angle; and the Energy Ratio Approach and Dissipated Energy Ratio approach.

From the outcomes of the experimentation, it was found that both temperature and mixture composition strongly affected the fatigue behaviour, as demonstrated by the better performance showed by the binder course material at the higher temperature. Moreover, it should be pointed out that different failure criterion led to distinct fatigue lines. A statistical analysis was used to highlight how the fatigue behaviour is significantly affected by both air void content and initial stiffness variability.

**Keywords:** Asphalt mixtures, Fatigue behaviour, Temperatures, Failure criteria, Binder course, Base course.

# Contents

CHAPTER 1 INTRODUCTION.....	11
1.1 Research Objectives .....	14
1.2 Thesis Outline .....	14
CHAPTER 2 BACKGROUND AND LITERATURE .....	16
2.1 Fatigue cracking .....	19
2.2 Factors affecting asphalt fatigue life .....	21
2.2.1 Volumetric properties .....	21
2.2.2 Stiffness.....	25
2.2.3 Type of loading.....	27
2.2.4 Test type, boundary conditions and support layer stiffness.....	29
2.2.5 Effect of environment temperature .....	29
2.3 Fatigue testing .....	29
2.3.1 Testing procedures .....	30
2.4 Literature on Fatigue failure criteria .....	37
2.4.1 Fatigue life, conventional criterion (50% of $E_0$ ).....	38
2.4.2 Damage analysis, ENTPE (50% of $E_{00}$ ).....	38
2.4.3 Peak in phase angle criterion .....	39
2.4.4 Energy ratio criterion .....	41
2.4.5 Dissipated Energy ratio criterion: .....	44
2.5 Fatigue modelling.....	47
2.6 Effect of the temperature on fatigue.....	51
2.7 Effect of mixture type on fatigue .....	52
CHAPTER 3 MATERIALS AND METHODOLOGY .....	54
3.1 Experimental campaign.....	55
3.2 Material characterization.....	56
3.2.1 Ignition test .....	57
3.2.2 Theoretical maximum density of the mixture / Aggregate density.....	60
3.2.3 Aggregate size distribution .....	63
3.3 Compaction methods and specimen preparation.....	67
3.3.1 Gyratory compaction .....	67
3.3.2 Roller compaction.....	72
3.4 Beams preparation.....	75
3.4.1 Sawing.....	75

3.4.2	Specimen Dimensions.....	76
3.5	Evaluation of the Air void content .....	77
3.5.1	Bulk density calculation.....	77
3.6	Fatigue testing .....	80
3.6.1	Four-point bending test on prismatic shaped specimens (4PB-PR).....	81
	CHAPTER 4 RESULTS AND DISCUSSION .....	86
4.1	Beams Characterization.....	87
4.1.1	Air voids.....	87
4.1.2	Stiffness.....	96
4.2	Fatigue failure analysis.....	105
4.2.1	Fatigue failure criterion 1: Reduction of initial modulus.....	105
4.2.2	Fatigue failure criterion 2: Reduction of the Extrapolated Modulus .....	106
4.2.3	Fatigue failure criterion 3: Peak in phase angle.....	108
4.2.4	Fatigue failure criterion 4: Energy ratio.....	108
4.2.5	Fatigue failure criterion 5: Dissipated Energy Ratio .....	110
4.3	Comparison of fatigue test results .....	111
4.4	Fatigue Curves.....	114
4.5	Comparing the effect of temperatures on fatigue life .....	118
4.6	Comparing the effect of mixture type on fatigue life.....	123
	CHAPTER 5 CONCLUSION AND RECOMMENDATIONS.....	127
5.1	Conclusions .....	128
5.2	Recommendations and future work.....	129

## List of Figures

Figure 1 Representation of the stresses due to single wheel load.....	12
Figure 2 Sketch of the global process due to the action of cyclic loading [21].....	18
Figure 3 Plot showing No. of cycles to failure vs applied strain.....	18
Figure 4 Sketch of the random propagation of fatigue damage that appeared in the bituminous mixtures [21].....	20
Figure 5 Stiffness modulus variation during fatigue test.....	20
Figure 6 Bituminous mixtures phase diagram.....	22
Figure 7 volumetric relationship of bituminous constituents.....	22
Figure 8 Plot showing the stress and strain-controlled tests.....	28
Figure 9 Schematic Demonstrating the Main Forms of Fatigue Test: (a) Two-Point Bending; (b) Four Point Bending; (c) Centre Point Bending; (d)Rotating Bending; (e) Direct Axial Loading; (f) Direct Axial Loading(Necked Specimen) and (g) Diametral Loading.....	30
Figure 10 Trapezoidal shaped specimen.....	31
Figure 11 Sinusoidal displacement at the head of specimen.....	32
Figure 12 Three point bending device.....	34
Figure 13 Indirect tensile test on cylindrical shaped specimens (IT-CY).....	35
Figure 14 Four point bending loading configuration.....	37
Figure 15 Stiffness Modulus versus cycles.....	39
Figure 16 Asphalt mixture stress–strain responses under a sinusoidal load for different viscoelastic behaviours [57].....	40
Figure 17 Fatigue life defined by Reese’s (1997) approach. [58].....	41
Figure 18 Energy Ratio (after Hopman, 1989)[60].....	42
Figure 19 Energy ratio of stress-controlled fatigue test.....	43
Figure 20 DER approach.....	46
Figure 21 The fatigue lives of the mixture at different temperatures and strain levels: (a) $N_{f50}$ of the neat mixture, (b) $N_{f50}$ of SBS-modified mixture, (c) $N_{fNM}$ of the neat mixture [76].....	52
Figure 22 Fatigue diagrams of HMA types H1, H2 and SMA type A in 25 °C and 40 °C.....	53
Figure 23 High temperature furnace and sample baskets for ignition test.....	59
Figure 24 Sample distribution inside the basket and sample.....	59
Figure 25 Mixture distribution after cooling down.....	61
Figure 26 Asphalt particles inside the pycnometer.....	61
Figure 27 Vacuum system.....	61
Figure 28 Sample washing.....	64
Figure 29 Mechanical vibrator and Sieves column.....	64
Figure 30 Aggregate gradation – Binder mixture.....	66
Figure 31 Aggregate gradation – Base mixture.....	66
Figure 32 Test piece motion diagram.....	67
Figure 33 Typical gyratory molds and samples.....	69
Figure 34 Compaction curve of all gyratory samples - Binder.....	70
Figure 35 Compaction curve of gyratory samples - Base.....	71
Figure 36 The roller compactor without the auxiliary elements.....	74

Figure 37 The wheel compactor auxiliary elements .....	74
Figure 38 finishing of the slab compaction and removing from the mould.....	74
Figure 39 Completed slab .....	75
Figure 40 Slab sawing.....	76
Figure 41 Four point bending beams .....	77
Figure 42 4PB measurement points .....	77
Figure 43 Gyratory samples inside the water bath and temperature measurement .....	79
Figure 44 The slab inside the water bath .....	79
Figure 45 The 4PB beams inside the water bath.....	79
Figure 46 The water bath and the balance .....	79
Figure 47 Basic principles of 4-point bending.....	81
Figure 48 Clamping system .....	82
Figure 49 Four point bending machine with thermostatic chamber .....	83
Figure 50 Electronic data registration equipment.....	83
Figure 51 Plot showing the comparison of air voids in all slabs – Binder .....	88
Figure 52 Plot showing the air voids distribution in the beams - Binder .....	90
Figure 53 Theoretical air voids histogram - Binder mixture .....	91
Figure 54 Real air voids histogram - Binder mixture .....	91
Figure 55 Comparison of theoretical air voids distribution w.r.t position of the beams in slabs - Binder .....	91
Figure 56 Comparison of real air voids distribution w.r.t position of the beams in slabs - Binder.....	92
Figure 57 plot showing the comparison of air voids in all slabs - Base .....	93
Figure 58 Plot showing the air voids distribution in the beams -Base.....	94
Figure 59 Theoretical air voids histogram - Base mixture .....	95
Figure 60 Real air voids histogram - Base mixture .....	95
Figure 61 Comparison of theoretical air voids distribution w.r.t position of the beams in slabs - Base .....	95
Figure 62 Comparison of theoretical air voids distribution w.r.t position of the beams in slabs - Base .....	96
Figure 65 Plot showing the Initial modulus variation - Bind.....	97
Figure 66 Plot showing the Extrapolated stiffness modulus variation - Binder .....	98
Figure 67 Initial stiffness Histogram - Binder .....	98
Figure 68 Extrapolated stiffness Histogram - Binder .....	99
Figure 69 Graph showing the trend in Initial modulus variation w.r.t. air voids of beams - Binder.....	100
Figure 70 Graph showing the trend in Extrapolated modulus variation w.r.t. air voids of beams – Binder .....	100
Figure 71 Plot showing the Initial modulus variation - Base.....	102
Figure 72 Plot showing the Extrapolated modulus variation - Base.....	102
Figure 73 Initial stiffness Histogram - Base .....	102
Figure 74 Extrapolated stiffness modulus Histogram - Base.....	103
Figure 75 Graph showing the trend in Initial modulus variation w.r.t. air voids of beams -	

Base.....	104
Figure 76 Graph showing the trend in Extrapolated modulus variation w.r.t. air voids of beams – Base.....	104
Figure 77 Typical graph of the 50 % reduction of initial modulus criterion .....	105
Figure 78 Typical graph showing the extrapolated stiffness reduction criterion.....	107
Figure 79 Typical graph showing the peak phase angle .....	108
Figure 80 Typical graph showing the Energy ratio criterion.....	109
Figure 81 Typical graph showing the DER criterion.....	110
Figure 82 Fatigue curves of a Binder mixture (a) 50 % E <sub>0</sub> (b)50 % E <sub>00</sub> (c) Energy Ratio (d) Dissipated Energy Ratio .....	114
Figure 83 Fatigue curves of the Base mixture (a) 50 % E <sub>0</sub> (b)50 % E <sub>00</sub> (c) Energy Ratio (d) Dissipated Energy Ratio .....	115
Figure 84 Fatigue curves - ALL - Binder @ 10 °C .....	117
Figure 85 Fatigue curves - ALL - Base @ 20 °C .....	118
Figure 86 Comparison of the fatigue curves at different temperature - 50 % E <sub>0</sub> - Binder....	118
Figure 87 Comparison of the fatigue curves at different temperature - 50 % E <sub>00</sub> - Binder..	119
Figure 88 Comparison of the fatigue curves at different temperature - Energy Ratio - Binder .....	119
Figure 89 Comparison of the fatigue curves at different temperature - DER – Binder.....	120
Figure 90 Fatigue curves showing the comparison of temperatures tested with the same mixture (Binder).....	122
Figure 91 Comparing the effect of mixture on fatigue behaviour – 50% E <sub>0</sub> .....	123
Figure 92 Comparing the effect of mixture on fatigue behaviour – 50% E <sub>00</sub> .....	123
Figure 93 Comparing the effect of mixture on fatigue behaviour – Energy Ratio .....	124
Figure 94 Comparing the effect of mixture on fatigue behaviour – DER .....	124
Figure 95 Fatigue curves showing the Comparison of mixtures tested at same temperature	126

## List of Tables

Table 1 Comparison of the Tests under $\sigma - N$ and $\epsilon - N$ .....	28
Table 2 Testing methods and the European standards .....	55
Table 3 Size of the ignition test sample .....	57
Table 4 Ignition test results for two mixtures .....	60
Table 5 Theoretical maximum density of the two mixtures .....	62
Table 6 Minimum size of test portion for aggregate gradation .....	63
<i>Table 7 Limiting values of aggregate gradation for the binder and base mixtures</i> .....	65
Table 8 Sieve analysis of Binder and Base mixtures .....	65
Table 9 Gyratory sample's mass inside the mold.....	68
Table 10 Reference compaction temperature .....	68
<i>Table 11 Thickness measurements of gyratory samples - Binder</i> .....	69
<i>Table 12 Thickness measurements of gyratory samples - Base</i> .....	70
Table 13 Samples workability and Compatibility of binder and Base Mixtures.....	71
Table 14 Wheel compactor to be compacted mass - Binder.....	72
Table 15 Sweep plan, specimens 500 mm $\times$ 180 mm $\times$ e, heavy compaction .....	73
Table 16 Compacted slab thickness.....	75
Table 17 Sample Beam measurements .....	77
Table 18 Theoretical and Actual air voids calculation of the Gyratory samples.....	79
Table 19 Typical theoretical and actual air voids calculation of the slabs .....	80
Table 20 typical calculation of Theoretical and Actual air voids in 4PB beams.....	80
Table 21 Minimum time required to bring specimens to test temperature .....	84
Table 22 Comparison of the theoretical and real air voids in all slabs for Binder mixture .....	88
Table 23 Comparison of the theoretical and real air voids in all beams for Binder mixture...	89
Table 24 Comparison of the theoretical and real air voids in slabs for Base mixture .....	92
Table 25 Comparison of the theoretical and real air voids in all the beams - Base mixture ..	93
Table 26 Tables showing the Initial modulus and Extrapolated modulus of the beams - Binder .....	96
Table 27 Beams Initial stiffness and their corresponding air voids - Binder.....	99
Table 29 Tables showing the Initial modulus and Extrapolated modulus of the beams - Base .....	101
Table 30 Beams Initial stiffness and Extrapolated stiffness with their corresponding air voids - Base .....	103
Table 32 Fatigue test results for all beams considering classical fatigue analysis .....	106
<i>Table 33 Fatigue test results for all beams considering 50 % <math>E_{00}</math> analysis</i> .....	107
Table 34 Fatigue test results for all beams considering Energy Ratio analysis.....	109
Table 35 Fatigue test results for all beams considering Dissipated Energy Ratio analysis...	110
Table 36 Fatigue results of the all the fatigue failure criteria in the Binder mixture tested at 300 $\mu$ s strain level and 10 $^{\circ}$ C .....	111
Table 37 Fatigue results of the all the fatigue failure criteria in the Binder mixture tested at	

200 $\mu\text{s}$ strain level and 10 $^{\circ}\text{C}$ .....	112
Table 38 Fatigue results of the all the fatigue failure criteria in the Binder mixture tested at 140 $\mu\text{s}$ strain level and 10 $^{\circ}\text{C}$ .....	112
Table 39 Fatigue results of the all the fatigue failure criteria in the Base mixture tested at 300 $\mu\text{s}$ strain level and 20 $^{\circ}\text{C}$ .....	113
Table 40 Fatigue results of the all the fatigue failure criteria in the Base mixture tested at 200 $\mu\text{s}$ strain level and 20 $^{\circ}\text{C}$ .....	113
Table 41 Fatigue results of the all the fatigue failure criteria in the Base mixture tested at 140 $\mu\text{s}$ strain level and 20 $^{\circ}\text{C}$ .....	113
Table 42 Fatigue test parameters for the bituminous mixtures.....	116
Table 43 Temperature effect on fatigue life parameter for Binder mixture .....	120
Table 44 Gradation effect on Fatigue life of asphalt mixtures .....	125

# **CHAPTER 1 INTRODUCTION**

## CHAPTER 1 INTRODUCTION

The designer attempts to avoid two types of structural failure during the pavement's design life: cracking and rutting. The idea of design life is especially significant for pavements since they do not fail suddenly (unless in extremely rare cases of massive thermal or ground movements, which are not economically possible to account for at the design stage) but deteriorate gradually over time. This is essentially a fatigue phenomenon, in that the degradation produced by stresses and strains in the structure is driven by both the magnitude and quantity of load applications that the pavement receives.

Asphalt concrete pavements when subjected to the traffic loads repeatedly undergo several distresses. Fatigue cracking is one of the major distresses which causes failure in the flexible pavements. Fatigue cracking can be classified as bottom-up fatigue cracking or top-down fatigue cracking depending upon the dominant mechanism and location of the crack initiation in both these cases, cracks not only decrease the load distributing capacity of the bituminous layers, but also allow water to percolate to the base and subgrade, leads to the acceleration of the complete destruction of the pavement.

Fatigue is one of the main failure modes of pavement structures, which results in the degradation of the pavement materials and finally the pavement structure [1]. A single wheel load passing over the pavement may cause high tensile strains at the bottom of the asphalt layers. Under tandem axle, also high tensile strains may be caused at the top and bottom of the asphalt layers [2]

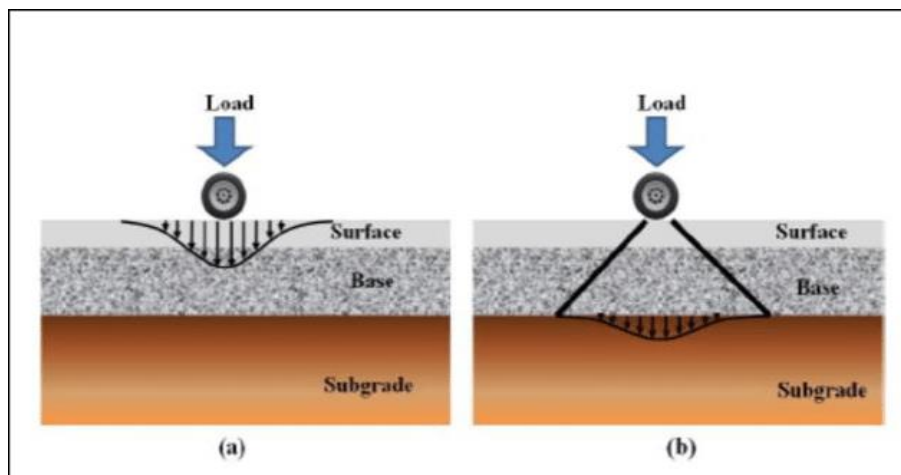


*Figure 1 Representation of the stresses due to single wheel load*

Bituminous mixtures used in different layers of the pavement have a complex behaviour, thus the fatigue characteristics need to be carefully evaluated [3].

Several methods, including a full-scale field test, a field survey and a laboratory fatigue test, were used to evaluate the fatigue properties of the asphalt mixtures [1], [4] – [8]. In comparison

to a full-scale field test or field survey, the laboratory fatigue test can be used to analyse the fatigue resistance of an asphalt mixture in a cost-effective and timely manner [3].

Using the controlled stress fatigue test, the initial decrease of the modulus can be largely due to the effect of permanent deformations, which can mask the true damage caused by the fatigue process [3]. Given this possibility, the bulk of fatigue experiments are performed under controlled strain circumstances (to reduce the impacts of irreversible deformations when researching fatigue damage) [1], [9], [10]. However, this type of test does not reproduce the same load conditions that affect bituminous materials during their service life (a stress relaxation and fatigue process under constant strain occur in the laboratory tests, whilst creep, strain hardening and fatigue process occurring the roads due to the presence of constant loads). Therefore, significant differences can be obtained between laboratory fatigue-life predictions and real fatigue lives [11], [12], and between laboratory tests carried out at controlled stress or strain conditions.

The laboratory fatigue test for the bituminous mixtures is most commonly conducted at the temperature ranging between 10 °C and 20 °C [13] – [16], as the fatigue cracking in the asphalt layer is generally regarded to occur within this temperature range [17].

Another factor that effects the analysis of the fatigue response of the bituminous mixtures is the selection of an accurate fatigue failure criteria. Fatigue damage starts with the network of micro cracks, which randomly in the three dimensions of a certain volume of the material where the fatigue process occurs. This accumulation of the micro cracks creates the macro cracks that propagates inside the volume of material until causing its total failure. Thus, the propagation of the global damage depends on many variables [18] such as the type of bituminous mixture tested, the test conditions such as amplitude, frequency, temperature, the type of test used or the geometry of the test specimen. As a result, it is very complicated to clearly identify a damage limit that defines the uniform failure criterion that could be universal to any fatigue test [10]. Many researchers have studied recently on defining a criterion to minimize the influence of all these mentioned variables during the evaluation of the fatigue behaviour of the asphalt mixture.

### 1.1 Research Objectives

The focus of this study is on the fatigue characterisation of bituminous mixtures. In particular, the effects of temperature and material type has been studied by use of the four-point bending test following the European standards.

The effect of temperature was investigated by performing tests on the binder course mixture at two test temperatures. The temperatures 10 °C and 20 °C are chosen to compare the effects on fatigue characterisation. These temperatures are preferred, since the real pavement conditions corresponds within this range.

In addition, the effect of mixtures was studied by taking two different kind of mixtures, base course mixture and a binder layer mixture containing the same binder type using the similar test conditions.

To compare the results, recent study that was conducted by Ahmad Salah (Politecnico di Torino, 2022) was taken into consideration following the five fatigue failure criteria, to characterise the fatigue resistance.

On the other hand, to define the non-homogeneity of the results, statistical analysis has been made which shows the effect of air voids on the initial stiffness modulus and also the extrapolated stiffness modulus.

### 1.2 Thesis Outline

The thesis is organized into five chapters including the following contents:

Chapter 1: Introduction

A general overview on the fatigue characterization of the bituminous mixtures, which is followed by the research objectives and the outline of the thesis.

Chapter 2: Background and Literature review

Discussion on general aspects related to the fatigue of bituminous mixtures. The most common fatigue failure criteria were also presented. Also, the discussion on effect of temperatures and effect of gradation on fatigue life of bituminous mixtures from the previous investigations.

Chapter 3: Materials and methods:

In this chapter a detailed description of the experimental campaign is explained. Starting with describing the material and then going through the material characterization with the complete explanation of the testing procedure and their results. Then the specimens

preparation steps are illustrated to obtain the final beams which will be tested for the four-point bending test. Also, the four-point bending test following the European standards is briefly discussed.

### Chapter 4: Analysis of the results

The crux of the thesis is contained in this section, where a thorough examination of the findings is provided. Five distinct fatigue failure criteria are used in this analysis to estimate the fatigue resistance using the two different temperatures at three different strain levels. After that, the obtained results of the fatigue curves for each failure criterion are compared. The collected data are then subjected to a reliability analysis to determine a representative value for the fatigue life for each failure criterion.

### Chapter 5: Conclusion and Recommendations

The most pertinent test findings are used to draw conclusions, and as a result, certain suggestions are made in this section. There is also a recommended path for future work presented.

**CHAPTER 2 BACKGROUND AND LITERATURE**

In this chapter, background of the fatigue cracking is briefly discussed, to understand the phenomena of cracking, fatigue testing is also mentioned. There are classical and new failure approaches to obtain the fatigue life, those which followed in this study are mentioned which are observed from the other research studies. A literature review on the effect of temperature and effect of the gradation is also represented.

Bituminous mixes are viscoelastic materials with mechanical characteristics that are greatly dependent on the temperature of service and the applied loading rate [19]. In this regard, bituminous mixtures behave more viscously at the high temperatures and low loading rates, and they are vulnerable to flow, which causes the plastic deformations formation. Inversely, when the temperature of the pavement is low or the applied load has a high frequency, these materials behave in more elastic way, therefore they can support the stresses without flow.

Fatigue occurs when a pavement is subjected to repeated stress levels that are less than the ultimate failure stress. Hveem (1955) was among the first to identify fatigue failure induced by repetitive loads on asphalt pavement over very resilient soils. He concluded that there was a correlation between observations of cracking and fatigue type failures in bituminous pavements and the observed deflections that the pavement must endure with each passing wheel. Hveem proposed that a well-designed pavement must be able to bear deflections or have enough stiffness to minimize deflections to acceptable levels [2].

Fatigue that occurs in the asphalt mixtures due to the cyclical loads can be considered a global process (Figure 2) which involves three main phenomena [20].

- i. Accumulation of the permanent deformations.
- ii. Reversible degradation and initiation of irreversible damage.
- iii. Crack propagation (cumulative micro cracks produces the localization and propagation of the macro cracks).

During study of the fatigue behaviour of the asphalt mixtures, the occurrence of the mentioned three phenomena can be identified observing the changes in their mechanical properties [1]. Consequently, the results that obtained from the typical cyclic loading test can be sub-divided into three stages: (i) a sudden reduction of the modulus and the increase of the phase angle; (ii) a quasi-static stage where the changes attained are very minimal; (iii) a rapid decrease of the modulus and the phase angle, due to the occurrence and propagation of the micro cracks.

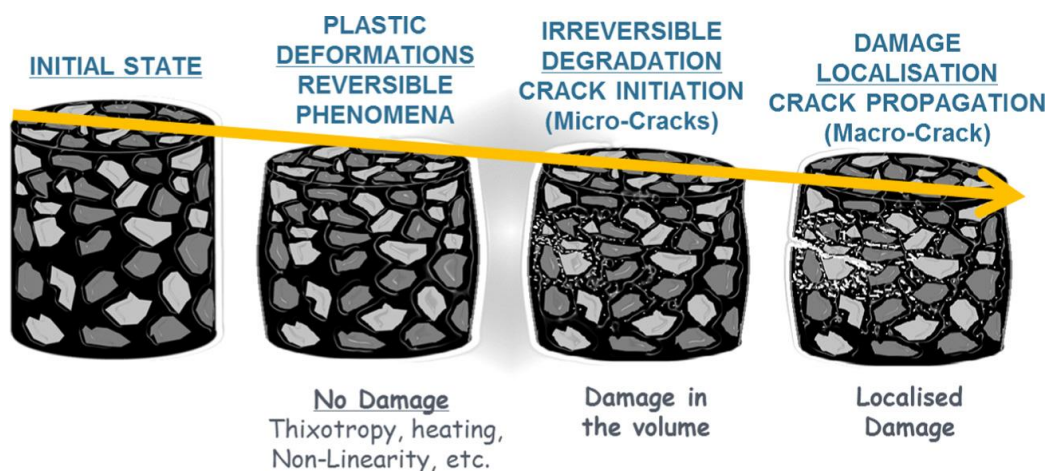


Figure 2 Sketch of the global process due to the action of cyclic loading [21]

For many years, researchers have been studying the fatigue life of asphalt pavement systems. These studies may be divided into three categories: phenomenological investigations, energy-based studies, and fracture mechanics studies. The phenomenological technique examines the connection between the number of load cycles to failure and repetitive stress or strain in the test specimen. This method is based on the stress number of cycles to failure and Miner's linear law, which relates to cumulative damage in pavement. For example, shows a general fatigue curve, plotting strain (or stress) against load repetitions on a log-log scale.

The energy-based approach uses the concept of the dissipated energy to evaluate fatigue behaviour. This approach assumes that fatigue damage is a depletion of dissipated energy from one load cycle to the next.

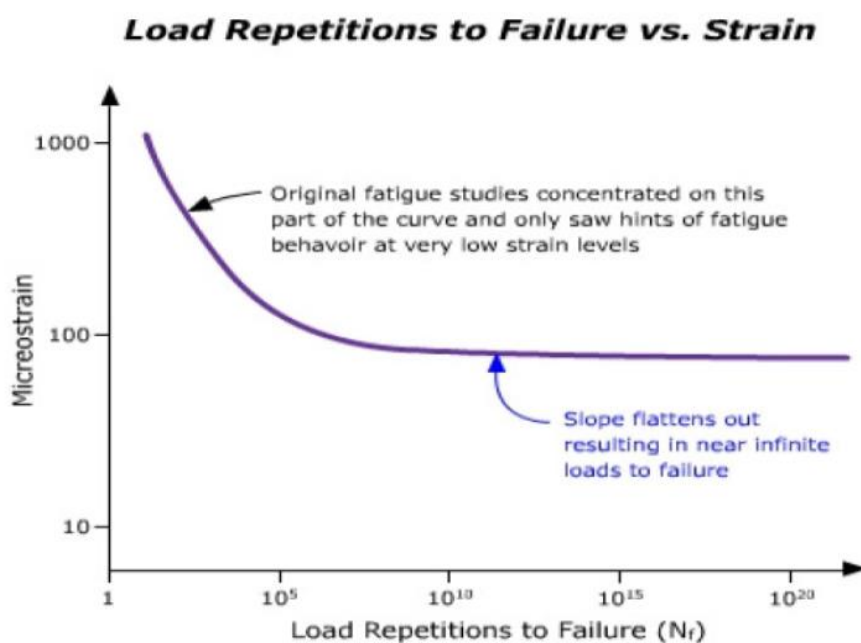


Figure 3 Plot showing No. of cycles to failure vs applied strain

Finally, the fracture approach, which is based on the idea of fracture mechanics, investigates the development and propagation of cracks. The stages of crack growth are often broken down into three stages: crack initiation, propagation, and unstable fracture. This approach attempts relate a characteristic of the crack propagation in the pavement to fracture parameters such as the stress intensity factor.

However, evaluation of fatigue life for field asphalt concrete pavements is extremely difficult due to lack of knowledge to fatigue damage relations for real pavements, reliable testing data for only a limited number of mixtures, and limited knowledge about how the fatigue life potential of an asphalt concrete pavement varies with temperature and mixture characteristics.

## 2.1 Fatigue cracking

Fatigue cracking occurs in two phases, crack initiation and crack propagation. Crack initiation is commonly defined as the coalescence of micro-cracks to form a macro crack when tensile forces are applied repeatedly. Crack propagation is the growth of the macro crack across the material tensile strains as tensile forces are applied (Figure 4). There are several complicated tests that can measure the life to crack initiation but no test that can, reliably measure crack propagation at the moment and as previously said, analytical approaches, which are the way ahead, require this information. It should be noted at this point that the fatigue parameters of a bituminous mixture cannot be evaluated in isolation, as stiffness dictates the degree of the tensile strain experienced by the material. This then determines the material's life to crack initiation.

Over the previous 30 years, substantial study has been conducted in the field of fatigue, but relatively little has been converted into practice. This is thought to be related to the complexity and hence cost of testing, as well as difficulty in applying the results of the element testing to the pavement's reaction [22].

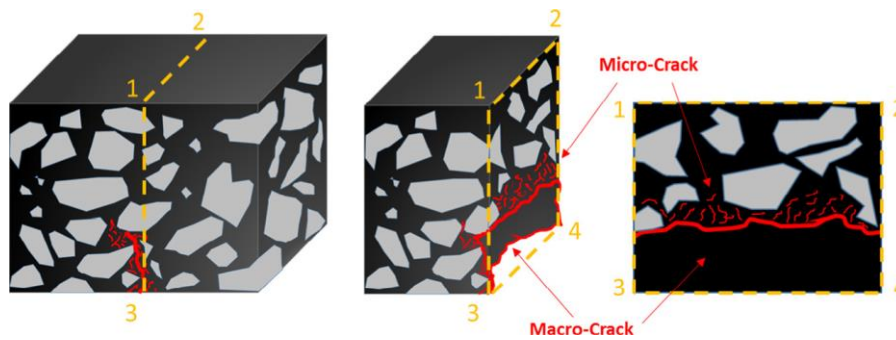


Figure 4 Sketch of the random propagation of fatigue damage that appeared in the bituminous mixtures [21]

Sridhar (2008) presented a brief review on Top-Down Cracking (TDC). It defines as longitudinal and/or transverse cracks that initiate at the surface of asphalt layer and propagate downward. They are usually longitudinal cracks appearing just outside the wheel paths.

Brown et al., demonstrated that for thin pavements, fatigue cracking started at the bottom of the bituminous layer due to high tensile strains and migrated to the top surface [23]. For thick pavements, cracks started on the surface of bituminous layer due to tensile strains at the surface and migrated downward.

During a fatigue test, modulus value declines according to Figure 5, where three phases can be recognized:

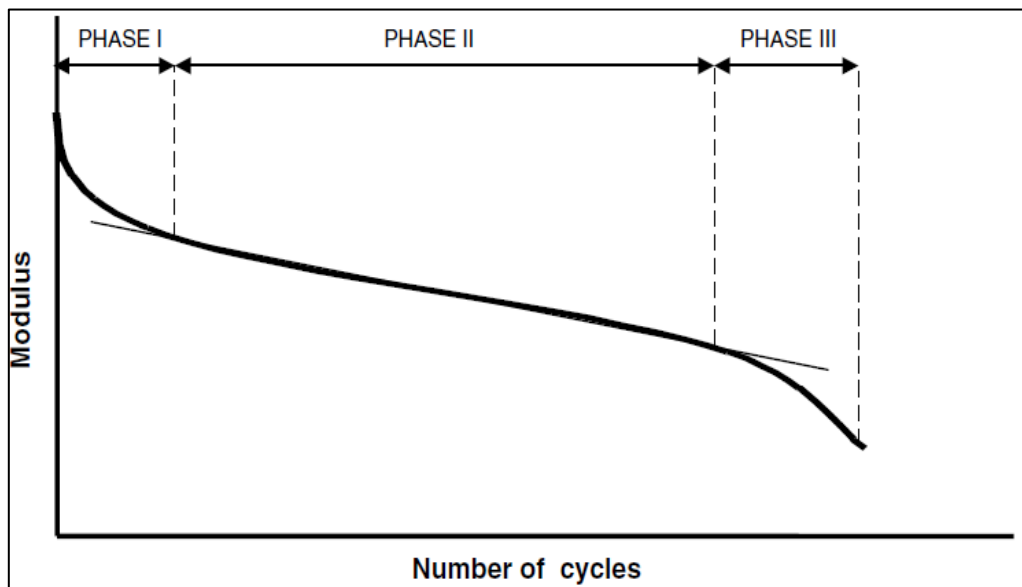


Figure 5 Stiffness modulus variation during fatigue test

Phase I: at the beginning of the test there is a rapid reduction of the modulus value.

Phase II: modulus variation is approximately linear.

Phase III: rapid decrease of the modulus value.

Since the first half of the 1950s, numerous different test setups have been used in widespread fatigue testing. There are numerous tests available now to determine fatigue resistance.

According to BS EN 12697-24:2018 [24]. “This European Standard defines alternate tests for assessing the fatigue of bituminous mixtures, including as bending tests, direct and indirect tensile tests. The tests carried out on compacted bituminous material under sinusoidal loading or other controlled stress, with various types of specimens and supports”.

In the sections that follow, these tests will be explained. The four-point bending test, which will be explained in detail, will be the main topic of this thesis.

### 2.2 Factors affecting asphalt fatigue life

These are the below mentioned important properties among which plays a crucial role in designing that also effect the pavement performance [2].

- ✓ Volumetric properties
- ✓ Type of Loading
- ✓ Stiffness
- ✓ Test type, border conditions and support layer stiffness
- ✓ Effect of Temperature Environment

#### 2.2.1 Volumetric properties

The properties of a specified material confined in a known volume are referred to as volumetric properties. These properties include bulk density, theoretical maximum density, air voids and voids in mineral aggregate. The volumetric properties are reflected in the volume of binder and aggregates required to produce a mixture of desired properties. Mixture volumetric properties are important for the long-term performance and durability of pavements.

All the parameters which involve in the volumetric properties can be seen in a phase diagram (Figure 6) with respective to their volumes and mass.

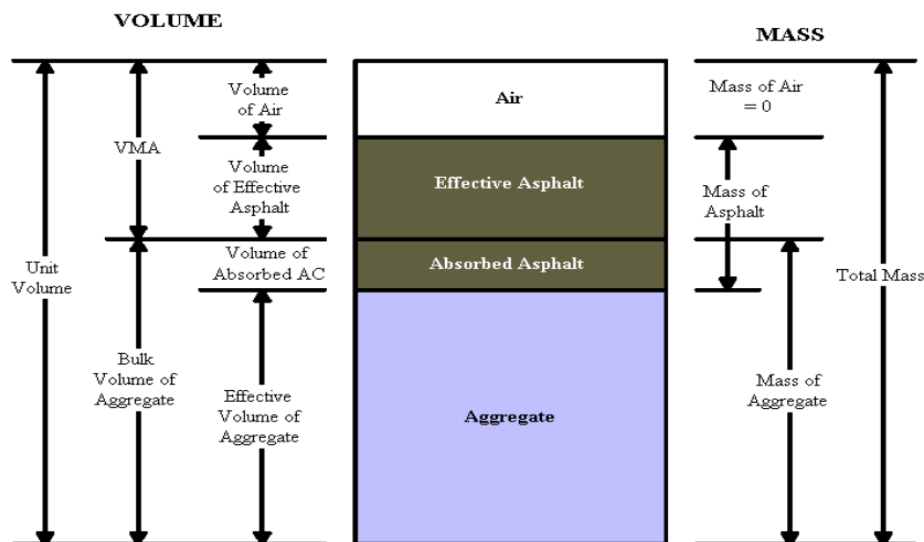


Figure 6 Bituminous mixtures phase diagram

Each of the attributes and corresponding volumes in the diagram from earlier can be quantified. The air voids, voids in the mineral aggregate, voids filled with asphalt binder, and effective asphalt binder content of a compacted asphalt mixture all give some indication of the mixture's likely performance. There is a need to be aware of the precise masses and gravities of each component in order to calculate those amounts.

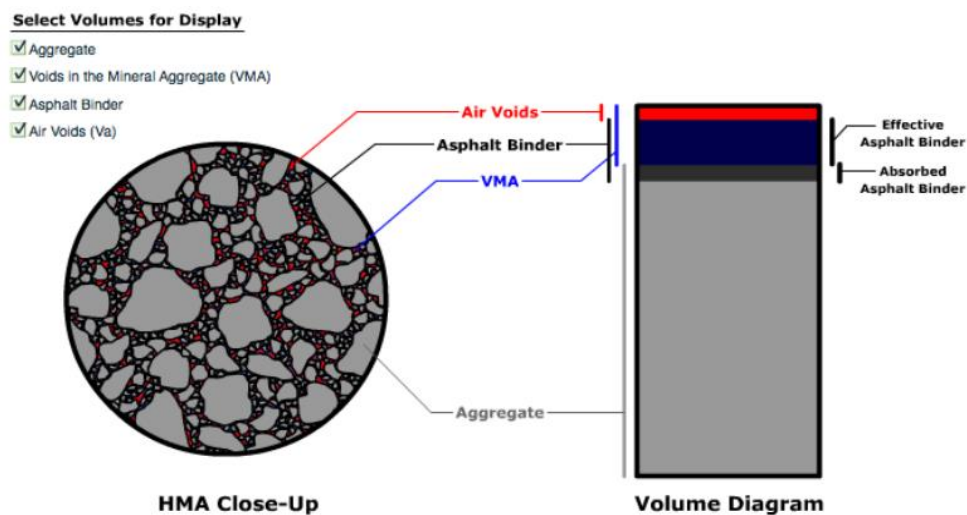


Figure 7 volumetric relationship of bituminous constituents

### 2.2.1.1 Air voids ( $V_a$ )

Air voids are small air spaces or pockets of air that occurred between the coated aggregate particles in the final compacted mix. The air voids content of a bituminous specimen is calculated using the maximum density of the mixture and the bulk density of the specimen. For

mixtures with water in their composition (e.g., mixtures produced with bituminous emulsion or foamed bitumen), the bulk density of the specimen shall refer to its dry bulk density.

The air voids content shall be calculated to the nearest 0,1 % (by volume) as follows:

$$V_a = 100 \left[ \frac{G_{mm} - G_{mb}}{G_{mm}} \right]$$

where,

$V_a$  = air voids in compacted mixture, percent of total volume.

$G_{mm}$  = maximum specific gravity of paving mixture.

$G_{mb}$  = bulk specific gravity of compacted mixture.

### 2.2.1.2 Percent Aggregate (Stone) ( $P_s$ )

$P_s$  represents the aggregate's share in the mix, represented as a percentage of the sample's total mass.

$$P_s = 100 - P_b$$

where,

$P_s$  = percent aggregate (stone) percent by total weight.

$P_b$  = asphalt binder content.

### 2.2.1.3 Voids in the Mineral Aggregate (VMA)

This component communicates the intergranular void space, expressed as a percentage of the specimen's total volume, that exists between the aggregate particles of the compacted paving mixture and contains the air voids and the effective binder content.

$$VMA = 100 \left[ \frac{G_{mb} * P_s}{G_{sb}} \right]$$

where,

VMA = voids in mineral aggregate, percent of bulk volume.

$G_{sb}$  = bulk specific gravity of combined aggregate.

$G_{mb}$  = bulk specific gravity of compacted mixture.

$P_s$  = aggregate content, percent by total weight =  $100 - P_b$

$P_b$  = asphalt binder content percent by total weight.

### 2.2.1.4 Voids Filled with Asphalt (binder) (VFA)

This is the percentage of the sample's overall volume that represents the volume of voids present among the compacted asphalt-covered aggregate particles. It is the percentage of voids

## CHAPTER 2 BACKGROUND AND LITERATURE

that are packed with asphalt and excludes absorbed asphalt therefore, the quantity rises as the asphalt binder content does.

$$VFA = 100 \left[ \frac{VMA - V_a}{VMA} \right]$$

where,

VFA = voids filled with asphalt, percent of VMA.

VMA = voids in mineral aggregate, percent of bulk volume.

$V_a$  = air voids in compacted mixture, percent of total volume.

### 2.2.1.5 Effective Specific Gravity of the Aggregate (Stone) ( $G_{se}$ )

This quantity is used to measure the asphalt binder absorbed into the aggregate particle. This is a determined quantity based on the maximum specific gravity of the mix, and the specific gravity of the asphalt binder. This measurement takes into account the volume of each aggregate particle as well as the volume of voids that fill up with water throughout the test soak period but not the volume of voids that take in asphalt binder. Between apparent and bulk specific gravities is effective specific gravity.

The effective specific gravity of the aggregate is defined as the ratio of the mass in air of a unit volume of a permeable material (excluding voids permeable to asphalt binder) at a specified temperature to the mass in air (of equal density) of an equal volume of a void free distilled water at a specified temperature.

$$G_{se} = \frac{P_s}{\left[ \frac{100}{G_{mm}} - \frac{P_b}{G_b} \right]}$$

where,

$G_{se}$  = effective specific gravity of combined aggregate.

$P_s$  = aggregate content, percent by total weight =  $100 - P_b$

$G_{mm}$  = maximum specific gravity of mix.

$P_b$  = asphalt binder content percent by total weight.

$G_b$  = specific gravity of asphalt binder.

### 2.2.1.6 Percent of Absorbed (asphalt) Binder ( $P_{ba}$ )

$P_{ba}$ , which is given as a percentage of aggregate mass rather than as a percentage of the entire mass of the mixture, is the total percent of the asphalt binder that is absorbed into the aggregate.

The performance of the mix is not impacted by this part of the asphalt binder component.

$$P_{ba} = 100 \left[ \frac{G_{se} - G_{sb}}{G_{sb} * G_{se}} \right] * G_b$$

where,

$P_{ba}$  = absorbed asphalt binder percent of aggregate.

$G_{se}$  = effective specific gravity of combined aggregate.

$G_{sb}$  = bulk specific gravity of combined aggregate.

$G_b$  = specific gravity of asphalt binder.

### 2.2.1.7 Percent of Effective (asphalt) Binder ( $P_{be}$ )

$P_{be}$ , is the total amount of asphalt binder in a paving mixture less the amount lost through absorption into the aggregate particles, represented as a percentage of aggregate mass. It is the portion of the asphalt binder that is still present on the aggregate particles' exterior as a coating. The amount of asphalt in the mix is what determines how well it performs.

$$P_{be} = P_b - \left[ \frac{P_{ba}}{100} * P_s \right]$$

where,

$P_{be}$  = effective asphalt binder content percent by total weight.

$P_s$  = aggregate content, percent by total weight =  $100 - P_b$

$P_b$  = asphalt binder content percent by total weight.

$P_{ba}$  = absorbed asphalt binder.

## 2.2.2 Stiffness

To simulate the response of bituminous mixtures due to fatigue, stiffness parameter plays a vital role. The elastic stiffness in a pavement is a measure of a material capacity to disperse the traffic loading over an area. The higher the elastic stiffness of the pavement and, hence, the individual layers the wider the area which reduces the level of strain experienced minimises in the pavement structure, dependent upon both the temperature and speed of loading [22].

It is defined according to BS EN 12697-26:2018 [25], the relation between the maximum applied stress and maximum strain response and expressed as:

$$E = \frac{\sigma}{\varepsilon}$$

where,

$E$  = elastic stiffness modulus in MPa

$\sigma$  = applied stress in MPa

## CHAPTER 2 BACKGROUND AND LITERATURE

$\varepsilon$  = applied strain in micrometre per metre or in micro strain( $\mu\text{m}/\text{m}$ ).

Complex Modulus:

The dynamic (complex) modulus is determined by applying sinusoidal vertical loads to cylindrical samples while measuring their deformation (Roberts et al., 1996). This describes the relationship between stress and strain for a linear visco-elastic material introduced to a sinusoidal load wave from at time,  $t$ , where applying a stress  $\sigma \times \sin(\omega \times t)$  results in a strain  $\varepsilon \times \sin(\omega \times t - \Phi)$  that has a phase angle,  $\Phi$ , with respect to the stress.

The amplitude of strain and the phase angle are functions of the frequency,  $f$ , and the testing temperature,  $\theta$ .

The stress - strain ratio which implies the complex modulus  $E^*$ , given as:

$$E^* = E^* \cdot (\cos(\Phi) + i \cdot \sin(\Phi))$$

The complex modulus depends on the frequency,  $f$  and the temperature,  $\theta$ . The complex modulus is characterised in two ways:

- 1- By the real component  $E_1$  and the imaginary components  $E_2$ :

$$E_1 = |E^*| \cdot \cos(\Phi)$$

$$E_2 = |E^*| \cdot \sin(\Phi)$$

- 2- By the absolute value of the complex modulus  $|E^*|$  and the phase angle,  $\Phi$ :

$$|E^*| = \sqrt{E_1^2 + E_2^2}$$

$$\Phi = \arctan\left(\frac{E_2}{E_1}\right)$$

where,

$E^*$  = the visco-elastic complex modulus, in megapascals (MPa).

$|E^*|$  absolute modulus of the complex modulus, in megapascals (MPa).

$E_1$  the real component of the complex modulus, in megapascals (MPa).

$E_2$  the imaginary component of the complex modulus, in megapascals (MPa).

$\Phi$  the modulus phase angle of the material (argument), in degrees ( $^\circ$ ).

The later description is usually used in practice. In linear elastic multi-layer calculations for instance the  $E^*$  modulus is commonly used as input value for young's modulus.

To describe the correlation between stress and strain at the loading time,  $t$ , for a material exposed to controlled loading (force or displacement), the secant modulus is used

$$E(t) = \frac{\sigma(t)}{\varepsilon(t)}$$

with stress,  $\sigma(t)$ , and strain,  $\varepsilon(t)$ , at time  $t$ .

A very stiff asphalt mixture in-situ may not display a good behaviour towards fatigue when the asphalt layer is thin, however, in thick asphalt layers the opposite may occur. This response is not completely simulated in the laboratory and because of this reason, it is difficult to mathematically model it.

Now, this degree of difficulty increases if we consider that that the asphalt mixture stiffness is a function of multiple factors such as asphalt binder stiffness, asphalt binder content and type (asphalt cement, asphalt emulsion, cutback asphalt, foamed asphalt, modified asphalt binders, etc.) [26], form, texture and absorption of the aggregate [27], [28], filler type and content [29], [30], volumetric composition of the mix (air void contents ( $V_a$ ), voids filled with asphalt (VFA), among others) [31], temperature, load frequency, traffic and environment [32], chemical composition, the ageing of the asphalt [33] among others. Generally, mixtures with higher air voids shows shorter fatigue life comparatively with the lesser air voids.

### 2.2.3 Type of loading

When fatigue resistance tests are performed in laboratory, samples are commonly subjected to two types of loads: stress-controlled ( $\sigma$ -C) and strain-controlled ( $\varepsilon$ -C). In  $\sigma$ -C tests, while the stress that is applied on the sample is remains constant during the test, strain increases [34]. While sample strain is constant throughout the entire  $\varepsilon$ -C tests, stress is reduced. In other words, under  $\varepsilon$ -C, with the increase of load repetitions, the asphalt mixture deteriorates, losing stiffness, and therefore it requires less load and less stress to produce the same strain [35].

Some factors associated to the type of load that add difficulty in obtaining models that predict the fatigue life process of asphalt mixtures are the following

- The response of bituminous mixtures in both types of loading ( $\sigma$ -C and  $\varepsilon$ -C) is often inverse (see Table 1). When the stiffness of the mix increases it has high fatigue resistance under  $\sigma$ -C. The reverse occurs the load mode is  $\varepsilon$ -C [1], [36], [37].
- For laboratory tests to simulate what happens on the field as closely as possible, it is necessary to know the load mode under which the asphalt mixture works when in service. Thin asphalt layers (with thickness equal or under 2 inches) are put under  $\varepsilon$ -C, while those with a thickness over 6 inches are under  $\sigma$ -C mode [38]. Failure criteria applied to both types of loads are different [34]. Generally, under  $\varepsilon$ -C, the sample is

## CHAPTER 2 BACKGROUND AND LITERATURE

supposed to fail when it has lost half of its initial stiffness, while under  $\sigma$ -C, it is assumed that failure occurs when the initial deformation is duplicated or when there is total rupture of the sample [39], [40].

- According to previous studies, tests performed under  $\varepsilon$ -C provides more disperse results than the ones performed under  $\sigma$ -C. [1], [34], [35], [41].
- During loading and unloading, dissipated energy (area of the stress-strain curve) [42] is created. This energy increases under  $\sigma$ -C and decreases under  $\varepsilon$ -C [43].

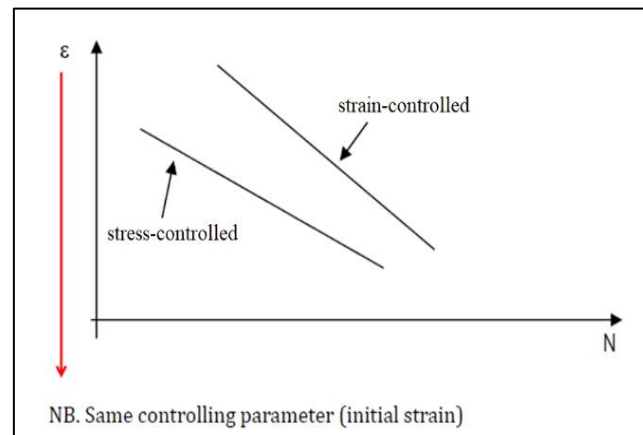


Figure 8 Plot showing the stress and strain-controlled tests

Table 1 Comparison of the Tests under  $\sigma - N$  and  $\varepsilon - N$

Description	$\sigma$ -N	$\varepsilon$ -N
Usual failure criterion	Sample rupture	Loss of one half of initial stiffness
Fatigue life	Shorter	Longer
Results dispersion	Reduction of life	Increase of life
Stiffness increase	Increase of life	Reduction of life
Rest time period	Increase of life	Reduction of life

On the other hand, on the field, the application of load is different to the one used in laboratory tests. The type, magnitude, frequency, and rest periods between load applications are different. Generally, laboratory fatigue tests are done by applying a continuous load. However, discontinuous tests, or tests that present rest periods between the application of load, better represent in situ conditions [44].

### 2.2.4 Test type, boundary conditions and support layer stiffness

Another factor that complicates the prediction of fatigue life of asphalt mixtures is the test type (tension-compression, 2,3,4 points bending, indirect tensile, dynamic shear, etc.), the geometry of samples (cylindrical, beams, trapezoidal samples, etc.), boundary conditions (lateral confinement, thickness, topography, etc.) and support layers (base, subbase, subgrade) stiffness [45].

These factors cause results of laboratory test findings to vary. As a result, some studies discovered large differences between the deformations measured in laboratory and in situ and derived various correlation coefficients known in the reference literature as “shift factor”. The issue with these coefficients is that they are dispersed (they fluctuate between 13 and 700) [46], [47].

### 2.2.5 Effect of environment temperature

Since asphalt fatigue is affected by the stiffness of the mixture, which is again depending on temperature, the distribution of load applications with time can have a substantial impact on the fatigue life. For instance, if all traffic loads are applied at times of low temperatures, then a different fatigue life will result compared with the situation where the loading occurs at higher temperatures. The real difference is determined by the amount of the loads, the thickness of the asphalt layer, the pavement composition, and the various traffic load proportions applied at low and high temperatures. Such a condition can arise for pavements that are heavily used at night by huge numbers of heavy vehicles. Since this study is also focused on the effect of temperature on bituminous mixtures, there is dedicated section which further explains briefly with the previous considerations.

## 2.3 Fatigue testing

From the early 1950s, significant amount of fatigue testing has been carried out, during this time a variety of different test configurations have emerged. It is possible to classify the most often used ones into categories dependent upon the mode of loading as follows:

#### 1. Simple flexure

- ✓ Centre point beam flexure (three-point bending) [48]
- ✓ Four-point flexure [49]
- ✓ Rotating cantilever beam flexure [50]

## CHAPTER 2 BACKGROUND AND LITERATURE

- ✓ Two-point beam flexure (trapezoidal cantilever) [51]
2. Direct axial loading
- ✓ Cylindrical specimens in tension and compression [50]
3. Diametral Loading [52]

The schematic representation of all the type of fatigue tests in Figure 9 which have had the most extensive use. In the arrows indicate the direction of the applied loading which induce the tensile stresses and strains and, hence, cause fatigue failure.

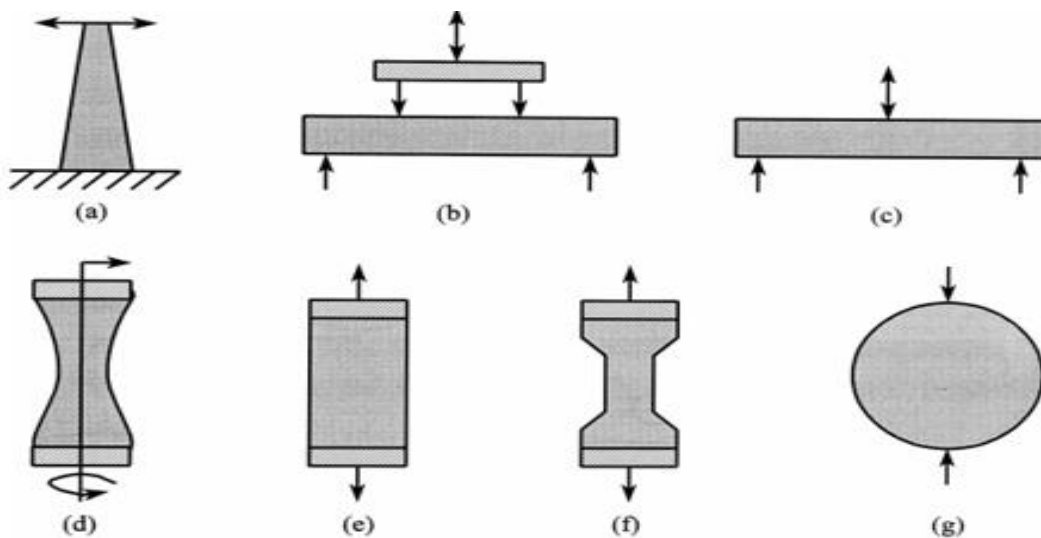


Figure 9 Schematic Demonstrating the Main Forms of Fatigue Test: (a) Two-Point Bending; (b) Four Point Bending; (c) Centre Point Bending; (d) Rotating Bending; (e) Direct Axial Loading; (f) Direct Axial Loading (Necked Specimen) and (g) Diametral Loading

### 2.3.1 Testing procedures

The European Standard introduced several methods to evaluate fatigue resistance of asphalt mixtures. These tests are briefly described here, more details about four point bending method are provided in section 3.3. The full testing protocol is described in the EN 12697-24:2018 [24].

#### 2.3.1.1 Two-point bending test on trapezoidal shaped specimens (2PB-TR)

“This method characterizes the behaviour of bituminous mixtures under fatigue loading with controlled displacement by two-point bending using trapezoidal shaped specimens. The procedure can be used for bituminous mixtures with a maximum aggregate size of up to 20 mm

on specimens prepared in a laboratory or the obtained specimens which are cored directly from the road layers with a thickness of at least 40 mm [24].

For mixtures with an upper size  $D$  between 20 mm and 40 mm, the test can be performed using the same principle but with adapted specimen sizes. For a given frequency of sinusoidal displacement, the method shall be carried out on several elements tested in a ventilated atmosphere at a controlled temperature.

An element test shall consist of:

- Placing a test piece with an isosceles trapezoidal head (Figure 10) under a sinusoidal displacement with constant amplitude.
- Recording the change in the force at head amplitude relative to the reaction of the test piece.
- Determining the test piece's fatigue life after the failure condition has been met.

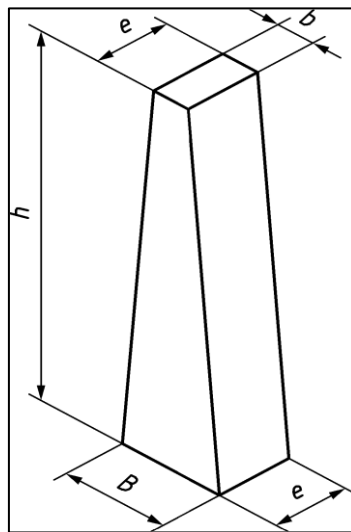


Figure 10 Trapezoidal shaped specimen

The test device must have a system that enables the application of a sinusoidal displacement with constant frequency to the specimen's top. Throughout the test, the displacement must fluctuate by no more than 0.12 m/N. The test device must be able to apply the load to the specimens at  $(25 \pm 1)$  Hertz and, if necessary for specific objectives, at alternative frequencies  $\pm 4\%$ . It's possible that the outcomes of tests conducted at wholly unrelated frequencies cannot be properly compared.

## CHAPTER 2 BACKGROUND AND LITERATURE

The sample  $i$  will be pushed sinusoidally up to the failure threshold at its peak at the enforced displacement amplitude of  $\pm 5 \mu\text{m}$ . The response forces must be recorded to an accuracy of  $\pm 2\%$  or better between 100 and 500 cycles in order to calculate the average reaction force.

The displacement  $z_i$  shall be measured and  $\varepsilon_i$  calculated for this element test. A accuracy of 300 cycles must be used while counting the number of cycles  $N_i$  at the failure criteria.

At the various strain amplitude levels where the tests are conducted, the fatigue line of the mixture element tests must be shown. The fatigue line will be evaluated as a linear regression of fatigue life versus amplitude levels in a dual decimal logarithmic system. These findings will be used to define the strain equal to an average of one million cycles  $\varepsilon_6$  and the slope of the fatigue line  $1/b$ . It is also possible to determine the quality index relative to  $\varepsilon_6$ ,  $\Delta\varepsilon_6$  and the standard deviation of the residual dispersion of fatigue life  $sN$ .

The deformations  $\varepsilon_i$  must be chosen in such a way that either:

- On a logarithmic scale, the strain levels are evenly spaced approximately.
- There are at least 3 levels of deformation, with a homogeneous number of specimens (to 1 or 2 specimens) at each level. On a logarithmic scale, the average values must be about evenly spaced.

A minimum of 18 element tests must be carried out to estimate the result.

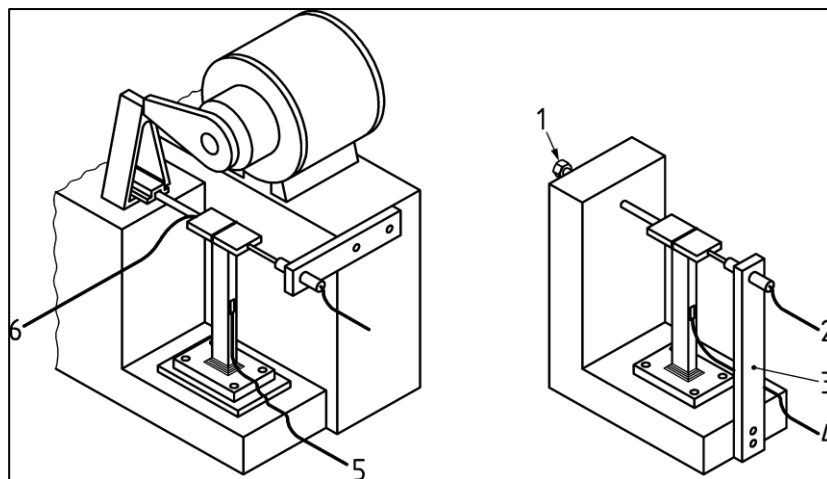


Figure 11 Sinusoidal displacement at the head of specimen

### Key:

- 1- Screw to apply the deformation.
- 2- Displacement measurement.
- 3- Support.
- 4- Measured strain.
- 5- Recorded strain.
- 6- Recorded stress.

### 2.3.1.2 Two-point bending test on prismatic shaped specimens (2PB-PR)

“This method examines the behaviour of bituminous mixtures under fatigue loading by 2-point bending using square-prismatic shaped specimens. The method can be used for bituminous mixtures with a maximum aggregate size of up to 20 mm and on specimens prepared in a laboratory or obtained from road layers with a thickness of at least 40 mm[24]”

The test equipment must have a mechanism that allows a sinusoidal displacement with a predefined frequency to the top of the specimen. The displacement must fluctuate by less than 0.1 m/N during the test.

The test device must be capable of delivering displacement to samples at a frequency of  $(25 \pm 1)$  Hz and, if required for specific objectives, at various frequencies  $\pm 4\%$ . If a frequency different than 25 Hz is utilized, information must be included in the test report. There doesn't seem to be a direct correlation between the results of tests conducted at completely different frequencies.

There must be a minimum of three tension levels, each with a minimum of six duplicates. The tension levels must be chosen for the material to ensure that the series' mean fatigue life is between  $10^4$  and  $10^6$  cycles for at least two levels and between  $10^6$  and  $10^7$  cycles for at least one level. Minimum of three levels of tension with a minimum of six duplicates per level must be carried out. The levels of tension shall be selected for the material in order to obtain a mean fatigue life of the series lies between  $10^4$  and  $10^6$  cycles for not less than 2 levels, and between  $10^6$  and  $10^7$  for a minimum of one level.

### 2.3.1.3 Three-point bending test on prismatic shaped specimens (3PB-PR)

“This method characterizes the behaviour of bituminous mixes under fatigue loading, with controlled displacement by three-point bending using prismatic beam shaped specimens. The behaviour is characterized through the determination of the fatigue law in terms of strain (relation between strain and number of load cycles at failure) and the associated energy law. The method can be used for bituminous mixture specimens with maximum aggregate size of 22 mm or for samples from road layers with a thickness of at least 50 mm. For a given frequency of sinusoidal displacement, the method shall be carried out on several elements tested at a controlled temperature [24]”.

A beam-shaped specimen supported at both ends and subjected to an element test must have a sinusoidal displacement applied to its midpoint with a consistent amplitude. The conclusion

## CHAPTER 2 BACKGROUND AND LITERATURE

will be drawn from the relationship between the maximal initial strain at the specimen's mid-span section and the quantity of cycles required to reduce the initial stiffness of the specimen by half. The strain at the mid-span region of the specimen must be continuously recorded against the number of cycles during the element test.

Any equipment that has a servo-hydraulic control press installed and capable of producing sinusoidal cyclic loading with the necessary frequency and amplitude can be employed (Figure 12).

At various strain amplitudes, test duplicates must be conducted on samples obtained from a homogeneous group. A preliminary computation using the results of the element tests must be used to establish a fatigue line for the mixture being tested.

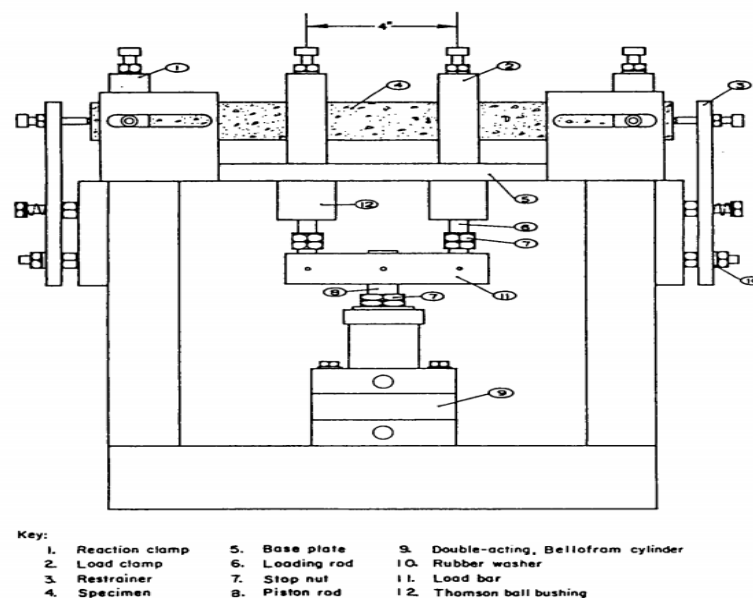


Figure 12 Three point bending device

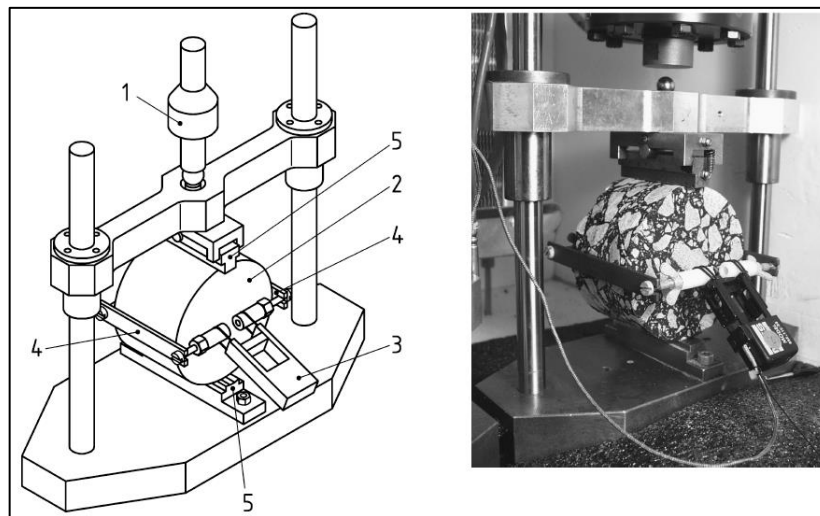
### 2.3.1.4 Indirect tensile test on cylindrical shaped specimens (IT-CY)

A cylindrical specimen manufactured in a laboratory or cored from a road layer can be used in this test. A cylindrical shaped specimen shall be subjected to repeated compressive loads with a haversine load signal through the vertical diametral plane. This loading develops a relatively uniform tensile stress perpendicular to the direction of the applied load and along the vertical diametric plane, which causes the specimen to fail by splitting along the central part of the vertical diameter. The resulting horizontal deformation of the specimen shall be measured, and

an assumed Poisson's ratio shall be used to calculate the tensile strain at the centre of the specimen. Fracture (fatigue) life shall be defined as the total number of load cycles before a fracture of the specimen occurs. Further failure criteria can be defined according to the dissipated energy during loading [24].

- The testing apparatus must be able to apply repeated haversine load pulses with rest intervals at a minimum loading range of 15 kN with an accuracy of 0.25 percent.
- To record the displacements along the horizontal diametral plan, a sensor with a suggested measuring range of  $\pm 2.0$  mm and a measurement accuracy of at least  $\pm 2$   $\mu\text{m}$ .
- The thermostatic chamber must have a temperature control range of  $-10$   $^{\circ}\text{C}$  to  $30$   $^{\circ}\text{C}$  and precision of at least  $\pm 0.5$   $^{\circ}\text{C}$ .
- To evaluate the fatigue behaviour at least 15 to 18 specimens shall be prepared.

Approximately  $70$   $\mu\text{m}/\text{m}$  to  $400$   $\mu\text{m}/\text{m}$  initial tensile strain range is recommended for fatigue tests. The consequent fatigue life of the tested material shall fall within a range between  $10^3$  and  $10^6$  per number of load cycles. A minimum of three stress levels must be carried out, with at least five replicates at every single level.



Key

- 1- load cell
- 2- asphalt specimen
- 3- extensometer
- 4- deformation strips
- 5- loading strip

*Figure 13 Indirect tensile test on cylindrical shaped specimens (IT-CY)*

### **Cyclic indirect tensile test on cylindrical shaped specimens (CIT-CY)**

A cylindrical shaped specimen shall be subjected to cyclic compressive load through the

vertical diametral plane. This type of loading causes a relatively uniform tensile stress perpendicular to the direction of the applied load and along the vertical diametric plane, which causes the specimen to fail by splitting along the central part of the vertical diameter. The resulting horizontal deformation of the specimen shall be measured, and an assumed Poisson's ratio shall be used to calculate the tensile strain at the centre of the specimen. As failure criterion, the energy ratio concept based on dissipated energy shall be applied [24].

It is necessary to use test equipment that enables sinusoidal loading of the specimen while maintaining the desired precision. It is necessary to have a computer and software for collecting and storing the data.

A minimum of two displacement transducers must be mounted on the specimen for the measurement system to accurately capture the specimen's horizontal deformation. The minimum measurement range for displacement transducers must be 4 mm, with a precision of 1  $\mu\text{m}$  for each displacement transducer. Additionally, displacement transducers must measure the vertical specimen's deformation for test control.

The desired test temperature in the vicinity of the specimens can be maintained in a thermostatic chamber with an accuracy of 0.5 °C. The link between the quantity of load cycles and the energy ratio yields the fracture life.

### **2.3.1.5 Four-point bending test on prismatic shaped specimens (4PB-PR)**

“This method characterizes the behaviour of bituminous mixtures under fatigue loading using four-point-bending test equipment in which the inner and outer clamps are symmetrically placed, and slender prismatic beams are used. The prismatic beams shall be subjected to four-point periodic bending with free rotation and translation at all load and reaction points. The bending shall be realized by loading the two inner load points (inner clamps) in the vertical direction, perpendicular to the longitudinal axis of the beam. The vertical position of the end bearings (outer clamps) shall be fixed. This load configuration shall create a constant moment, and hence a constant strain, between the two inner clamps. The sinusoidal type of loading shall apply. During the test, the load required to bend the specimen, the deflection, and the phase lag between these two signals shall be measured as a function of time. Using these measurements, the fatigue characteristics of the material tested shall be determined[24]”

Two inner and two outer clamps must be evenly spaced from the prismatic sample's centre. At the middle third, constant and equal loads must be applied (Figure 14). It is required to record

every applied force, deflection, and phase lag. According to the selected failure situation, the test sample's fatigue life must be estimated, as will be covered in the following chapters.

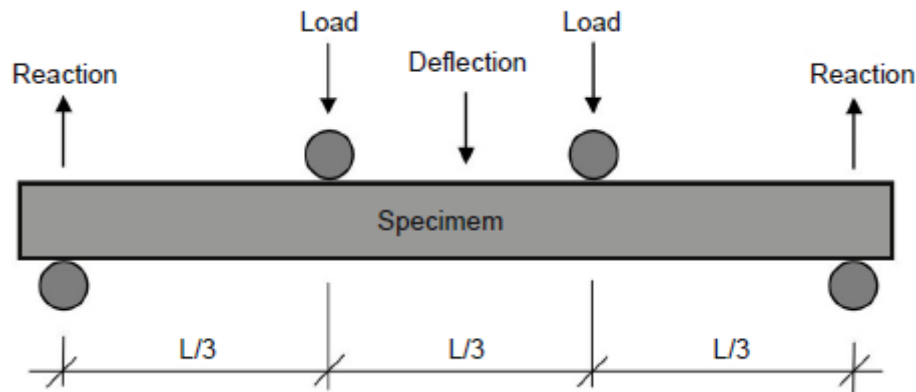


Figure 14 Four point bending loading configuration

This study is mainly focused on the fatigue resistance using the four – point bending beam test, this topic is further briefly discussed in the section 3.6, about the details of test equipment, specimen preparation and testing procedure.

## 2.4 Literature on Fatigue failure criteria

From the past two decades researchers has been doing humungous work in developing the fatigue test equipment and analysis techniques. Four point bending beam test and the trapezoidal fatigue equipment were created to investigate the fatigue performance of the bituminous mixtures, these testing procedures require at least 4 - 6 test repetitions to make the analysis. This analysis scheme further provides the chance to evaluate the rate of micro-cracks formation, besides the corresponding effect on the apparent stiffness of the mixture. This upgraded testing instrumentation permits to precisely estimate the point where fatigue failure happens [53]

The failure criterion defines the applicable region associated with the continuum damage model and is important in characterising the service life of asphalt mixtures. A proper failure criterion should consistently predict the failure of the material that reaches macro-fracture [54].

The number of cycles required to bring a sample to failure under a certain fatigue criterion is known as the fatigue life of the sample. To address this issue, a variety of criteria have been proposed. Some of these criteria are based on the modulus being reduced to a specific value,

while others are based on energy concepts or other stiffness-unrelated characteristics, such as the phase angle.

In the following sections five different criteria are presented.

### 2.4.1 Fatigue life, conventional criterion (50% of $E_0$ )

The concept of fatigue failure for asphalt concrete in LAB testing has always been debatable, especially when strain-controlled cyclic loading is used and there is no evidence of catastrophic failure or fracture. Examination of historical wear specifies that a material has failed when its modulus has decreased by 50% from its starting value, and the corresponding number of cycles is denoted by the symbol  $N_{F50}$ . However, because of its arbitrary premise, this failure criteria may not provide a cogent forecast for the damage state when used with continuum damage models (Modulus reduction to half its initial value) [55].

The traditional criteria ignore both the material characteristics and the actual fatigue phenomena, reflecting simply the sample stiffness. Other effects that have been mentioned by some researchers include thixotropy, self-heating, and non-linearity [56].

### 2.4.2 Damage analysis, ENTPE (50% of $E_{00}$ )

“The first proposed developments, made at ENTPE, supposed a linear variation of the modulus with the number of cycles in well-chosen intervals. A fatigue slope associated with a given interval could be used to characterize fatigue.[1] The method developed at the laboratory "DGCB" of ENTPE was employed to characterize fatigue in this approach. The method assumes a linear evolution of the modulus with number of applied load cycles within prescribed intervals.

In fatigue test the relationship between the modulus and the number of cycles can be identified in three phases:

**Adaptation phase:** This phase is distinguished by sudden decrease in initial modulus due to the laborious excitation of load application. However, the reduction is not mainly justified by fatigue damage. Heating and other phenomenon such as thixotropy can occur.

**Quasi stationary phase:** Throughout this phase, the fatigue contribution to stiffness decrease is dominant. Even if the parasitic effect (thermal heating and thixotropy) is minor in this phase, it must be considered. this phase is examined in the "DGCB" practice, to characterize the fatigue damage evolution, from which we can estimate the modulus ( $E_{00}$ ) value by linear

extrapolation when we have a linear reduction of the modulus. The  $E_{00}$  represents the intercept of this line, as shown in Figure 15

Failure phase: If the first two phases crack-initiation phases, this third phase is crack propagation, in which macro-cracks begin to grow, until the total failure is achieved at the end of this phase.

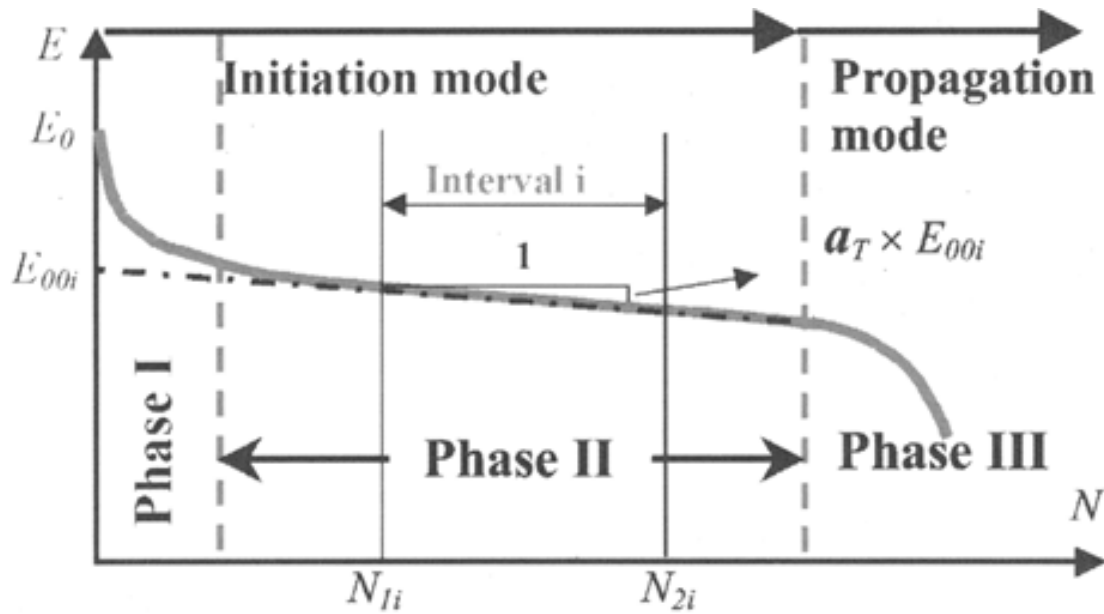


Figure 15 Stiffness Modulus versus cycles

In summary, the number of cycles corresponding to 50% reduction of the modulus value ( $E_{00}$ ) obtained through linear extrapolation of the stage at which we have linear reduction of the modulus when drawn versus the number of cycles is the considered failure criterion.

### 2.4.3 Peak in phase angle criterion

The phase angle is simply the angle at which  $\epsilon_0$  lags  $\sigma_0$ , is an indicator of the viscous (or elastic) properties of the material being evaluated [57]. Mathematically, this is expressed as

$$\phi = \frac{t_i}{t_p} \cdot (360^\circ)$$

where,  $t_i$  is the time lag between a cycle of stress and strain (s)

$t_p$  is the time for a stress cycle (s).

## CHAPTER 2 BACKGROUND AND LITERATURE

For a pure elastic material,  $\phi = 0$  and for a pure viscous material,  $\phi = 90^\circ$ . The below Figure 16 shows the relationship and degree of lag between the stress and strain of an asphalt mixture under a given sinusoidal load.

It demonstrates three different viscoelastic responses: dominantly elastic behaviour with phase angles below  $5^\circ$ , viscoelastic behaviour with phase angles between  $5^\circ$  and  $45^\circ$  (typical of asphalt mixtures) and dominantly viscous behaviour with phase angles  $>45^\circ$  (Figure 16).

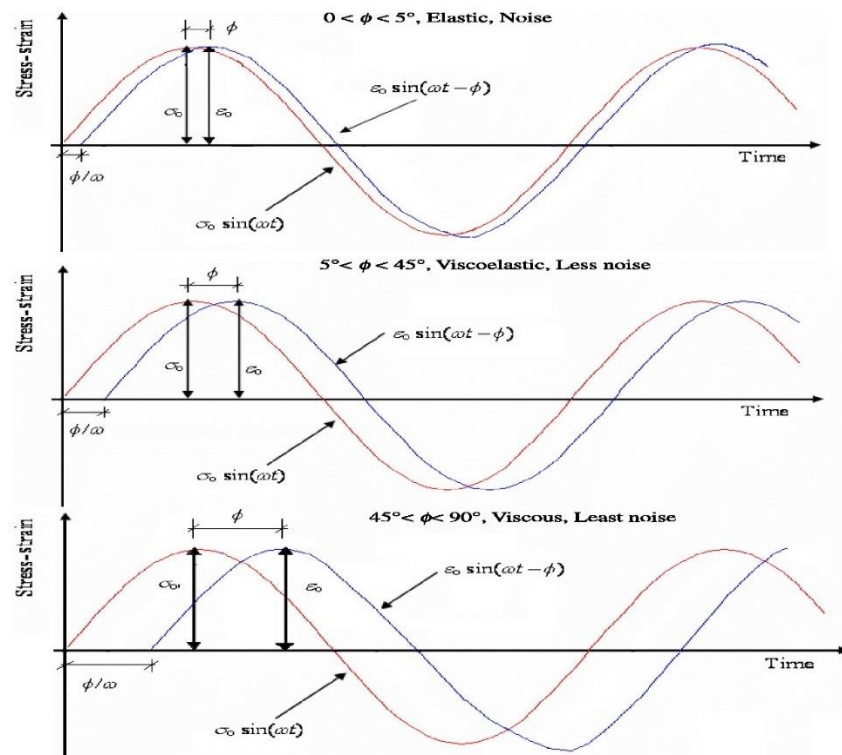


Figure 16 Asphalt mixture stress–strain responses under a sinusoidal load for different viscoelastic behaviours [57]

Reese [58] proposed a novel strategy by defining fatigue failure using the peak of the phase angle. The observed phase angle of asphalt concrete under cyclic stress typically shows a steady increase followed by a rapid reduction. The cycle during which this abrupt decline takes place is known as the number of cycles at failure, or  $N_f$  (Figure 17).

Because the definition of failure is tracked through the material's viscoelastic behaviour and the enormous variation in phase angle must represent a transformation in the dominant mechanism inside the material, which is most likely macro-fracture, this approach is generally thought to have more theoretical support than the traditional approach [59].

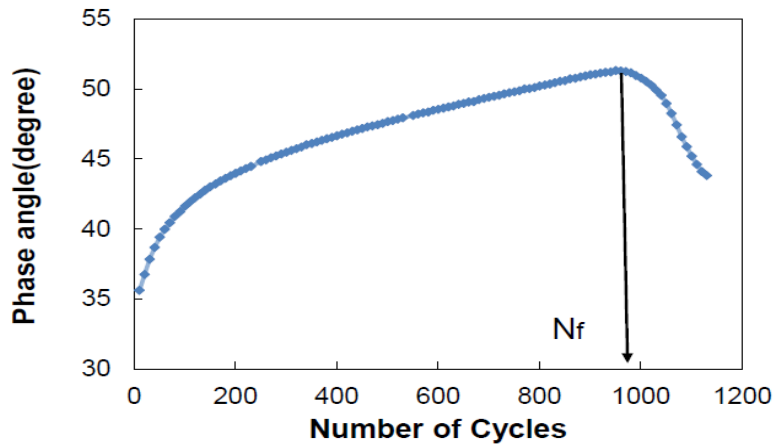


Figure 17 Fatigue life defined by Reese's (1997) approach. [58]

#### 2.4.4 Energy ratio criterion

In a stress-controlled test, the load amount is fixed, and following the period of fracture initiation when crack tips are present, the stress increases significantly. As a result, it is simple to estimate the value of  $N_1$  from the peak of  $R_n^\sigma$  vs  $n$ , because the data obtained from either stress or strain-controlled test configuration characterizes the material in the same state of damage instead of the modulus reduction criteria (The classical approach), which is an arbitrary definition, the idea of determining fatigue life by the  $N_1$  peak point is highly desirable.

In order to determine the number of cycles ( $N_1$ ) at which the formation of macro-cracks in a strain-controlled test (macro-cracks results when the microcracks merge to form a sharp crack, which then propagates up to failure), Hopman et al. [60] recommended the use of a "energy ratio" (Figure 18). The following is a definition of the energy ratio,  $W_n$ :

$$W_n = \frac{n \cdot w_0}{w_n}$$

where,

$n$  = cycle number

$w_0$  = dissipated energy in first cycle

$w_n$  = dissipated energy in  $n^{\text{th}}$  cycle

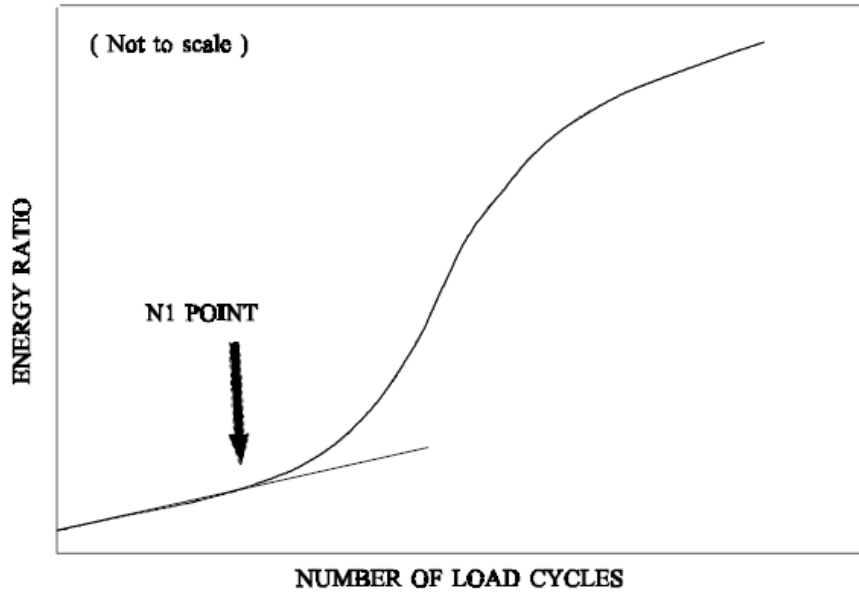


Figure 18 Energy Ratio (after Hopman, 1989)[60]

When plotting the energy ratio with the number of cycles, a noticeable modification of the slope can be plainly observed at a crucial number of cycles,  $N_1$ . This was proposed to be consistent with the sharp fracture development and typically correlates to a 40% reduction in extensional complex modulus. The energy ratio is expressed as follows:

$$W_n = \frac{n(\pi\sigma_0\varepsilon_0\sin\delta_0)}{\pi\sigma_n\varepsilon_n\sin\delta_n}$$

where,

$n$  = cycle number

$\sigma_0$  = stress in the initial cycle

$\sigma_n$  = stress in  $n^{\text{th}}$  cycle

$\varepsilon_0$  = strain in the initial cycle

$\varepsilon_n$  = strain in  $n^{\text{th}}$  cycle

$\delta_n$  = phase lag in cycle  $n$

If the stress term is substituted by  $(\varepsilon \cdot E^*)$  we get (for a strain- controlled test) the energy ratio, as follows:

$$W_n = \frac{n(\pi\varepsilon_0^2 E^* \sin\delta_0)}{\pi\varepsilon_0^2 E^* \sin\delta_n}$$

All constant terms in this equation could be shortcut into one single constant. Furthermore, the change in  $\sin \delta$  is insignificant compared to the change in  $E^*$  as indicated by (Rowe, 1993) [26]

and, therefore, the ratio of the  $\sin \delta$  can be taken as unity. So, the reduced energy ratio for a strain-controlled fatigue test,  $R_n^\epsilon$ , could be written as follows:

$$R_n^\epsilon = \frac{n}{E_n^*}$$

For strain- controlled test the value of  $N_1$  is identified in the point at which the slope of the ( $R_n^\epsilon$ ) versus ( $n$ ) diverges from a straight line.

For a stress- controlled test the same approach yields  $R_n^\sigma$  as follows:

$$R_n^\sigma = nE_n^*$$

In a stress- controlled test, the amount of the load stays fixed, and after the phase of crack initiation when we have the presence of crack tips, the stress increases sharply. Accordingly, the value of  $N_1$  can be easily estimated from the peak of  $R_n^\sigma$  vs  $n$  graph (Figure 19). This idea of identifying fatigue life by the  $N_1$  peak point is extremely desirable because the data attained from either stress/strain-controlled test configuration characterizes the material in the same state of damage instead of the modulus reduction criteria (The classical approach), which is an arbitrary definition.

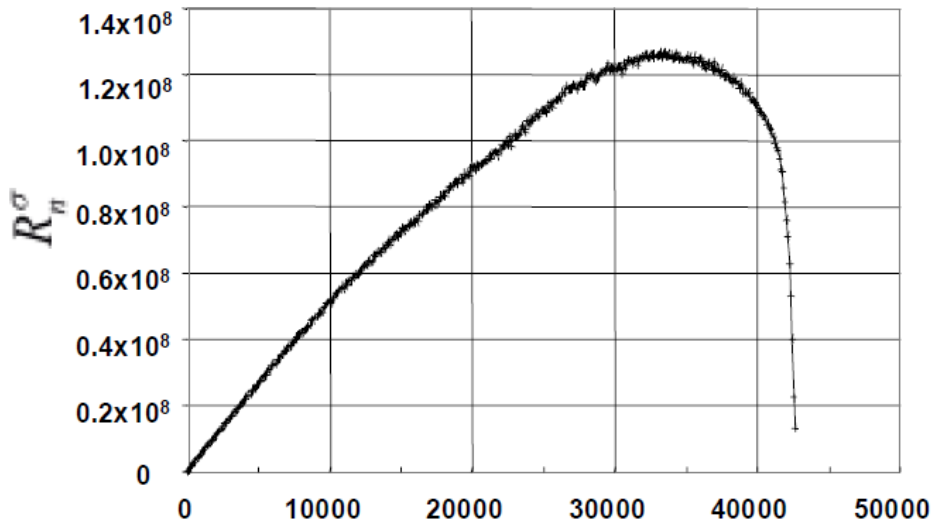


Figure 19 Energy ratio of stress-controlled fatigue test

If the results from the strain-controlled test were plotted, a standard graph might be produced. However, a further step of behaviour is detected. As the load in the controlled strain test decreases, a gradual crack spreads throughout the specimen at this latter stage.

The  $N_1$  condition is significantly more difficult to define for strain- controlled when compared to stress- controlled tests (This is because of the decrease of the stress at the crack tip as the

crack progresses, resulting in a reducing rate of crack propagation). By using the same analysis for the controlled stress approach as was previously described, this issue might be solved.

Hopman's analysis for stress-controlled testing may be applied, even when the fatigue tests are conducted using strain-controlled tests. A pronounced peak at failure  $N_1$  [62] when graphing the product ( $nE^*$ ) vs  $n$ , as shown in Figure 19.

The decline in modulus during the microcrack development phase is linear ( $dE^*/dn = \text{constant}$ ). The slope ( $dE^*/dn$ ), which measures relative damage, increases when fractures form and begin to spread. As a result, the product ( $nE^*$ ) decreases as a result.

$$E^* = 1 + n \frac{dE^*}{dn} + \frac{n^2}{2!} \cdot \frac{d^2E^*}{dn^2} + R$$

$$R \ll \left( 1 + n \frac{dE^*}{dn} + \frac{n^2}{2!} \cdot \frac{d^2E^*}{dn^2} \right)$$

$$E^*n \approx n + n^2 \frac{dE^*}{dn} + \frac{n^3}{2!} \cdot \frac{d^2E^*}{dn^2}$$

The second differential is equal to zero throughout the microcrack generation phase, and  $nE^*$  equals  $n(1 + nE^*)$ . When a sharp fracture starts to form, the damage rate increases, the second differential turns negative, and the product  $nE^*$  falls. The ensuing peak denotes the phase change from microcrack creation to macrocrack propagation.

#### 2.4.5 Dissipated Energy ratio criterion:

The application of the dispersed energy technique for fatigue damage assessments has received support from several studies. This method makes it possible to develop an independent fatigue rule independently of the loading mode, frequency, length of rest periods, and temperature.

Viscoelastic materials produce hysteresis loops when they are subjected to cyclic loading because they take distinct routes during the loading and unloading cycles [63]. The area inside the hysteresis loop, which is used to determine the dissipated energy per cycle, may be calculated as follows:

$$w_i = \pi \cdot \sigma_i \cdot \varepsilon_i \cdot \sin \delta_i$$

where,

$w_i$  is the dissipated energy at cycle  $i$

$\sigma_i$ , stress amplitude at cycle  $i$

$\varepsilon_i$  strain amplitude at cycle  $i$ ;  $\delta_i$  phase angle at cycle  $i$

Since the three primary viscoelastic parameters—stress, strain, and phase angle—are included in this method, it is possible to infer an intrinsic fatigue law by tracking how these values change as fatigue develops. Van Dijk and his colleagues provided the first research that used the dissipated energy technique to describe fatigue cracking in asphalt mixes. They demonstrated that no matter the manner of loading, frequency, or temperature, the relationship between cumulative dissipated energy ( $W_{fat}$ ) at failure and the number of cycles ( $N_f$ ) until failure depended exclusively on the material parameters. After  $n$  cycles, the total energy that has been lost may be estimated as follows:

$$W_n = \sum_{i=0}^n w_i$$

The relationship between cumulative dissipated energy to the number of load cycles to failure was found to follow a power law relation as following:

$$W_{fat} = A \cdot N_{fat}^z$$

where,

$W_{fat}$  = total dissipated energy until failure due to fatigue cracking.

$N_{fat}$  = number of loading cycles to fatigue.

$A$  and  $z$  = material constants.

The fundamental issue with this method is that it includes energies like recoverable viscoelastic energy and heat energy, which are not responsible for fatigue damage, in the total amount of dissipated energy calculated using the first equation. In order to examine the fatigue behaviour, Ghuzlan and Carpenter [40] suggested using the Dissipated Energy Ratio (DER).

The fatigue life under repeated cyclic stress should coincide with the boundary between crack initiation and propagation. To precisely pinpoint the fatigue failure point, a variety of strategies have been used.

The conventional approach of a 50% reduction in the initial stiffness is the most frequently used method to identify the fatigue failure in bituminous materials. This criterion, however, may not always be adequate for analysing fatigue properties, as several researchers have demonstrated. If this arbitrary definition is used, it is also possible that several stress/strain loading modalities may not necessarily result in a particular intrinsic fatigue law.

Finding alternative methods that are not arbitrary and can characterize the fatigue failure based on a more basic analysis. A feasible standard for characterizing the fatigue failure of

## CHAPTER 2 BACKGROUND AND LITERATURE

bituminous mixes was presented using the Dissipated Energy Ratio (DER) idea, which is shown below.

$$DER = \frac{\sum_{i=1}^n W_i}{W_n}$$

where,

$W_i$  = dissipated energy per cycle.

$W_n$  = dissipated energy at cycle  $n$ .

The graph of the correlation between DER and number of cycles in the stress-controlled mode offers a unique approach to assess the stage of fatigue damage at which the material experiences a transition from crack initiation to crack propagation. Figure below indicates the relationship between DER and loading cycles. Throughout the first part the damage is negligible and  $DER = n$  (the dissipated energy is roughly equal for successive cycles). As the relative difference in dissipated energy between successive cycles becomes substantial, the dissipated energy ratio starts deviating from the equality line which is interpreted as crack initiation. The fatigue failure  $N_f$  point in Figure is characterized by the sudden change in DER which can be linked to the point of transition from crack initiation to crack propagation. This change is believed to be highly material-specific and independent of the mode of loading.

For the strain-controlled test configuration the failure point  $N_f$  is described by the intersection of two tangents as shown in the following in the Figure 20

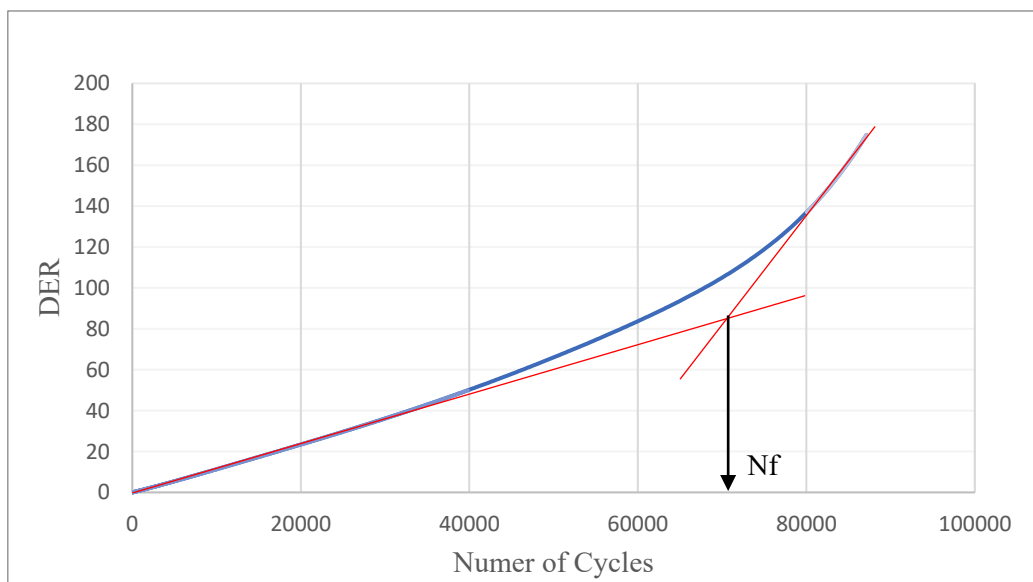


Figure 20 DER approach

## 2.5 Fatigue modelling

To predict fatigue cracking there are numerous fatigue models that have been developed across the world. Fatigue models are commonly classified into two main types, the strain-based models and the strain-modulus based models. These models are termed phenomenological models because they provide observable relationships rather than theoretical analysis established from the pavement mechanics' study.

A review of the literature reveals some main models used to calculate fatigue damage from the stresses or strains in the asphalt layer for fatigue cracking from both the surface and the base of the bound layers.

This first approach is to determine the fatigue life of the asphaltic material from the maximum tensile strain or stress in the asphalt layer. Longitudinal cracking observed on the surface of a flexible pavement is commonly considered as being related to traditional fatigue except for temperature cracks and long-term weathering cracks, and the newly proposed mechanism of top down cracking. This type of fatigue model has been developed from laboratory experiments and is typically a power-law relationship. This relationship has been expressed in the following form, [64]

$$N_f = k_1 (1/\epsilon_0)^{k_2}$$

Material constants  $k_1$ , and  $k_2$  are typically determined from simple laboratory fatigue tests on specimens of asphaltic material [see, for example, references [65]–[67]]

Experimental studies have shown that the major factors affecting the constants  $k_1$ , and  $k_2$ , in equation (1) are: (a) asphalt mixture stiffness, (b) bituminous binder content, (c) bituminous binder viscosity, (d) gradation and characteristics of the aggregate, (e) air void content and (f) pavement temperature [66], [68].

Bonnaure et al. and Finn et al. noted differences in the coefficients of this equation for different temperatures. They proposed a fatigue formula using modulus as follows:

$$N_f = K_1 (1/\epsilon_0)^{K_2} (E^*)^b$$

where,

$E^*$  = the dynamic stiffness modulus of the HMA,

$\epsilon_0$  = the tensile strain,

$K_1$ ,  $K_2$ , and  $b$  = fitting coefficients to the data.

## CHAPTER 2 BACKGROUND AND LITERATURE

To account for strain variations, the Miner's hypothesis of damage has been used in conjunction with these phenomenological fatigue relationships, Miner (1945). Miner's hypothesis is represented as a relative damage factor where the crack will occur when the sum of the damage factors equals one. Miner's damage hypothesis is given as follows:

$$D_i = n_i / N_i$$

where,

$D_i$  = relative damage during some period  $i$ ,

$n_i$  = number of load applications during a period  $i$ ,

$N_i$  = the ultimate number of load applications the pavement could carry

These basic models have served as the framework for various agencies in calibrating these models to their specific pavements and mixtures. Given below are the fatigue models of several agencies with some details about the coefficients developed and the assumptions used.

### ❖ The Asphalt Institute Model

The fatigue relation for the Asphalt Institute (AI) was developed based on laboratory fatigue data for selected sections of the AASHO road test by Asphalt Institute (1982), and Finn et al.(1977). The following fatigue relation was developed by the Asphalt Institute (1982):

$$N_f = 18.4 \times (C) (4.325 \text{ E-}3) (\epsilon_t)^{-3.291} |E^*|^{0.854}$$

where,

$N_f$  = number of 18,000 lb equivalent single axle loads,

$\epsilon_t$  = tensile strain in asphalt layer (in/in),

$|E^*|$  = asphalt mixture dynamic modulus (psi),

$C$  = function of volume of voids and volume of asphalt.

The fatigue relationship in Equation (9) was modified to reflect the effect of the air voids and asphalt content in the asphalt mixture. This was done by introducing the correction factor ( $C$ ), equal to:

$$C = 10^M$$

where,

$M = 4.84 (V_b / (V_v + V_b) - 0.69)$ ;  $V_b$  = volume of asphalt;  $V_v$  = volume of air voids.

The M value was obtained from laboratory fatigue data developed by Pell and Cooper (1975). The value of C was set to be 1 when the volume of binder equals 11 and the volume of air voids equal 5. It can be noted that the fatigue life is reduced by increasing the air voids content or reducing the asphalt content in the asphalt mixture.

❖ The Tayebali (1996) Model (SHRP Project A-003A)

$$N_f = S_f * 2.738 * 10^5 * e^{0.077VFB} * \varepsilon_t^{-3.6224} * S_0''^{-2.720}$$

Where  $S_f$  = shift factor to convert laboratory results to field expected results (the recommended factor is 10 for 10% cracked area and 14.0 for 45% cracked area),  $e$  = base of natural logarithm,  $VFB$  = percentage of voids filled by bitumen,  $\varepsilon_0$  = strain level, and  $S_0''$  = loss of stiffness as measured in flexure [69].

❖ Bodin Model [70]

This model suggests a non-local damage model to forecast pavement fatigue cracking, which was employed in a finite-element code along with a self-adaptive jump-in-cycle procedure for high-cycle fatigue computations. The mathematical model used to illustrate mechanical damage is an elasticity-based damage model for fatigue.

$$N_{crit} = \frac{F(d_{crit})(\beta + 1)}{\varepsilon_a^{\beta+1}}$$

$$F(d_{crit}) = constant$$

$$F(d) = \sum_{cycle\ 1}^N \frac{\varepsilon_a^{\beta+1}}{\beta + 1}$$

where,  $d$  is the damage variable;  $\varepsilon_a$  is the amplitude of the equivalent strain over one cycle;  $f(d)$  is the function of damage and  $F(d)$  is the scalar function of damage; and  $b$  is a model parameter.

❖ IRC model

Based on large amount of filed performance data of pavements of south, north, east, and west zones in India collected under the Research Schemes R-6<sup>4</sup> and R-19<sup>5</sup> of Ministry of Surface

## CHAPTER 2 BACKGROUND AND LITERATURE

Transport. Govt. of India. The relation between the fatigue life of the pavement and the tensile strain in the bottom of the bituminous layer was obtained as:

$$N_f = 2.21 \times 10^{-4} \times [1/\varepsilon_t]^{3.89} \times [1/E]^{0.854}$$

where,

$N_f$  = Number cumulative standard axel to produce 20% cracked surface area,

$\varepsilon_t$  = initial strain on the bottom of the asphalt concrete,

E = Elastic modulus of asphalt concrete layer.

### ❖ NCHRP 1-37A Calibrated Fatigue Model

This model contains significant modifications to the standard form of the fatigue equation, but still relies on the basic strain-modulus form. Thick and thin pavements exhibit different behaviour when analysed with the standard phenomenological model, changing from constant strain in a thin pavement to constant stress in a thick HMA layer, the 1- 37A research team elected to add a variable to change coefficients as the HMA layer becomes thicker.

The Asphalt Institute equation serves as the foundation for this model. To define the coefficients for different mixes and different locations of the United States, a thorough calibration process was carried out utilizing field data and LTPP sections. The final form of El-Basyouny and Witzcak's (2005) model is:

$$N_f = \beta_{f1} \cdot K_1 (\varepsilon_t)^{-\beta_{f2}} \cdot K_2 (E)^{-\beta_{f3}} \cdot K_3$$

where,

$N_f$  = Number of load repetitions to fatigue failure,

$\varepsilon_t$  = tensile strain at the critical location,

E = the dynamic modulus of the HMA,

$k_1, k_2, k_3$  = Laboratory regression coefficients,

$\beta_{f1}, \beta_{f2}, \beta_{f3}$  = Calibration parameters.

## 2.6 Effect of the temperature on fatigue

The laboratory fatigue test for the asphalt mixture is most commonly conducted at the temperatures ranging between 10 °C and 20 °C, as the fatigue cracking in the asphalt layer is generally regarded to occur within this intermediate temperature scope [71], [72].

The SHRP project report [73] also proves that the fatigue life of the asphalt mixture increases with the rising temperature within the range of 5 °C to 25 °C in the bending test with controlled strain mode.

Tsai et al [16] investigated the fatigue characteristics of the asphalt mixtures at 5 °C, 20 °C and 30 °C using the four-point bending (4 PB) test with controlled strain mode. They reported that as the temperature increases, fatigue life of asphalt mixture was increase, however the initial stiffness of the mixture exhibit inversely.

Hoffman (2008) evaluated the influence of temperature on fatigue performance of bituminous mixes prepared with regular binder (50/70) and polymer modified (PMB 45A and PMB 25H). Fatigue tests were conducted in indirect tensile mode at 10, 15, 20, 25 and 30 °C temperatures. The results show that for a given strain level, the mix with softer binder (PMB 45A) failed earlier than the mix having PMB 25H binder because of its low stiffness. Furthermore, the fatigue resistance decreased with increase in temperature (due to decrease in resilient).

Fatigue life of asphalt concrete (AC 0/14) at different temperatures 5, 15 and 25 °C was studies by two researchers Silva and Oliveira (2008) [74]. The results depict, at high strain levels (above  $200 \times 10^{-6}$ ) the AC 0/14 mixture presents the highest fatigue cracking resistance at a temperature of 25 °C. In contrast, at lower strain levels the AC 0/14 mixture presents the highest fatigue cracking resistance at a temperature of 5 °C.

Chen also found that the fatigue life of asphalt mixture increases with the rise of temperature in the 4 PB fatigue test [75] .

Cheng et al. [76] has done some rigorous study on the temperature affects the fatigue life of the asphalt mixture oppositely in the 4 PB and IDT tests. In the 4 PB test, the rising temperature causes an increase in the fatigue life of the mixture. Below shown Figure 21 are the typical results of this study. However, in the IDT test, the fatigue life of the mixture decreases obviously with the increase of temperature.

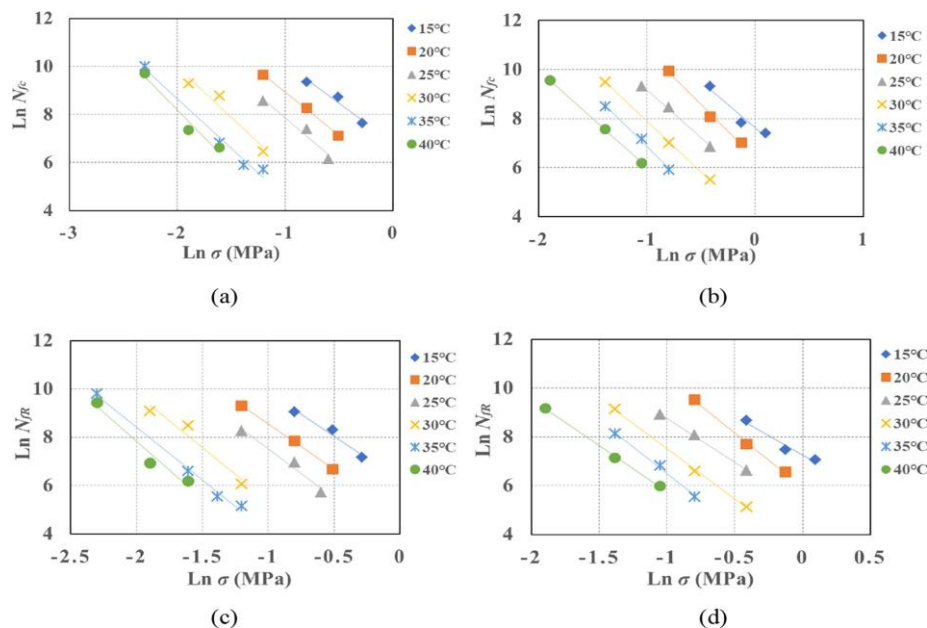


Figure 21 The fatigue lives of the mixture at different temperatures and strain levels: (a)  $N_{f50}$  of the neat mixture, (b)  $N_{f50}$  of SBS-modified mixture, (c)  $N_{fM}$  of the neat mixture [76]

The above-mentioned studies disclose the apparent effect of temperature on the fatigue life of asphalt mixture. Although, to clarify the fatigue behaviours of asphalt mixture at different temperatures two issues still need to be addressed. First, the current findings imply the tendency that the temperature affects the mixture’s fatigue life 4 PB test with controlled strain mode. This phenomenon needs to be further identified, as the fatigue life of the bituminous mixtures depend on the various factors. Secondly, a particular study is needed to estimate the fatigue life on the different layers of the asphalt pavement possessing the same binder type and obviously with the different aggregate gradation.

## 2.7 Effect of mixture type on fatigue

The effect of aggregate gradation on fatigue of modify bituminous concrete (BC) and dense bituminous macadam (DBM) mixes has studied by the two researchers, Shukla and Bose. A new gradation was adopted and termed as Large Size Aggregate Mix (LSAM) based on laboratory testing and analysis. Laboratory tests were carried out to determine Marshall and Modified Marshall Characteristics, indirect tensile strength and fatigue life cycles of bituminous mixes. The results indicated that fatigue life of (LSAM) mix was higher than (DBM) mix and slightly less than BC mix. Also, by use of (LSAM) mix, the optimum binder content is reduced from 5.3 percent to 5.0 percent, and shear strength (stability) of the mix also increased.

effects of aggregate size, temperature and asphalt content on fatigue characteristic of different bituminous mixtures was studied by Nejad et al. Indirect tensile stiffness modulus (ITSM) and indirect tensile fatigue test (ITFT) were performed in this study. The results (Figure 22) indicated that fatigue life was shortened with increasing temperature. Moreover, HMA mixtures had greater fatigue lives as compared to SMA mixtures and this arise from dense graded inherent structure which interlocked better to each other in comparison with SMA mixtures. It is concluded that increasing the asphalt content will make the mixture less stiff and therefore, less fatigue resistant (NCHRP, 2004). However, the effect of aggregate gradation on fatigue behaviour is more dominating than the effects of asphalt content.

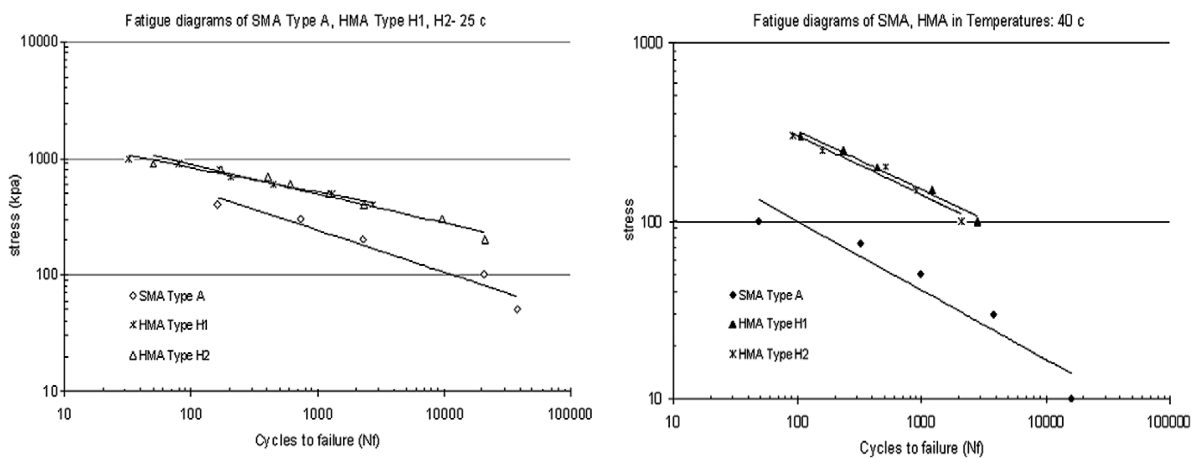


Figure 22 Fatigue diagrams of HMA types H1, H2 and SMA type A in 25 °C and 40 °C

### **3 CHAPTER 3 MATERIALS AND METHODOLOGY**

### 3.1 Experimental campaign

This section summarizes the experimental campaign initializing with the bitumen mixtures characterization and continuing with the specimen preparation which are then used in the four-point bending beam test. These mixtures were tested and compared following the objectives of the study.

According to the standards to obtain the final fatigue curve of bituminous mixtures, a minimum of six beams were prepared and tested for at least three strain levels which should obtain a fatigue life in the range of  $10^4 - 2 \times 10^6$  cycles [25].

This study employed one type of binder, 50/70 grade to prepare two bitumen mixtures are used for this study, binder course mixture and base course mixtures which is common in asphalt pavement surface layers. These two mixtures are plant-based mix obtained from local plant, SITALFA S.p.A, Torino.

The binder content was attained by performing two ignition tests according to the standard, BS EN 12697-39-2020 [77] and the average binder content was noted. Two aggregate gradation tests were performed using the burnt mixture in accordance with BS EN 933-1-2012 [78]. The aggregate density and theoretical maximum density of the mixture were then calculated using BS EN 12697-5-2018 [79] and BS EN 1097-6-2013 [80], using the pycnometer technique.

In accordance with BS EN 12697-31-2019 [81], four gyratory tests were conducted to determine the mixture's workability and compatibility. The slabs are then produced in accordance with BS EN 12697-33-2019 [82] using a roller compactor. The obtained slabs are then dimensionally measured according to BS EN 12697-29-2020 [83], and also measure the densities. These slabs are sawed precisely to the required size and made them into beams. Finally, the obtained beams dimensions are measures and checking the densities again after that these are further taken to testing using the four-point bending device in accordance with BS EN 12697-24-2018 [24].

*Table 2 Testing methods and the European standards*

TEST	STANDARD
Ignition test	BS EN 12697-39-2020
Aggregate gradation	BS EN 933-1-2012
Aggregate density	BS EN 12697-5-2018
Theoretical maximum density	BS EN 1097-6-2013
Gyratory compaction	BS EN 12697-31-2019

Roller compaction	BS EN 12697-33-2019
Dimensions	BS EN 12697-29-2020
Fatigue Testing	BS EN 12697-24-2018

The testing is performed at DIATI road materials laboratory in Politecnico di Torino, with the four-point bending beam testing device produced by IPC Ltd. The dimension of the beam specimen is 410 mm × 50 mm × 50 mm. the sinusoidal loading with the frequency of 10 Hz is applied during the test. The controlled strain mode is used. Two temperatures, 10 °C and 20 °C on the binder course mixture and base course mixture, respectively were employed. At each temperature, after the initial trial and error, three strain levels 140 µm/m, 200 µm/m, 300µm/m were chosen for testing.

This study is an extension and aimed to bring the completeness to the recent study that was made by Ahmad Salah from the DIATI road materials laboratory in Politecnico di Torino. A 4PB test with controlled strain on binder course mixture with the test conditions of frequency 10 Hz and temperature of 20 °C for the testing of fatigue resistance. To make a better comparison of the results, this study also follows the similar failure criteria. The effect of temperatures, 10 °C and 20 °C on fatigue life with the help of binder course mixture and effect of mixture type on fatigue life with the base course mixture at temperature 20 °C.

### 3.2 Material characterization

This section describes the characterization of the materials used in the laboratory activities and their properties. This chapter shows only the initial stages in which the material is selected, classified, prepared, and measured.

Two materials are to be used in this study as binder and base, same procedures is repeated for both the materials which are described and briefly explain in this section.

Mixture characterization tests are used to describe the crucial mixture parameters. The most basic tests include:

- Ignition test to estimate the binder content.
- Theoretical maximum density of the mixture.
- Aggregate density.
- Sieve analysis to estimate aggregate size distribution.

### 3.2.1 Ignition test

The estimation of the binder content of asphalt mixtures through the ignition test come as an alternative to the traditional method of separating the binder using solvents. The leftover aggregate may be utilized to assess aggregate gradation and density because the test temperature does not harm the aggregate particles, making the procedure useful for assessing the composition of mixtures. The results can be used to ensure and manage the mixture's quality.

Procedure:

According to BS EN 12697-39-2020 [77], the determination of the binder content by ignition test is performed using technique (B), which allows the use of a furnace and an external balance.

The size of the used sample is estimated as a function of the nominal maximum aggregate size according to the following table:

*Table 3 Size of the ignition test sample*

<b>Nominal maximum aggregate size mm</b>	<b>Mass of sample g</b>	<b>Maximum constant mass limit g</b>
4	1 000 to 1 400	0,15
5,6 or 6,3 or 8 or 10	1 000 to 1 600	0,15
11,2 or 12,5 or 14 or 16	1 000 to 1 700	0,20
20 or 22,4	1 000 to 2 400	0,25
31,5	1 000 to 3 000	0,30
40 or 45	1 000 to 4 000	0,40

The furnace had been preheated to 540 °C, the test temperature. In the meanwhile, the weight of the catch pan and empty sample baskets (Figure 23) ( $W_t$ ) was recorded. The sample was then placed into the baskets and dispersed uniformly, and the corresponding weight ( $W_{t+s}$ ) was recorded. The sample was put inside the furnace once it had attained temperature. When the mass loss becomes zero, halt the test, remove the sample, allow it to cool at ambient temperature, and then note the mass of the sample plus the sample basket plus the catch pan ( $W(t+a)$ ).

**Calculations:**

The total mass of bituminous mixture before the ignition ( $W_{S,W}$ ) is calculated as:

$$W_{S,W} = W_{t+s} - W_t$$

where,

$W_{S,W}$  is the total mass of bituminous mixture prior to ignition, in grams (g).

$W_{t+s}$  is the mass of bituminous mixture, sample basket(s) and catch pan prior to ignition, in grams (g).

$W_t$  is the mass of the sample basket(s) and catch pan, in grams (g).

The total mass of the remaining aggregate after the ignition test is:

$$W_a = W_{t+a} - W_t$$

where,

$W_a$  is the total mass of aggregate remaining after ignition, in grams (g).

$W_{t+a}$  is the mass of bituminous mixture, sample basket(s) and catch pan after ignition, in grams (g).

$W_t$  is the mass of the sample basket(s) and catch pan, in grams (g).

The corrected binder content by the mass of bituminous mixture is calculated as:

$$B = \frac{(W_s - W_a)}{W_s} \times 100 - C_F$$

where,

$B$  is the corrected binder content of the bituminous mixture sample, in percent (%).

$W_s$  is the dried total mass of the bituminous mixture prior to ignition, in grams (g).

$W_a$  is the total mass of aggregate remaining after ignition, in grams (g).

$C_F$  is the calibration value, in percent (%). (Was neglected in our calculations)



*Figure 23 High temperature furnace and sample baskets for ignition test*



*Figure 24 Sample distribution inside the basket and sample*

The results are presented in the table below:

*Table 4 Ignition test results for two mixtures*

<b>IGNITION TEST</b>					
<b>Binder content (%) by wt. of Mixture</b>			<b>Binder content (%) by wt. of Aggregate</b>		
<b>Test Sample</b>	Binder	Base	Test Sample	Binder	Base
<b>1</b>	5.76	4.55	1	6.11	4.76
<b>2</b>	5.49	4.99	2	5.81	5.25
<b>Average</b>	<b>5.62</b>	<b>4.77</b>	<b>Average</b>	<b>5.96</b>	<b>5.00</b>
<b>Std Deviation</b>	<b>0.135</b>	<b>0.22</b>	<b>Std Deviation</b>	<b>0.15</b>	<b>0.245</b>

### 3.2.2 Theoretical maximum density of the mixture / Aggregate density

The theoretical maximum specific gravity, or in other words could be indicated as the theoretical maximum density (TMD), is the hot mixed asphalt density excluding air voids. Therefore, if the air voids were theoretically excluded from a sample, the density of the remaining aggregate and asphalt binder would be the theoretical maximum density. TMD is a significant HMA characteristic because it is used to determine the air voids in compacted HMA and other volumetric-related properties of a compacted bituminous mixture, and also to offer a target value for the compaction.

#### **Procedure:**

The volumetric method is used to estimate the theoretical maximum density of the mixture in accordance with BS EN 12697-5-2018 [79].

- a. The mass of the loose sample used for this test should be more than 50 times of the nominal maximum aggregate size (12.5mm)
- b. To disaggregate the mixture, it was heated to  $(110 \pm 5) ^\circ\text{C}$ , in the oven. The sample was then put onto a table, allowed to cool, and then it was manually loosening and separating into coarse particles (Figure 25).
- c. Knowing the empty weight of the pycnometer with cap ( $m_1$ ), included is recorded along with the volume of the already calibrated pycnometer ( $V_p$ ).
- d. The sample is then put inside the pycnometer, where the total weight is then recorded ( $m_2$ ). De-aired distilled water was poured into the pycnometer to fill it halfway up (see Figure 26).
- e. The same procedure is followed for the aggregate density.

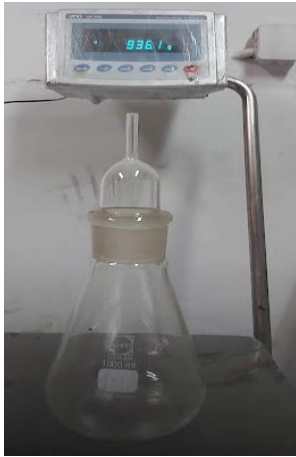


*Figure 25 Mixture distribution after cooling down*



*Figure 26 Asphalt particles inside the pycnometer*

The trapped air was then released by inserting the pycnometer into the vacuum system (see Figure 27). After the trapped air is released, disassemble the vacuum system, install the pycnometer cap, and fill the pycnometer with water to the top. The vacuum was applied for at least an hour, and the pycnometer was stirred every 15 minutes. At last, dry the pycnometer surface, note its weight in ( $m_3$ ), and take the temperature.



*Figure 27 Vacuum system*

Calculations:

The density of the water is calculated as follows:

$$\rho_w = 1,00025205 + \left( \frac{7.59xt - 5,32xt^2}{10^6} \right)$$

where,

$\rho_w$  is the density of water at test temperature, in megagram per cubic metre (Mg/m<sup>3</sup>).

$t$  is the temperature of the water in degrees Celsius (°C).

The maximum density  $\rho_{mv}$  of the bituminous mixtures determined by the volumetric procedure is calculated as follows:

$$\rho_{mv} = \frac{(m_2 - m_1)}{10^6 x V_p - \frac{m_3 - m_2}{\rho_w}}$$

where,

$\rho_{mv}$  is the maximum density of the bituminous mixture, as determined by the volumetric procedure, in megagrams per cubic metre (Mg/m<sup>3</sup>) to the nearest 0,001 Mg/m<sup>3</sup>.

$m_1$  is the mass of the pycnometer plus head piece, in grams (g).

$m_2$  is the mass of the pycnometer plus head piece, and test sample, in grams (g).

$m_3$  is the mass of the pycnometer plus head piece, test sample and water, in grams (g).

$V_p$  is the volume of the pycnometer, when filled up to the top, in cubic metres (m<sup>3</sup>).

$\rho_w$  is the density of the water at test temperature, in megagrams per cubic metre (Mg/m<sup>3</sup>) to the nearest 0,000 1 Mg/m<sup>3</sup>.

The same calculation is valid for the aggregate density. The results are presented in the table below:

*Table 5 Theoretical maximum density of the two mixtures*

Theoretical Maximum Density (TMD)		
Test sample	Binder [kg/m <sup>3</sup> ]	Base [kg/m <sup>3</sup> ]
1	2544	2754
2	2575	2745
3	2530	2739
4	2531	2739
<b>Average</b>	<b>2545</b>	<b>2744.25</b>
<b>Std Deviation</b>	<b>18.18</b>	<b>6.14</b>
<b>C.V</b>	<b>0.71</b>	<b>0.22</b>

### 3.2.3 Aggregate size distribution

The particle size distribution of an aggregate is one of the most important aggregate properties in estimation, it regulates the general behaviour of the pavement. Gradation in hot mixed asphalt assists in identifying the pavement qualities that have the most influence, including stiffness, stability, durability, permeability, workability, fatigue resistance, and friction resistance.

The gradation in Portland cement concrete aids in estimating strength, shrinkage, cement and water needs, workability, durability, and porosity. Particle size distribution is a significant consideration in the mix design because of these essential relationships. Consequently, the boundaries set out in the specification must always be observed.

#### Procedure

The estimation of the particle size distribution was carried according to the BS EN 933-1-2012 [78], using washing and dry sieving.

The size of the test portion for the test was estimated as a function of the aggregate size according to the following table:

*Table 6 Minimum size of test portion for aggregate gradation*

Aggregate size D (maximum) mm	mass of aggregates kg	volume of lightweight aggregates (litres)
90	80	-
32	10	2,1
16	2,6	1,7
8	0,6	0,8
≤ 4	0,2	0,3

- a. The estimated test portion's weight ( $M_1$ ) was noted.
- b. The sample was then put into a container and cleaned (see Figure 28 ).
- c. The residue that was returned on the 0.063 mm sieve was then dried, and the corresponding weight was noted ( $M_2$ ).
- d. The sample was then put into the sieving column (see Figure 29), which is made up of many sieves that are connected and organized in descending order from top to bottom.
- e. The column was placed in a mechanical vibration for shaking for 10 minutes.
- f. The sieves were then removed one by one, and the weight of each sieve as well as the weight of the empty sieve was recorded.



Figure 28 Sample washing



Figure 29 Mechanical vibrator and Sieves column

The masses of each sieve were determined as a percentage of the total masses ( $M_1$ ), all of the masses had been entered in a data sheet. Calculated was the cumulative percentage of the initial dry mass that passed through each filter down to the 0.063 mm.

The percentage of fines ( $f$ ) passing the 0.063 mm sieve was calculated as follows:

$$f = \frac{(M_1 - M_2) + P}{M_1} \times 100$$

where,

$M_1$  is the dried mass of the test portion, in kilograms.

$M_2$  is the dried mass of the residue retained on the 0.063 mm sieve, in kilograms.

$P$  is the mass of the screened material remaining in the pan, in kilograms.

The results were validated based on the difference between the sum of the masses and  $P$ , obtaining less than 1 % from mass  $M_2$ .

The limiting values for aggregate gradation was taken as follows:

*Table 7 Limiting values of aggregate gradation for the binder and base mixtures*

Sieve size (mm)	Lower limit (% passing)	Upper limit (% passing)	Sieve size (mm)	Lower limit (% passing)	Upper limit (% passing)
32	100	100	31.5	100	100
16	90	100	20	68	88
10	73	85	16	55	78
4	45	56	8	36	60
2	28	38	4	25	48
0.5	16	24	2	18	38
0.25	11	18	0.5	8	21
0.063	4	8	0.25	5	16
			0.063	4	8

*Table 8 Sieve analysis of Binder and Base mixtures*

BINDER MIXTURE		BASE MIXTURE	
Sieve size (mm)	Passing (%)	Sieve Size (Mm)	Passing %
16	100	31.5	100.00
14	98.6	20	86.72
12.5	95.1	16	74.00
10	87.7	8	55.84
8	80.7	4	38.92
6.3	72.8	2	24.57
4	53.4		
2	34.2		
1	23.9		

0.5	16	0.5	11.63
0.25	10.7	0.25	7.49
0.063	6.3	0.063	4.78
Pan	0	Pan	0.00

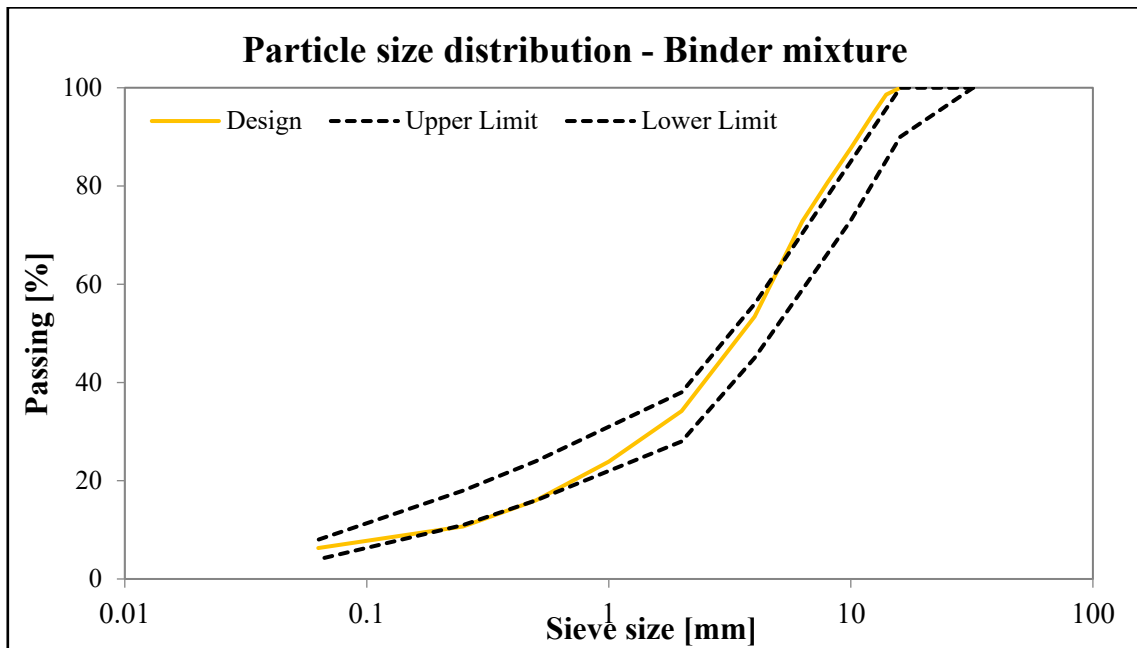


Figure 30 Aggregate gradation – Binder mixture

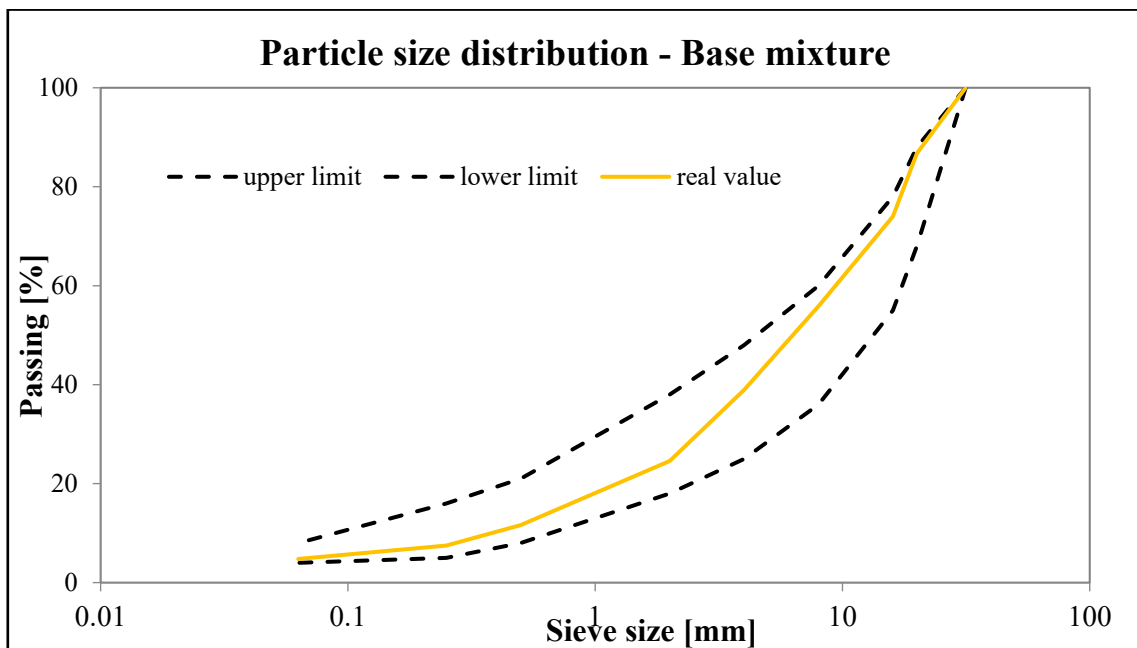


Figure 31 Aggregate gradation – Base mixture

The test is considered acceptable if the gradation must be in the assigned lower and upper limits. Otherwise, the test should be repeated. After making the sieve gradation curve for both the mixtures it is noticed that, curve is in between the limits and the tests of the results are represented for the Binder mixture in Figure 30 and the Base mixture in Figure 31

### 3.3 Compaction methods and specimen preparation

#### 3.3.1 Gyratory compaction

To estimate compatibility and workability for both the mixtures, using a gyratory compactor. The air voids content (or compaction ratio) of a mixture for a specific number of gyrations may be estimated using this approach. Additionally, it is utilized to prepare specimens of a specific height that will later be tested for their mechanical characteristics.

"During the entire course of the test, the bituminous mixture is maintained at a steady temperature within predetermined tolerances inside a cylindrical mould that is restricted by inserts. While the ends of the test piece should ideally remain perpendicular to the axis of the conical surface, compaction is achieved by the simultaneous action of a low static compression and of the shearing action resulting from the motion of the sample's axis, which generates a conical surface of revolution, of apex O, and of  $2\phi$  angle at the apex [81].

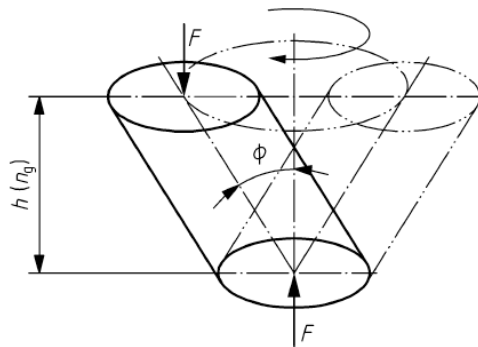


Figure 32 Test piece motion diagram

Procedure:

According to BS EN 12697-31:2019 [81], the gyratory compaction was performed. The mass ( $M$ ) that will be used in the mold is first estimated as follows:

$$M = 10^{-3} \pi \frac{D^2}{4} h_{min} \rho_M$$

where,

$M$  is the mass of a dry mixture to be introduced in the mould, in grams (g).

## CHAPTER 3 MATERIALS AND METHODOLOGY

$D$  is the internal diameter of the mould, in millimetres (mm).

$h_{min}$  is the minimum height of compacted specimen, corresponding to zero percent of voids, in millimetres (mm).

$\rho_M$  is the maximum density of the mixture, in Megagrams per cubic metre (Mg/m<sup>3</sup>).

$h_{min}$  is a constant value and must be taken as 0.66D and 1.05D.

**Note:** Since we employed a 100 mm diameter mould, the value of  $h_{min}$  should be taken between 66 and 105 mm, for mixtures BINDER and BASE, it was taken to be 70 mm and 75 mm, respectively.

- ❖ For Binder the mass of the dry mixture to be put in the mould equals 1375 gm.
- ❖ For Base mixture the mass of the dry mixture to be put in the mould equals 1499 gm.

D (mm)	H <sub>min</sub> (mm)	H <sub>min</sub> (mm)	TMD (Kg/m <sup>3</sup> )	M, MIN (g)	M, MAX (g)
100	66	105	2501	1296.42	2062.49
100	66	105	2545	1319.23	2098.78

Table 9 Gyrotory sample's mass inside the mold

- The inserts and moulds were placed in the oven to condition for at least two hours to reach the reference compaction temperature of  $\pm 5.0^\circ\text{C}$ , which is calculated as a function of bitumen grade as shown in the following table:

Paving grade of bitumen	Reference compaction temperature for: °C		Paving grade of bitumen	Reference compaction temperature for mixtures of types other than mastic asphalt °C
	Mixtures of types other than mastic asphalt	Mastic asphalt mixtures		
10/20 to 20/30	180	230	250/330	130
30/45	175	220	330/430	125
35/50	165	210	500/650	120
40/60	155	200	650/900	115
50/70	150	-	V12000	115
70/100	145	-	V6000	110
100/150	140	-	V3000	100
160/220	135	-	V1500	90

Table 10 Reference compaction temperature

- The bituminous mixture was simultaneously heated to the reference compaction temperature while avoiding overheating to prevent the loose mixture from aging further.

- When the mould, inserts, and mixture have reached the desired temperature, the mould with the bottom insert is put on a balance and the inside surface is lubricated. Following that, a funnel was used to pour the predetermined mass within the mold. The mixture's top layer was leveled, and the top insert was then positioned. Before conducting the test, the mould containing the mixture was returned to the oven for at least 15 minutes to ensure a uniform temperature.
- The test was then conducted once the mould was installed inside the gyratory compactor. Following the completion of the test, the compacted sample was removed from the mould and allowed to cool



Figure 33 Typical gyratory molds and samples

Following that, measurements of thickness were made at four locations (each 90 °) along the diameter as follows:

For Binder Mixture:

Table 11 Thickness measurements of gyratory samples - Binder

Sample 1, 100 GY				Sample 3, 180 GY			
Thickness measured at 90 ° (mm)				Thickness measured at 90 ° (mm)			
73.75	73.75	73.75	73.65	72.45	72.45	72.65	72.75
Average Thickness(mm)			73.7	Average Thickness (mm)			72.5
Sample 2, 100 GY				Sample 4, 180 GY			
Thickness measured at 90 ° (mm)				Thickness measured at 90 ° (mm)			
73.95	74.1	74.1	74.1	72.9	72.75	72.75	72.8
Average Thickness (mm)			74.0	Average Thickness (mm)			72.8

## CHAPTER 3 MATERIALS AND METHODOLOGY

The compatibility and workability were estimated from the compaction curve as we can see in the following graphs:

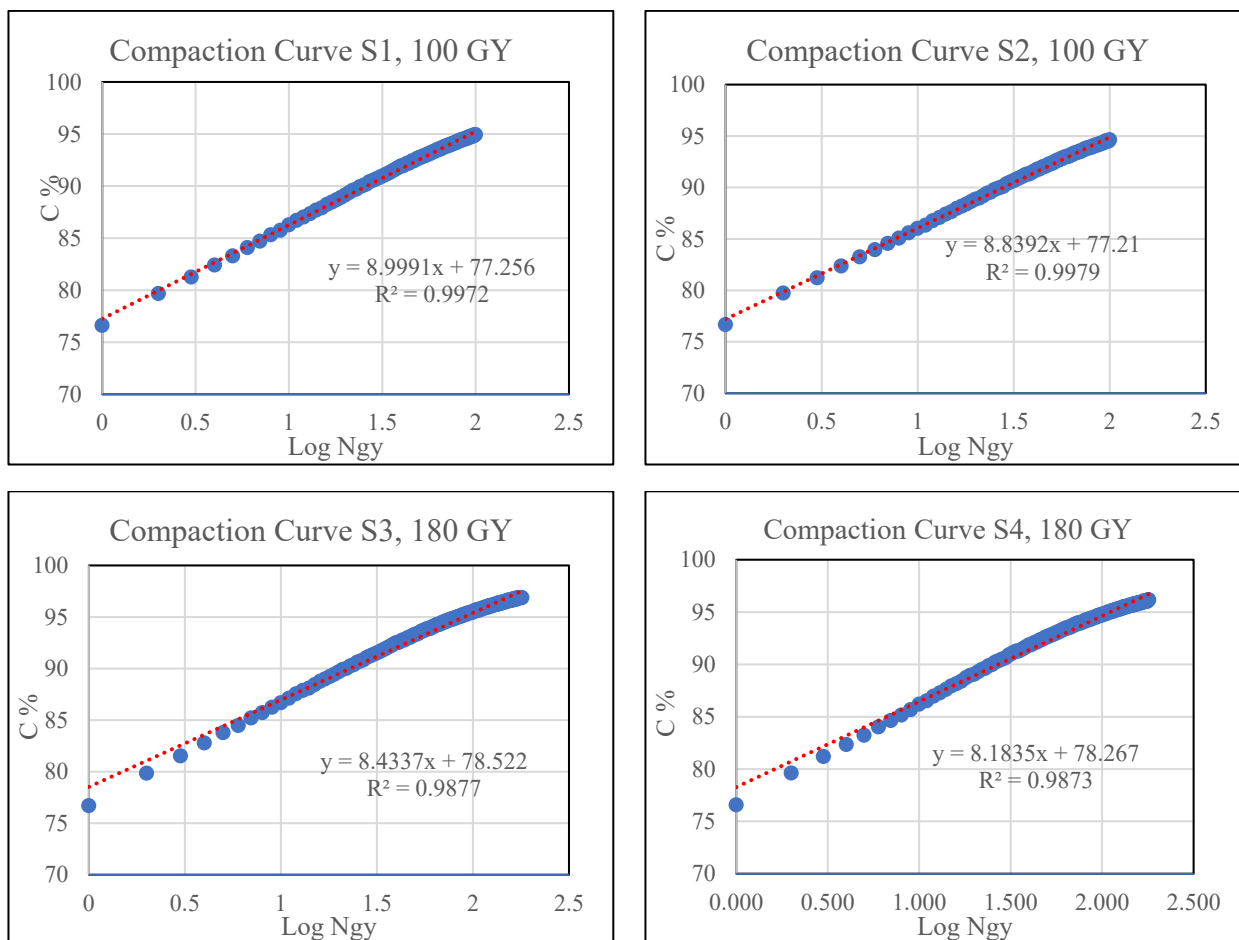


Figure 34 Compaction curve of all gyratory samples - Binder

Below mentioned tables are the results of the base mixture:

Table 12 Thickness measurements of gyratory samples - Base

Sample 1, 100 GY			
Thickness measured at 90 ° (mm)			
79.6	79.7	79.6	79.7
Average Thickness (mm)			<b>79.65</b>

Sample 3, 180 GY			
Thickness measured at 90 ° (mm)			
79.7	79.2	79.45	79.4
Average Thickness (mm)			<b>79.4375</b>

Sample 2, 100 GY			
Thickness measured at 90 ° (mm)			
79.9	79.9	80.05	79.9
Average Thickness (mm)			<b>79.9375</b>

Sample 4, 180 GY			
Thickness measured at 90 ° (mm)			
79	78.8	79.2	79.4
Average Thickness (mm)			<b>79.1</b>

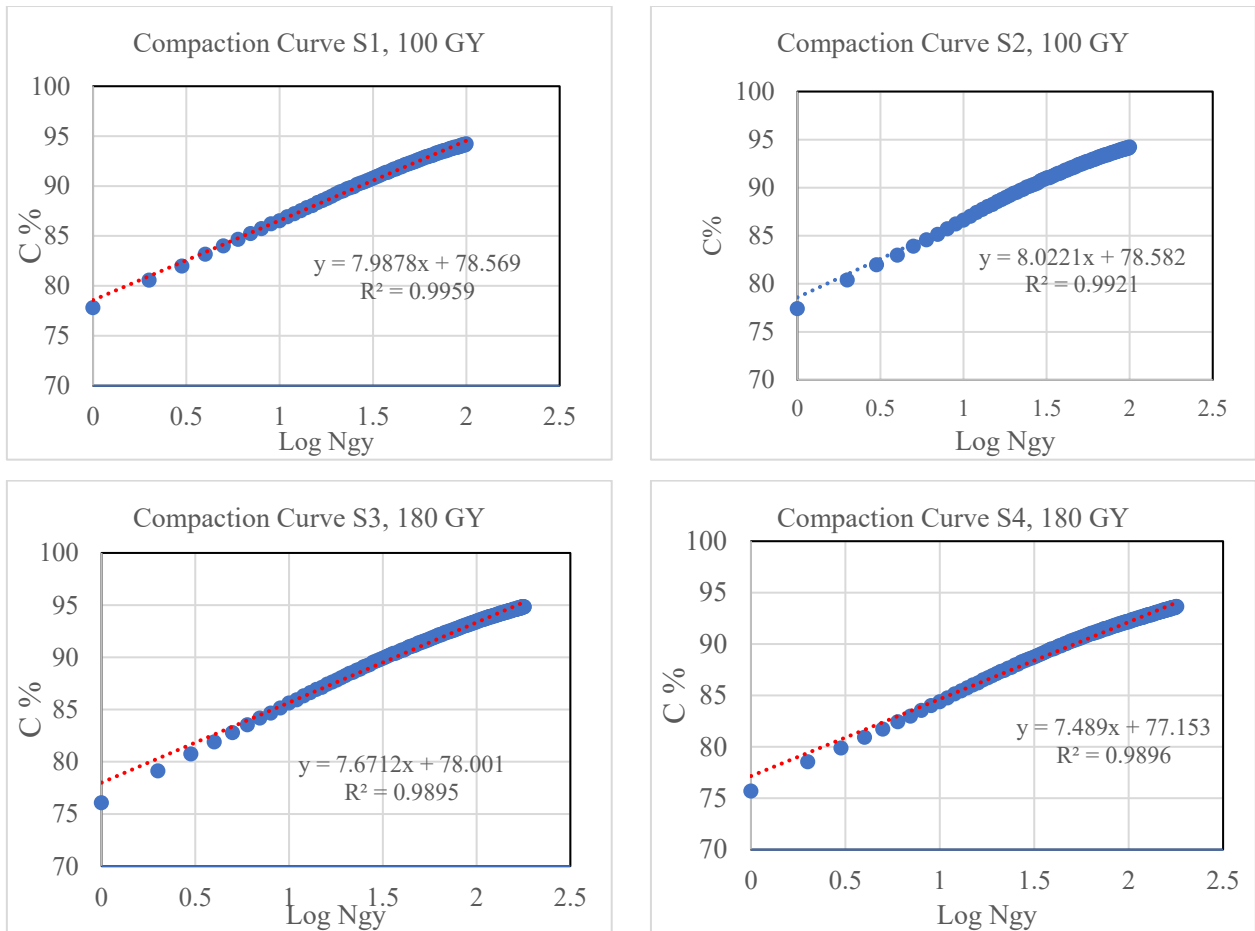


Figure 35 Compaction curve of gyratory samples - Base

The results are summarized in the following table:

Table 13 Samples workability and Compatibility of binder and Base Mixtures

Sample	Workability		Compaction	
	Binder	Base	Binder	base
1	9.00	7.99	77.3	78.6
2	8.84	8.02	77.2	78.6
3	8.43	7.67	77.5	77.2
4	8.18	7.49	77.3	76.3

### 3.3.2 Roller compaction

To obtain the slabs, which are used them to made into beams for testing in the four-point bending test equipment, roller compactor is used.

In the laboratory, the mould which is in the size of L=500 mm, B =180 mm, H= 50 mm, which is made in accordance with BS EN 12697-33-2019 [82].

The roller compaction is performed using a wheel fitted with pneumatic tire.

#### Procedure:

- The metal mould, frame, and base were first pre-heated for at least two hours to the reference compaction temperature. Once they achieved the test temperature, they were removed from the oven and put back into the compaction equipment right away.
- Silicon was applied to the metallic components covering the base and the inside surface of the mold.
- The mass of the bituminous mixture ( $M \pm 1\%$  by weight) was then added to the mold, and any segregation was eliminated by spreading the material uniformly with a shovel.

The mass of bituminous mixture to be introduced in the mold is calculated as:

$$M = 10^{-6} \times L \times l \times e \times \rho_m \times \left( \frac{100 - v}{100} \right)$$

where,

$M$  is the mass of slab, in kilograms (Kg).

$L$  is the interior length of the mold, in (mm).

$l$  is the interior width of the mold, in (mm).

$e$  is the final thickness of slab, in (mm).

$\rho_m$  is the theoretical maximum density of the mixture in ( $\text{Mg}/\text{m}^3$ ).

$v$  is the air voids content in slab, in percentage (%).

Table 14 Wheel compactor to be compacted mass - Binder

Mixture type	Target voids	Mould size			Volume [cm <sup>3</sup> ]	TMD [g/cm <sup>3</sup> ]	Mass [g]	MV, geo [g/cm <sup>3</sup> ]
		w [cm]	L [cm]	H [cm]				
<b>Binder</b>	7.5	18.0	50.0	5.0	4500.0	2.501	<b>10410.4</b>	2.313
<b>Base</b>	7.5	18.0	50.0	5.0	4500.0	2.545	<b>10593.6</b>	2.313

CHAPTER 3 MATERIALS AND METHODOLOGY

In order to achieve the target air voids (taken as 7.5 %), a heavy compaction was used following the sweep plan indicated in table (31), which gives the closest result above the desired air voids content, some additional passes are also applied to ensure that the slab is made even and to prevent uneven compaction and surface deformations.

In order to level the surface further, the passes in the blocked axis at the conclusion of the sweep plan might be replaced by 4 to 6 passes using a smooth steel roller with no transverse displacement.

Table 15 Sweep plan, specimens 500 mm × 180 mm × e, heavy compaction

Number of passes					Tyre pressure MPa	Load F kN	Start	Extent of lateral translation a mm	Axis mode
Position of the wheel									
Front	Centre		Rear						
Cumulative a		Cumulative <sup>a</sup>		Cumulative <sup>a</sup>					
1				1	0,1	1	right	75	blocked
		1							
1				1					
		1							
2	2				0,6	5	right	45	freed
				2					
		1	1						
2	4			2					
		1	2						
4	8								
				4					
		2	4						
8	16								
				8					
		4	8						
8	24								
				8					
		4	12						
4	28								
				4					
		2	14						
2	30								
				2					
		1	15						
2	32								
				2					
		1	16						
1					0,6	5		45	blocked
				1					
		1							
1									
				1					
		1							

<sup>a</sup> The cumulated number of passes is given only for the freed axis mode.



Figure 36 The roller compactor without the auxiliary elements

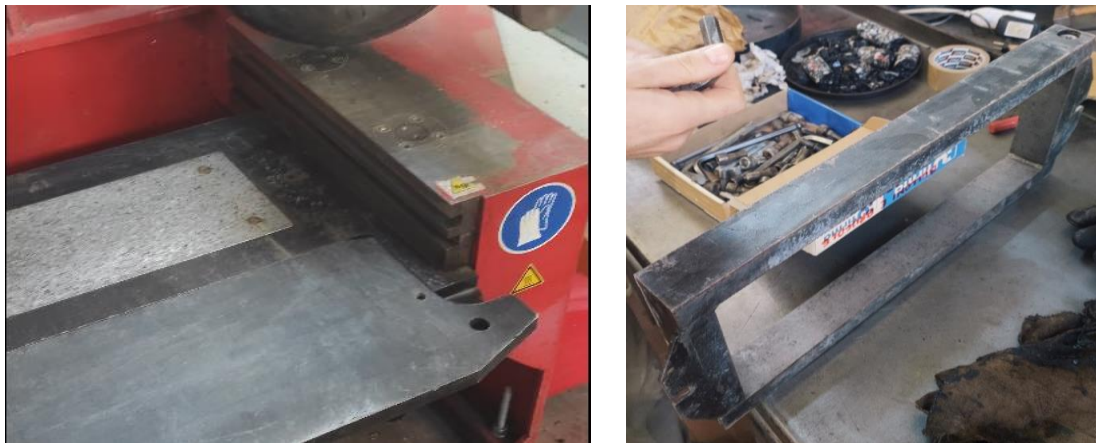


Figure 37 The wheel compactor auxiliary elements

Following the completion of the compaction process, the slab was removed from the roller compactor and allowed to cool before the thickness was measured along each of the slabs four sides, as shown in the example below:



Figure 38 finishing of the slab compaction and removing from the mould



Figure 39 Completed slab

Table 16 Compacted slab thickness

<b>1st wheel compaction</b>						
<b>Long Side 1 (mm)</b>						
50.5	50.6	50.3	49.9	49.2	49.9	50.5
<b>Long Side 2 (mm)</b>						
50.9	51	49.7	49.8	49.4	49.3	50.3
<b>Short Side 2 (mm)</b>						
49.7	49.8	50.3				
<b>Short Side 2 (mm)</b>						
49.7	50.8	50.5				

### 3.4 Beams preparation

#### 3.4.1 Sawing

The prismatic specimens which are attained by sawing from slabs that made in laboratory from the wheel compaction equipment or from the road layers. From each slab is marked and then cut into three beams of size 410mm × 50mm × 50mm.

Those beams are verified later in terms of density and voids ratio. The longitudinal axis of the beam shall be parallel with the axis of compaction.

The beams are checked visually for concerning non-homogeneity, compaction, void content, or the presence of large aggregate particles. Beams with irregularities with respect to required measurements and visually irregular are excluded.

Sawing must be done carefully and precisely, by marking the exact lengths and breadths.



*Figure 40 Slab sawing*

### 3.4.2 Specimen Dimensions

According to the standard [83], the specimen must have the nominal dimensions and tolerances listed below and be in the form of a prismatic shape:

- ❖ Total length must not surpass effective length by more than 10 %. (The effective length of this testing device is 380.5 mm).
- ❖ The difference between maximum and minimum measured value of the width and of the height is not greater than 1.0 mm; The difference between minimum and maximum measured value of the length shall not be greater than 2.0 mm. (beams fail to satisfy those limits were discarded). The angle between adjacent longitudinal surfaces should not deviate from a right angle by more than 1°.
- ❖ The effective length is not less than six times whatever the highest value is for the width or the height. The width and the height are always more than three times the maximum grain size in the tested material.
- ❖ The full length is determined four times with a ruler with an accuracy of 1.0 mm in the centre of the top and the bottom surfaces.
- ❖ The height and the width are measured with vernier callipers with an accuracy of 0.1 mm at the places where the clamps are to be installed ( $x = 0, x = A, x = L - A, x = L$ ).
- ❖ The length of the test specimen is calculated as the arithmetic mean of the length measurements. The width and the height of the specimen are calculated similarly. Beams that are not following the specimen specification are not tested.
- ❖ The thicknesses of the beams are measured at four points to check the uniformity throughout the length of the beam.



Figure 41 Four point bending beams



Figure 42 4PB measurement points

Table 17 Sample Beam measurements

Beam 11 C						
	B (mm)			Min	Max	Diff
<b>50</b>	49.6	49.5	49.3	49.3	50	0.70
	H (mm)			Min	Max	Diff
<b>50.8</b>	48.8	48.3	50.7	48.3	50.8	2.50
	L (mm)			Min	Max	Diff
<b>408.5</b>	408.5			408.5	408.5	0

### 3.5 Evaluation of the Air void content

#### 3.5.1 Bulk density calculation

Gyratory samples, Roller compacted slabs, and 4PB beams:

Since it is utilized to determine the actual air void in the mixture, the bulk density, which refers to the density of a compacted hot mixed asphalt, is one of the most essential parameters of a compacted mixture.

Bulk specific gravity can be measured in a number of ways, each of which uses a different method to estimate specimen volume. In this instance, we employed the saturated surface dry approach (SSD), the most popular technique for determining the specimen volume by deducting the mass of the specimen in water from the mass of a saturated surface dry (SSD)

## CHAPTER 3 MATERIALS AND METHODOLOGY

specimen. When the surface (including air voids attached to the surface) is dry and the internal air voids are filled with water, this state is known as SSD.

The compaction of the specimens was done using two different testing devices:

1. The gyratory shear compactor.
2. The wheel compactor.

And hence two bulk densities were estimated, according to [BS EN 12697-6-2020] [84].

### Procedure:

Using the same procedure for both gyratory compactor samples, the roller compactor samples, and the obtained four-point bending beam samples.

The dry specimen's mass ( $m_1$ ) is first measured, after which the specimen is submerged in water until it is sufficiently saturated for the mass to remain constant.

After the sample had been in the water for roughly an hour, the weight water ( $m_2$ ) was measured, being careful to ensure that there were no air bubbles that stuck to the surface.

The specimen was then taken out of the water bath, its surface was dried using a piece of chamois (a cloth made of leather), and the matching weight ( $m_3$ ), was noted right away.

Finally, the temperature of the water was recorded.

### Calculations:

The bulk density is calculated as follows:

$$\rho_{SSD} = \frac{m_1}{m_3 - m_2} \times \rho_w$$

where,

$\rho_{SSD}$  = bulk density (SSD), in megagram per cubic metre (Mg/m<sup>3</sup>).

$m_1$  = mass of the dry specimen, in gram (g).

$m_2$  = mass of the specimen in water, in gram (g).

$m_3$  = mass of the saturated surface-dried specimen, in gram (g).

$\rho_w$  = density of the water at test temperature, in megagram per cubic metre (Mg/m<sup>3</sup>).

$$V_a = 100 \left[ \frac{G_{mm} - G_{mb}}{G_{mm}} \right]$$

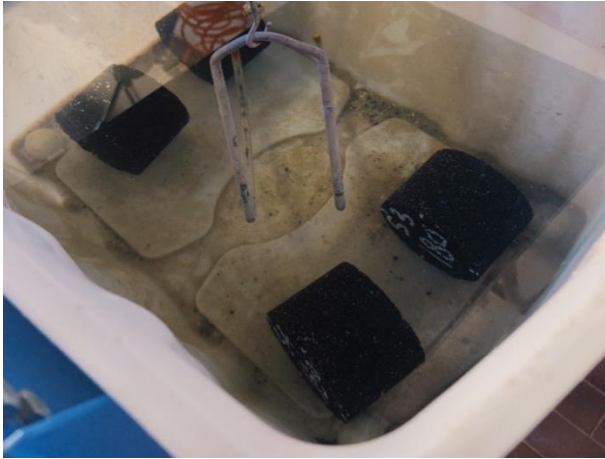


Figure 43 Gyratory samples inside the water bath and temperature measurement

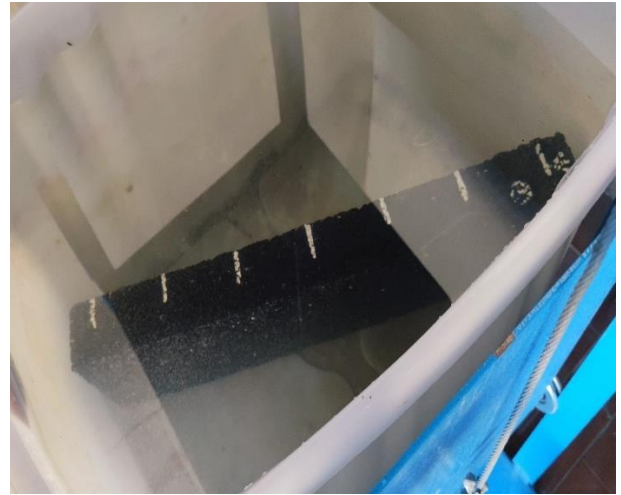


Figure 44 The slab inside the water bath



Figure 45 The 4PB beams inside the water bath



Figure 46 The water bath and the balance

Below mentioned tables are some results, for both the Gyratory compactor samples, Roller compaction samples and Four point bending beam samples:

Table 18 Theoretical and Actual air voids calculation of the Gyratory samples

Theoretical and Actual Air voids (%)								
ID	Volume (V)	Mass (M)	$\rho_{geo}$	TMD	V% theoretical	$\rho_w$	$\rho_{SSD}$	V% real
[-]	[m <sup>3</sup> ]	[g]	[kg/m <sup>3</sup> ]	[kg/m <sup>3</sup> ]	[%]	[kg/m <sup>3</sup> ]	[kg/m <sup>3</sup> ]	[%]
1	0.000626	1500.3	2398.3	2545.0	5.8	998.4	2442	4.0
2	0.000628	1498.4	2386.6	2545.0	6.2	998.4	2436	4.3
3	0.000624	1498.0	2401.0	2545.0	5.7	998.4	2448	3.8
4	0.000621	1496.8	2409.3	2545.0	5.3	998.4	2445	3.9
<b>Average</b>					5.7			4.0
<b>S D</b>					0.3			0.2

Table 19 Typical theoretical and actual air voids calculation of the slabs

Mould size			Volume	TMD	Mass	$\rho_{\text{geo,real}}$	V% geo
w [cm]	L [cm]	H [cm]	[cm <sup>3</sup> ]	[g/cm <sup>3</sup> ]	[g]	[g/cm <sup>3</sup> ]	(-)
18.0	50.0	5.01	4509.5	2.545	10540.2	2.337	8.2

M <sub>air</sub>	M <sub>water</sub>	M <sub>SSD</sub>	T	$\rho_w$	$\rho_{\text{SSD}}$	TMD	V% real
[g]	[g]	[g]	[°C]	[kg/m <sup>3</sup> ]	[kg/m <sup>3</sup> ]	[kg/m <sup>3</sup> ]	[%]
10540.2	6248.9	10626.8	20.9	998.1	2403	2545	5.58

Table 20 typical calculation of Theoretical and Actual air voids in 4PB beams

ID	$\rho_{\text{geo}}$	V% geo	$\rho_w$	$\rho_{\text{SSD}}$	V% real
[-]	[kg/m <sup>3</sup> ]	[%]	[kg/m <sup>3</sup> ]	[kg/m <sup>3</sup> ]	[%]
9 L	2320.8	8.8	998.0	2412	5.2
10 C	2361.5	7.2	998.0	2427	4.6
11 R	2351.2	7.6	998.0	2414	5.1

The remaining tables are presented in the Appendix.

### 3.6 Fatigue testing

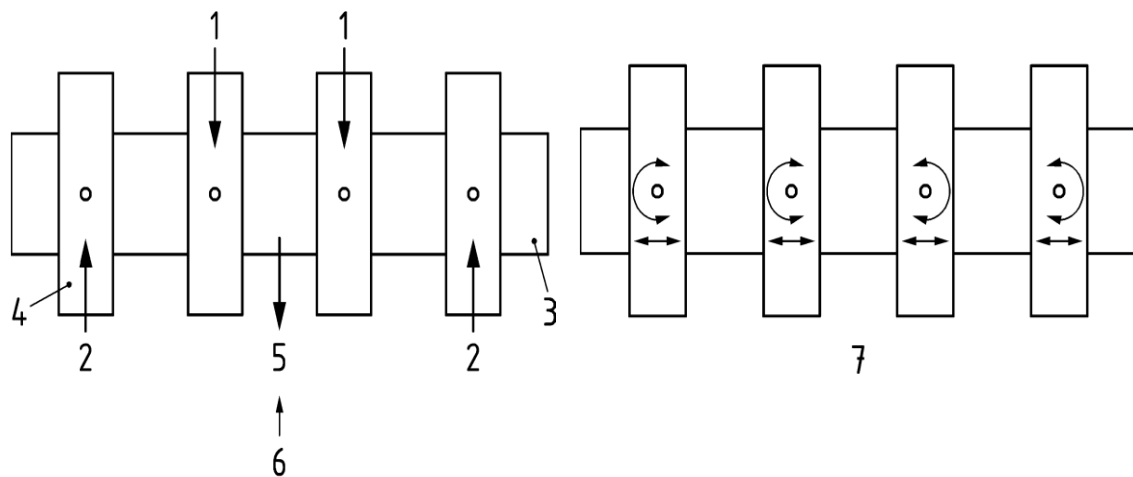
The asphalt fatigue tests were performed using the 4-point bending (4PB) setup. Two key parameters were defined for all two mixtures, i.e., their stiffness modulus and fatigue resistance. Tests were performed using the 4PB testing setup, as described in EN 12697-26:2018 [24]. To define the  $|E^*|$  modulus, cyclic tests were performed for both base and binder mixtures at 20 °C and 10 °C respectively, and their frequency was set for 10 Hz. The fatigue tests were performed under a strain-control mode, between 140, 200, 300  $\mu\text{m/m}$ . For the fatigue characterisation of each mixture, at least 6 replicates were tested at a minimum of 3 strain levels, with the total number of replicates as 18.

Four point bending testing procedure following the European standards is briefly explained in the next section.

### 3.6.1 Four-point bending test on prismatic shaped specimens (4PB-PR)

In this section, four point bending testing procedure will be explained clearly. Every step from specimen preparation to the testing of the beams are elaborated.

Two inner and two outer clamps must be evenly spaced from the prismatic sample's centre. At the middle third, constant and equal loads must be applied. It is required to record every applied force, deflection, and phase lag. According to the selected failure situation, the test sample's fatigue life must be estimated, as will be covered in the following chapters.



Key

- 1- Applied load.
- 2- Reaction.
- 3- Specimen.
- 4- specimen clamp.
- 5- Deflection.
- 6- Return to original position.
- 7- Free translation and rotation.

*Figure 47 Basic principles of 4-point bending*

#### Test equipment

Equipment that must be able to clamp two inner clamps onto a specimen and apply a sinusoidal load using a suitable mechanism (see Figure 47). The load's frequency,  $f$ , must be in the range between 0.1 and 60 Hz with a 0.1 Hz precision. Metal that is resistant to corrosion must be used to create the equipment. The testing system must be equipped with a mechanism to regulate the specimen's loading mode in a way that satisfies the test's execution requirements. The load cell must meet the requirements for transducers of accuracy class 0,2 and have a measuring range of at least  $\pm 2000$  N.

## CHAPTER 3 MATERIALS AND METHODOLOGY

The force should be measured halfway between the two inner clamps. The top surface or bottom surface of the specimen between or at one of the two inner clamps is where the displacement measurement must be done.

The displacement transducer has a measuring range of  $\pm 1.0$  mm fulfilling the specification for transducers of accuracy class 0.2 %. The deflection is measured at the centre of the bottom surface. In order to verify the necessary pure bending of the sample, the deflections of the two inner clamps are also be measured.

### Thermostatic chamber

Thermostatic chamber, Figure 49 with an accuracy of  $\pm 1$  °C and the ability to maintain the average air draught at least 10 mm away from the specimens (throughout the duration of the test). Regulation must be accurate to 0.5 °C.

### Clamping system

A tool that can clamp a specimen (beam) in the bending frame to provide freedom of rotation and horizontal translation at all supports. For a reference beam with a known stiffness modulus, the back-calculated stiffness modulus must be within 2% for the modulus and within 0.5° for the phase lag (see **Error! Reference source not found.**). The specimen within the clamps must be able to move horizontally and freely rotate inside the outer and inner clamps. By measuring the deflections at the inner clamp,  $x = A$ , and in the middle of the specimen,  $x = L/2$ , it will be possible to verify the presumed pure bending between the two inner clamps

Distance (A) should be selected in the range  $0,25 < A/L < 0,4$  and if possible close to one third of the effective length L (ASTM configuration). Here, the ratio will be 1,15. If A/L is chosen outside this range.

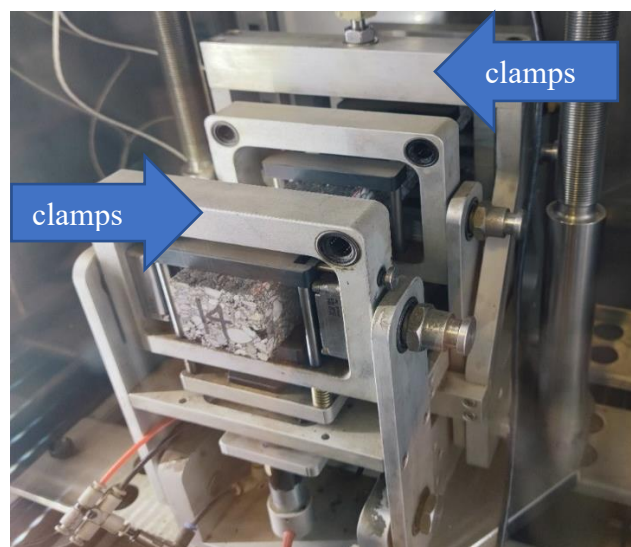


Figure 48 Clamping system



Figure 49 Four point bending machine with thermostatic chamber

### Electronic data registration

Electronic data registration apparatus (Figure 50) where the transducer signals are amplified by low-noise amplifiers, preferably so that a value of 10 V or  $\pm 10$  V corresponds to the full-scale deflection of the relevant transducer's measuring range.

Output outlets are provided for connecting both the data acquisition and processing equipment. A resolution of 1 N for the force and 0.1  $\mu\text{m}$  for the deformation is adopted with an accuracy class for the instruments must be 0.2 %.

The values of the frequency components at the test frequency  $f$  must be able to be recorded for the values of strain, stress, dynamic stiffness modulus, and (material) phase lag to be calculated.



Figure 50 Electronic data registration equipment

### Testing Procedure

The beams, thermostatic chamber and the loading equipment are set to the test temperature prior to the test. The minimum required conditioning time of the beams is shown in Table 21. For the considered temperatures, binder course mixture must be conditioned for at least 2 h and the base mixture must be kept in the thermostatic chamber for 1 h before the test starts.

Table 21 Minimum time required to bring specimens to test temperature

Test temperature °C	Time h
0	2
20	1

The beam must be placed into the load frame using the two outer and two inner clamps. The beam is then loaded sinusoidally at the chosen frequency (10Hz) at the initial imposed strain level. The necessarily force shall apply through the load frame connected to the two inner clamps. The strain-controlled loading mode must be confirmed by a view of the measured force or displacement. The force, displacement and phase lag must be recorded using the data processing equipment in the first 100 cycles (Cycles of the initial stiffness) and regularly thereafter (logarithmic capture).

The initial value of the modulus  $S_{mix}$  is calculated at the hundredth cycle ( $n = 100$ ). To improve the accuracy, also the average value of the parameters between the 98th and 102th load cycle (weighted average) can be used. The fatigue test is carried out until the calculated modulus  $S_{mix}$  dropped to 80% of its initial value (20% residual stiffness).

### Choice of test conditions

For a given temperature and frequency, the test is performed three levels (140  $\mu\text{m/m}$ , 200  $\mu\text{m/m}$ , 300  $\mu\text{m/m}$ ) in the strain-controlled with six replicates per each strain level. The levels for the chosen loading mode are chosen in such a way that the fatigue lives are within the range 10 thousand to 2 million cycles.

### Data processing

Using the obtained data of the force, deflection, and phase lag between these two signals measured at load cycles  $n(i)$ , the relevant results shall be calculated using the formula. The relevant test results shall be tabulated and graphically presented and related to the load cycle number  $n(i)$  at which they are measured. These test results are:

- ❖ Strain amplitude.
- ❖ Stress amplitude.
- ❖ Modulus of the complex modulus (dynamic stiffness modulus).

- ❖ Material phase lag.
- ❖ Dissipated energy per cycle.
- ❖ Cumulated dissipated energy up to cycle  $n(i)$ .

### Calculation and expression of results

Based on the results, representing the length of life  $N_{i,j,k}$  for the chosen failure criteria  $j$  and the set of test conditions  $k$ , the fatigue line is drawn by making a linear regression between the decimal logarithms of  $N_{i,j,k}$  and the decimal logarithms of the initial strain amplitude (strain amplitude at the 100th cycle). The shape of the fatigue line is expressed in the following formula:

$$\log(N_{i,j,k}) = A_0 + A_1 \cdot \log(\varepsilon_i)$$

where,

$i$  is the specimen number.

$j$  represents the chosen failure criteria.

$k$  represents the set of test conditions.

$\varepsilon_i$  is the initial strain amplitude measured at the 100<sup>th</sup> load cycle.

The most important outcome of this test is the strain correspondent with a fatigue life of  $10^6$  cycles, for the chosen failure criteria and set of test conditions since this  $\varepsilon_6$  is considered a crucial input parameter for pavement design.

## **4 CHAPTER 4 RESULTS AND DISCUSSION**

This chapter represents the results of the four-point bending test of the two mixtures. The fatigue data obtained from the two different mixtures were then analysed using five approaches discussed previously, along with the optimum course of action for characterization of fatigue resistance. The first two failure criteria are based on the modulus reduction: 50 % reduction in the initial modulus taken at the 100<sup>th</sup> cycle, and 50 % reduction in the modulus extrapolated from the phase of linear reduction of the modulus (Intermediate phase). The third failure criterion is the peak in the phase angle. The last two criteria are based on energy concepts, the energy ratio; dissipated energy approach.

The visco-elastic related modulus versus the void ratio of the beams and the fatigue related modulus versus the void ratio are two more relationships that will be discussed. There will also be a presentation of the relationship between the positions of the beams obtained from the wheel-compacted slab and the corresponding air spaces.

Comparison of the results of both the mixtures with different testing temperatures. To evaluate the effect of temperature on one mixture, on the other hand to evaluate the effect of mixture type on the fatigue resistance.

## 4.1 Beams Characterization

### 4.1.1 Air voids

In this section, the statistical analysis is carried out from the voids content results of slabs and beams obtained from employing the roller compaction is represented.

These below mentioned analysis is made to estimate the variability:

- a. The relationships of the theoretical and the actual air voids of the beams, and can clearly see the variability between them.
- b. The relationship between the actual air voids and the viscoelastic stiffness ( $E_0$ ).
- c. The relationship between the actual air voids and the fatigue-related stiffness (extrapolated  $E_{00}$ ).
- d. The relationship between the position of the beam in the wheel compacted slab and the air voids are presented.

#### **Binder mixture:**

For the four-point bending beam test at least 6 replicates are tested in 3 different strain levels for a binder mixture type, in total 18 beams are to be made, but due to some defects in the slabs

## CHAPTER 4 RESULTS AND DISCUSSION

and beams or the testing issues 24 beams are taken from the 8 slabs and all the results are tabulated below:

Table 22 Comparison of the theoretical and real air voids in all slabs for Binder mixture

Slab No	Theoretical Air Voids %	Real air voids %
1	7.7	4.5
2	8.7	5.0
3	9	5.9
4	8.5	4.4
5	8.8	5.8
6	8.8	5.6
7	10	7.5
8	9.5	5.
Average	8.87	5.59
Standard Deviation	0.636	0.912
Coeff Of Variation	7.1651	16.3

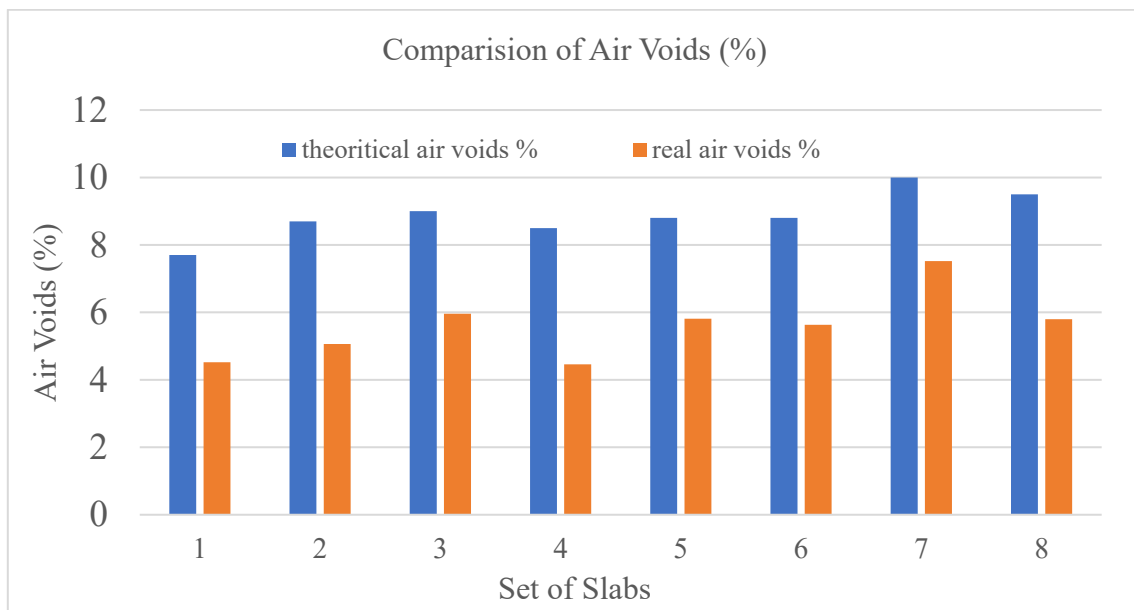


Figure 51 Plot showing the comparison of air voids in all slabs – Binder

From the above Figure 51, it is observed that the real air voids are always lesser than the theoretical air voids and it is reduced by 3.28%.

CHAPTER 4 RESULTS AND DISCUSSION

Table 23 Comparison of the theoretical and real air voids in all beams for Binder mixture

<b>BEAM ID</b>	<b>Theoretical Air Voids %</b>	<b>Real Air Voids %</b>
1 L	6.6	4.0
2 C	5.8	4.0
3 R	7.8	4.3
4 R	7.7	4.0
5 C	7.1	4.2
6 L	7.9	5.3
7 L	10.0	5.9
8 C	8.2	5.2
9 R	8.5	5.3
10 L	8.9	4.3
11 C	7.5	4.1
12 R	7.2	4.3
13 L	9.5	5.6
14 C	8.9	5.3
15 R	8.3	5.6
16 L	9.3	5.8
17 C	8.3	5.6
18 R	9.1	5.8
19 L	11.8	7.3
20 C	9.8	6.5
21 R	12	7.2
22 L	8.7	5.3
23 C	9.6	5.3
24 R	8.7	5
<b>Average</b>	<b>8.6</b>	<b>5.2</b>
<b>Std Deviation</b>	<b>1.419</b>	<b>0.945</b>
<b>Coefficient Of Variation</b>	<b>16.5</b>	<b>18.2</b>

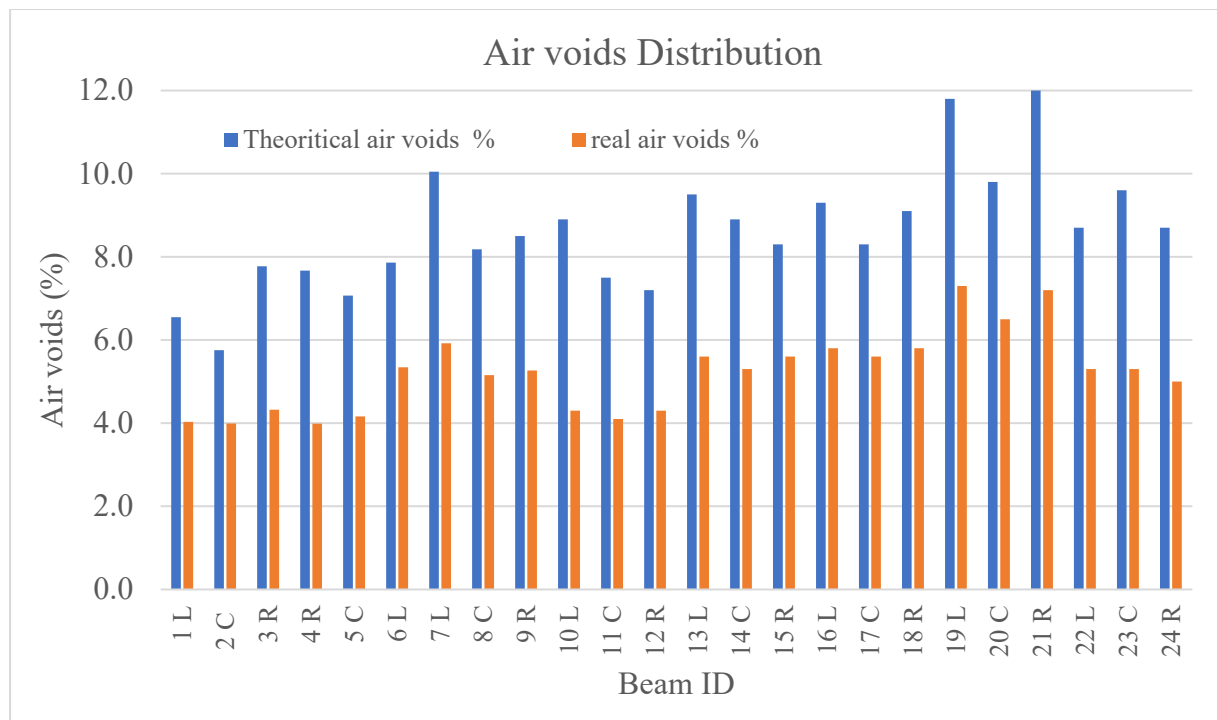


Figure 52 Plot showing the air voids distribution in the beams - Binder

From the above shown tables, theoretical air voids, actual air voids of the slabs and beams are presented with their corresponding average, standard deviation and coefficient of variation which shows the variability of the beams and slabs.

Since the slabs preparation is made each time individually, the compaction process is varied as the air voids of beams and slabs are expected to show some variability which can be seen in the above presented plots. Theoretical air void content is always higher compared to the real air voids.

There is a difference of 3.4% in average value from the theoretical air voids to the real air voids in this binder mixture case. While the theoretical air voids comprise between 5.8 % to 12 %, the corresponding actual air voids were in the range of 4 % to 7 %.

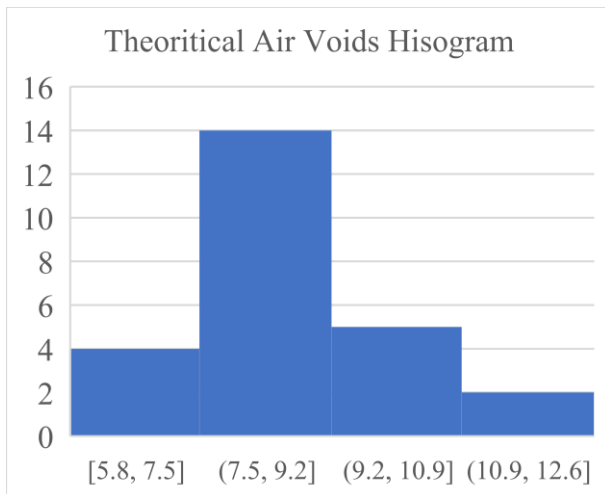


Figure 53 Theoretical air voids histogram - Binder mixture

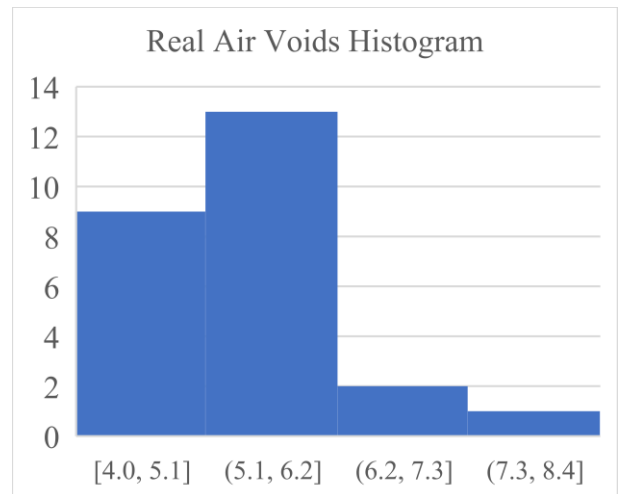


Figure 54 Real air voids histogram - Binder mixture

The above histograms presented shows values of air voids percentage of the beams that are fallen in certain range, for theoretical air voids in the range of 7.5 % to 9.2 % there are 14 beams, for the actual/real air voids 13 beams are in the range of 5.1 % to 6.2 %.

Comparison of the air voids corresponding to their position in the slab:

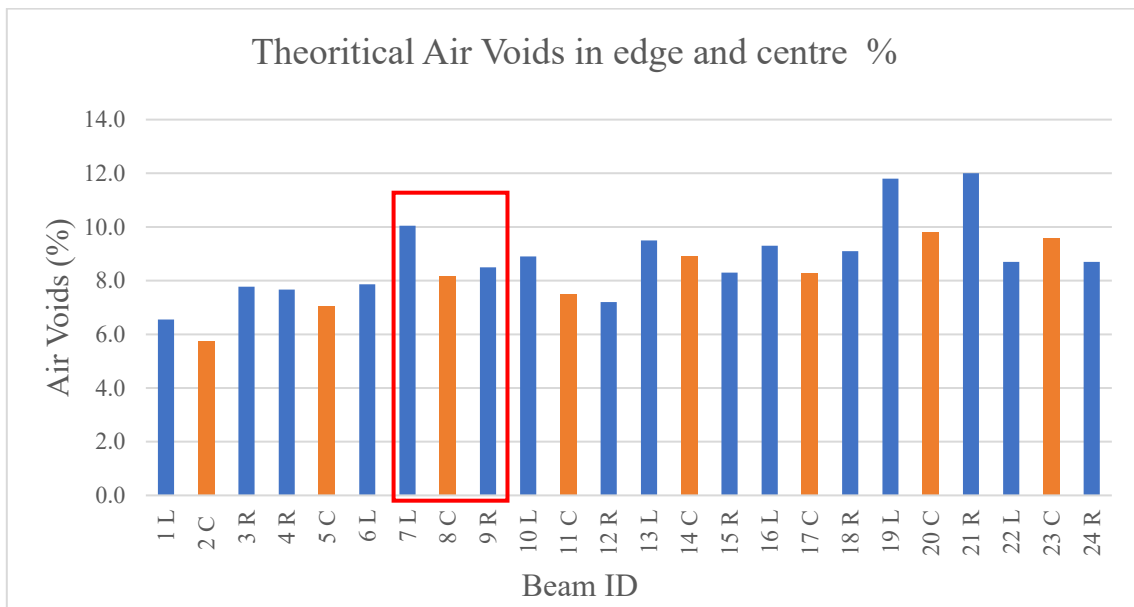


Figure 55 Comparison of theoretical air voids distribution w.r.t position of the beams in slabs - Binder

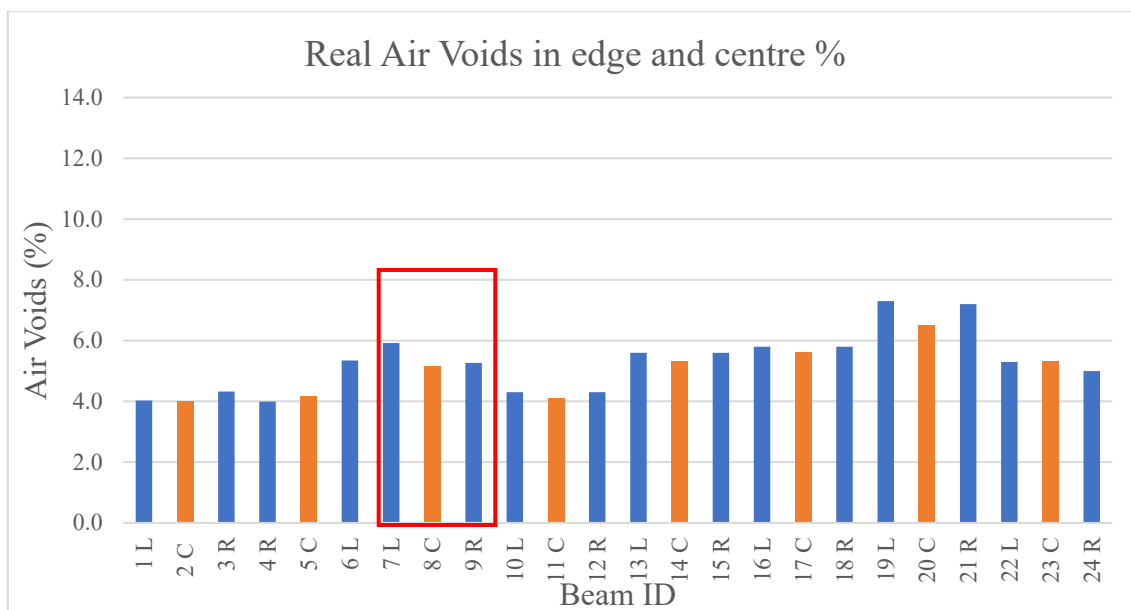


Figure 56 Comparison of real air voids distribution w.r.t position of the beams in slabs - Binder

In the above presented graphs, the highlighted box contains the comparison of the beams obtained from the single slab for both theoretical and actual voids.

The observation from this comparison is that beam which is taken from the central position of the slab is always have the lesser air voids than the either side of the slab, since the compaction in the centre is high when compare to the sides of the slab.

#### Base mixture:

For the base mixture same statistical analysis is repeated, the below mentioned tables and graphs shows the variability of the results. A minimum of 18 beams must be made for the test but due to defects found in the beams, 10 slabs and in total of 29 beams are prepared.

Table 24 Comparison of the theoretical and real air voids in slabs for Base mixture

Slab No	Theoretical Air Voids %	Real Air Voids %
1	10.1	6.48
2	10.8	7.00
3	10	6.78
4	8.2	5.58
5	7.7	5.02
6	8.2	5.59
7	9.3	6.34
8	9.8	6.48
9	8.2	5.65
10	9.1	6.2
<b>Average</b>	9.14	6.11
<b>Std Dev</b>	0.980	0.594
<b>C.V</b>	10.722	9.716

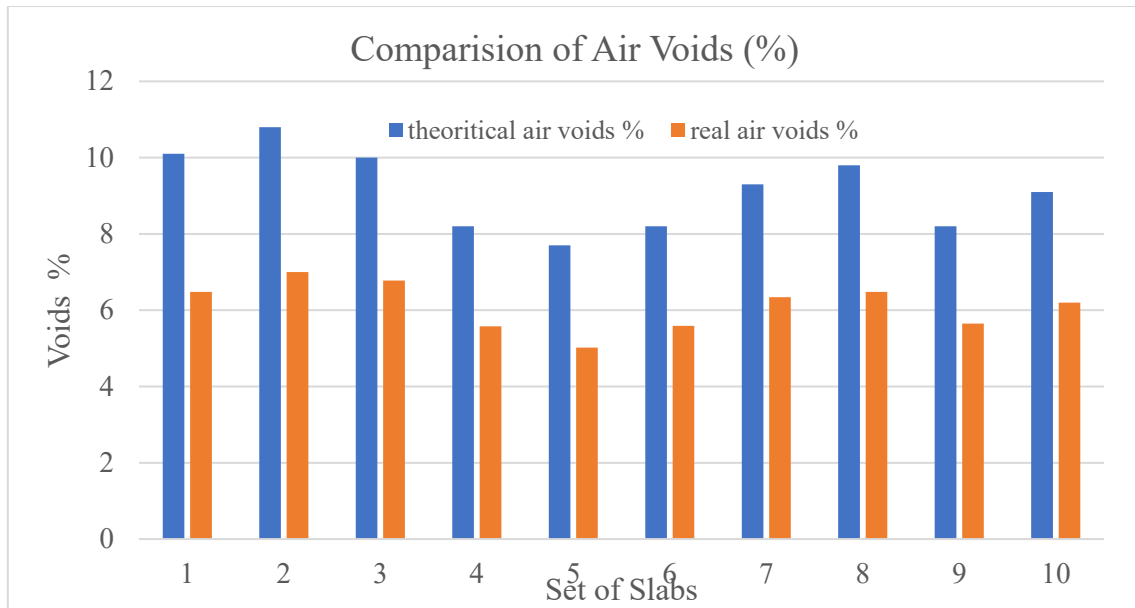


Figure 57 plot showing the comparison of air voids in all slabs - Base

Table 25 Comparison of the theoretical and real air voids in all the beams - Base mixture

Beam ID	Theoretical air voids (%)	Real Air Voids (%)
1 L	9.8	6.4
2C	8.9	5.5
3 R	8.0	5.5
4	10.8	6.9
5	8.5	6.3
6 R	8.7	5.2
7 C	8.8	5.0
8 L	10.3	5.6
9 L	8.8	5.2
10 C	7.2	4.6
11 R	7.6	5.1
12 L	7.4	4.6
13 C	7.8	4.2
14 R	6.4	4.7
15 L	7	5.4
16 C	6.3	5.2
17 R	8.4	5.4
18 L	10.2	5.9
19 C	9.7	5.5
20 R	8.9	6.1
21 L	8.9	5.7
22 C	9.9	5.5
23 R	9.4	5.5
24 L	10.4	5.4

## CHAPTER 4 RESULTS AND DISCUSSION

25 C	7.5	4.8
26 R	6.8	5.3
27 L	9.6	5.2
28 C	8.7	5.4
29 R	8.4	5.9
<b>Average</b>	<b>8.6</b>	<b>5.4</b>
<b>Std Deviation</b>	<b>1.229</b>	<b>0.663</b>
<b>Coeff Of Variation</b>	<b>14.3</b>	<b>12.3</b>

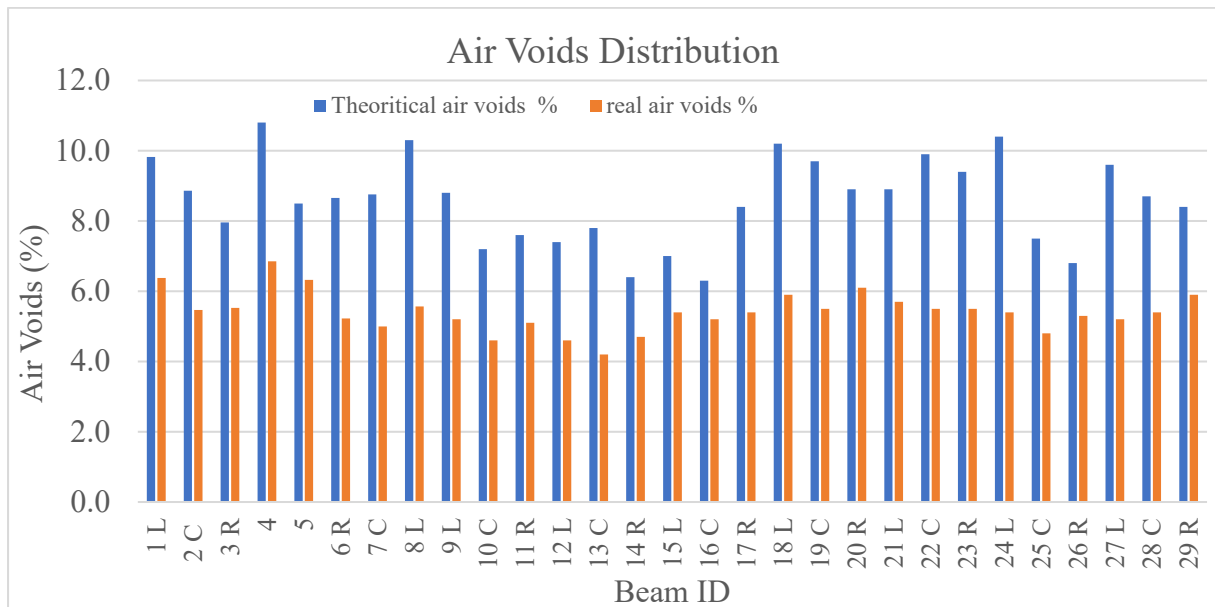


Figure 58 Plot showing the air voids distribution in the beams -Base

There is a difference of 3.2 % in average value from the theoretical air voids to the real air voids in this base mixture case. While the theoretical air voids comprise between 6.8 % to 10.8 %, the corresponding actual air voids were in the range of 5.2 % to 7 %.

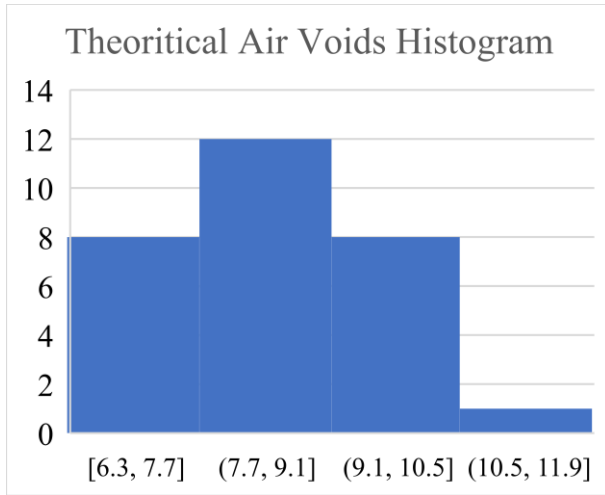


Figure 59 Theoretical air voids histogram - Base mixture

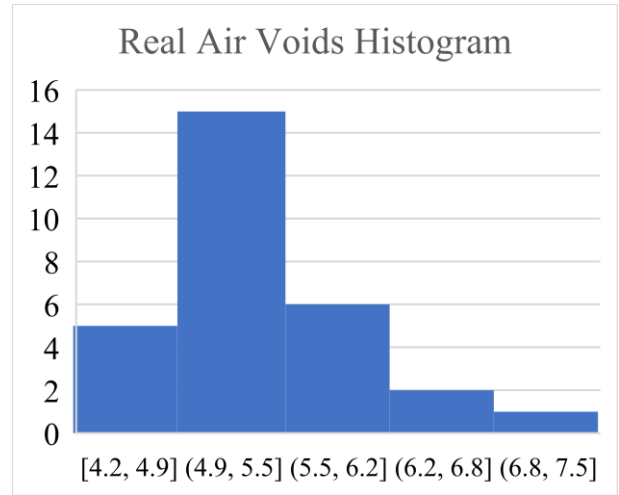


Figure 60 Real air voids histogram - Base mixture

From the above histograms

- For the theoretical air voids, and actual air voids, 20 beams are in the range of 7.7 % – 10.5 %, 21 beams are in the range of 4.9 % – 6.2 % respectively.

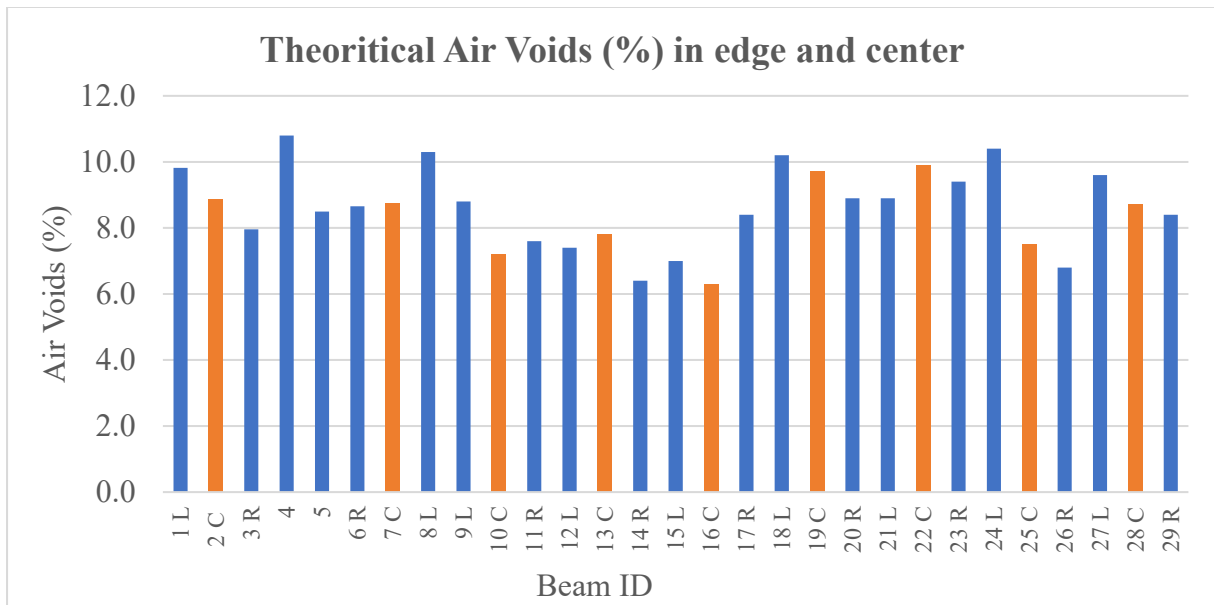


Figure 61 Comparison of theoretical air voids distribution w.r.t position of the beams in slabs - Base

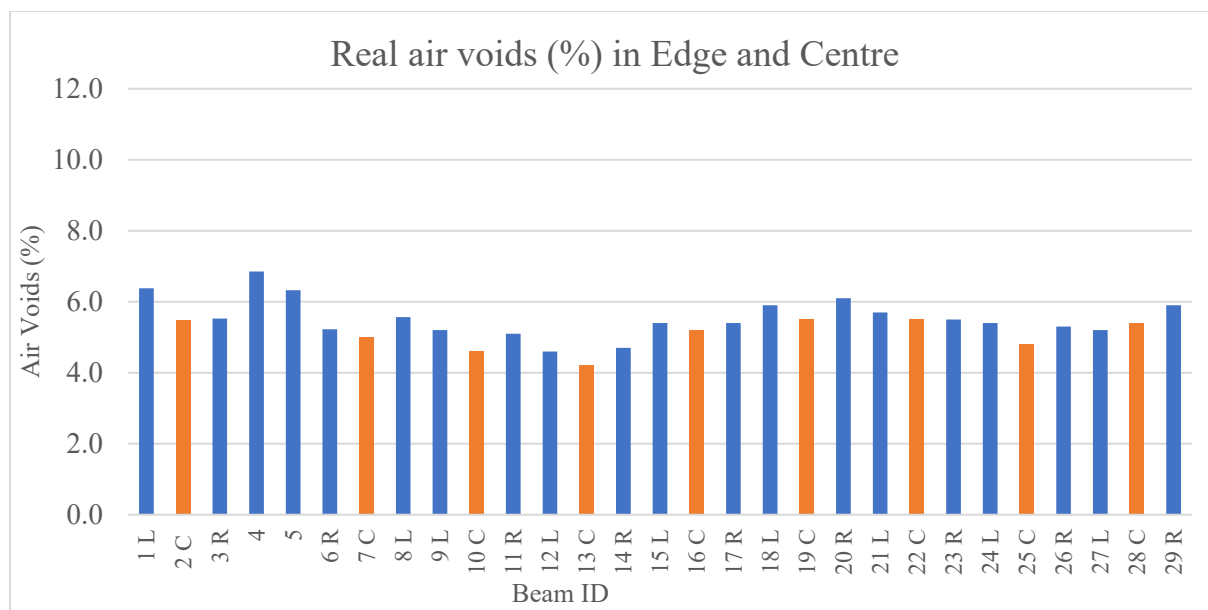


Figure 62 Comparison of theoretical air voids distribution w.r.t position of the beams in slabs - Base

As it is seen in the previous case, the beams in the central part of the slab always shows the lesser air voids when compared to the beams in the either side of the slab. For some slabs the voids of right position beams are lesser and left positioned beams have higher air voids, in some cases it is vice versa

#### 4.1.2 Stiffness

##### Binder mixture

To compare the results of the initial stiffness and the extrapolated stiffness of the beams, tested using their respective strain levels for the binder mixture are presented in the Table 26.

Statistical parameters like average, standard deviation and coefficient of variation are also mentioned in the table to see the variation in results.

Table 26 Tables showing the Initial modulus and Extrapolated modulus of the beams - Binder

200 $\mu\text{m/m}$		
Beam ID	Initial stiffness E0 (MPa)	Extrapolated stiffness E00 (MPa)
1 L	10091	8648
2 C	11113	9405
5 C	11170	8319
9 R	10156	7920
10 L	11322	8713
17 C	8511	7129
Avg.	10393.83	8355.67
STD	972.49	708.30
C.V	9.36	8.48

140 $\mu\text{m/m}$		
Beam ID	Initial stiffness E0 (MPa)	Extrapolated stiffness E00 (MPa)
6 L	10383	8617
7 L	8875	6970
8 C	9138	8642
11 C	11097	8656
12 R	11190	9588
15 R	10052	9201
Avg.	10122.50	8612.33
STD	883.89	816.35
C.V	8.73	9.48
300 $\mu\text{m/m}$		
Beam ID	Initial stiffness E0 (MPa)	Extrapolated stiffness E00 (MPa)
13 L	8066	6575
14 C	9760	7755
16 L	9193	7961
18 R	9585	7924
22 L	8734	7372
24 R	8297	7570
Avg.	8939.17	7526.17
STD	628.78	470.84
C.V	7.03	6.26

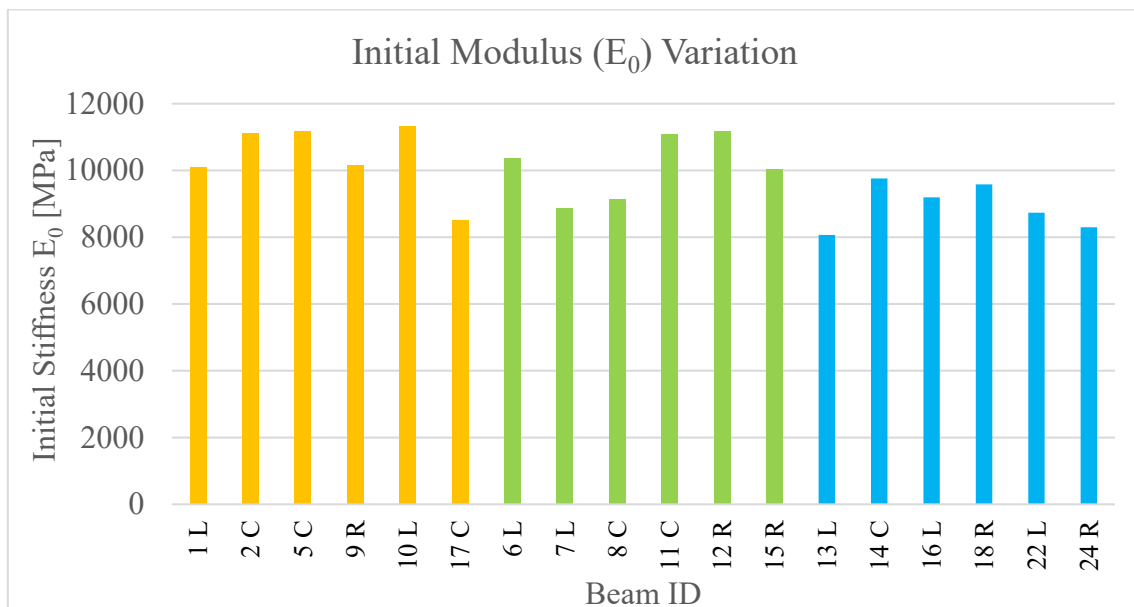


Figure 63 Plot showing the Initial modulus variation - Bind

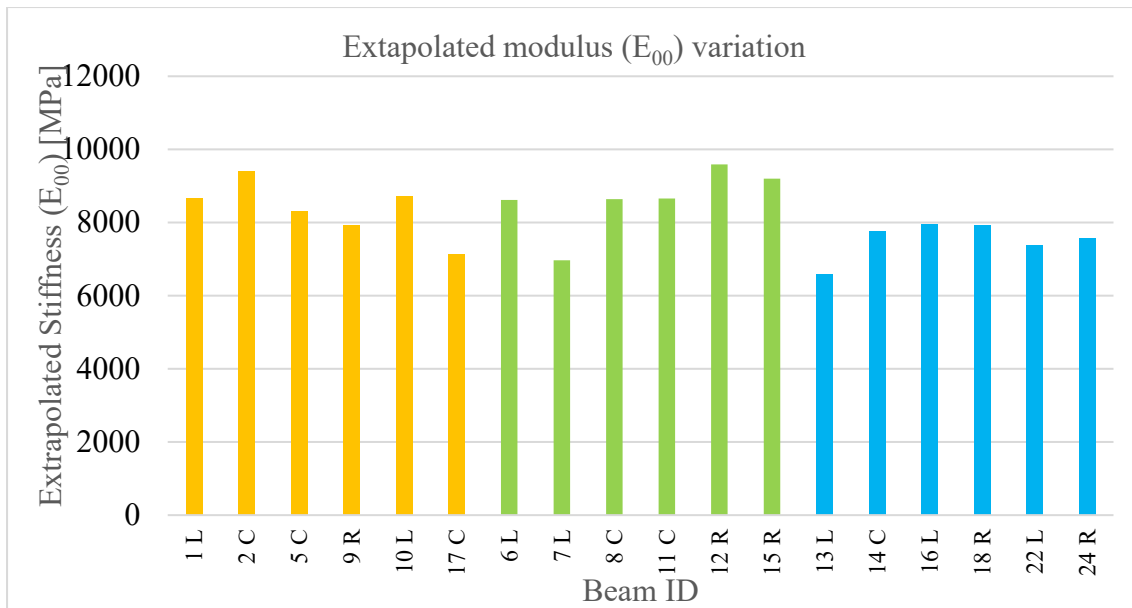


Figure 64 Plot showing the Extrapolated stiffness modulus variation - Binder

These graphs Figure 63 and Figure 64 shows the initial stiffness modulus (taken at 100<sup>th</sup> cycle) and Extrapolated stiffness modulus variation of binder mixture with respect to their corresponding strain level tested at 10 °C respectively.

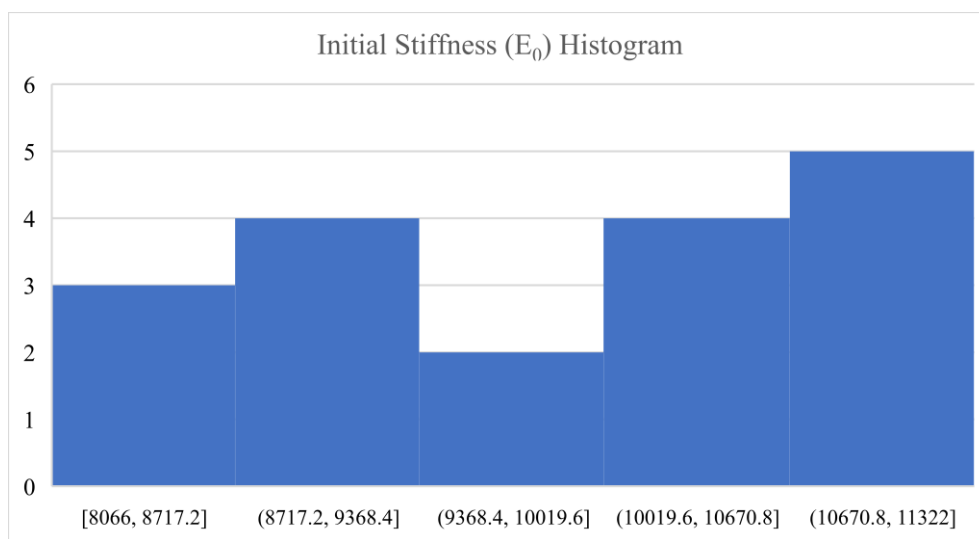


Figure 65 Initial stiffness Histogram - Binder

Based on the results, from the above histogram, there is a better consistency of the results in terms of the standard deviation. Most of the beams shows that the initial stiffness is in range of between 9300 MPa to 11300 MPa.

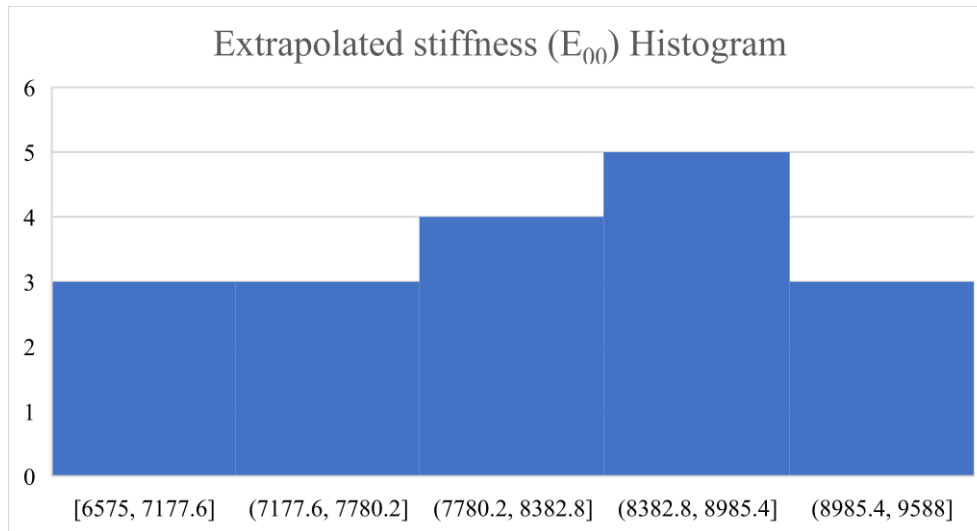


Figure 66 Extrapolated stiffness Histogram - Binder

From the above histogram Figure 66, Extrapolated stiffness modulus is in the range of 6575 MPa – 9588 MPa. There are 12 beams that are tested fall in the range of 7177 MPa – 8985 MPa.

Both the values for the initial stiffness ( $E_0$ ) and the corresponding air voids are tabulated as follows:

Table 27 Beams Initial stiffness and their corresponding air voids - Binder

Strain Level	Beam ID	Initial Stiffness (MPa)	Extrapolated Stiffness (E <sub>00</sub> ) (MPa)	Air Voids %
300 μm/m	13 L	8066	6575	5.6
	14 C	9760	7755	5.3
	16 L	9193	7961	5.8
	18 R	9585	7924	5.8
	22 L	8734	7372	5.3
	24 R	8297	7570	5
200 μm/m	1 L	10091	8648	4
	2 C	11113	9405	4
	5 C	11170	8319	4.2
	9 R	10156	7920	5.3
	10 L	11322	8713	4.3
	17 C	8511	7129	5.6
140 μm/m	6 L	10383	8617	5.3
	7 L	8875	6970	5.9
	8 C	9138	8642	5.2
	11 C	11097	8656	4.1
	12 R	11190	9588	4.3
	15 R	10052	9201	5.6

CHAPTER 4 RESULTS AND DISCUSSION

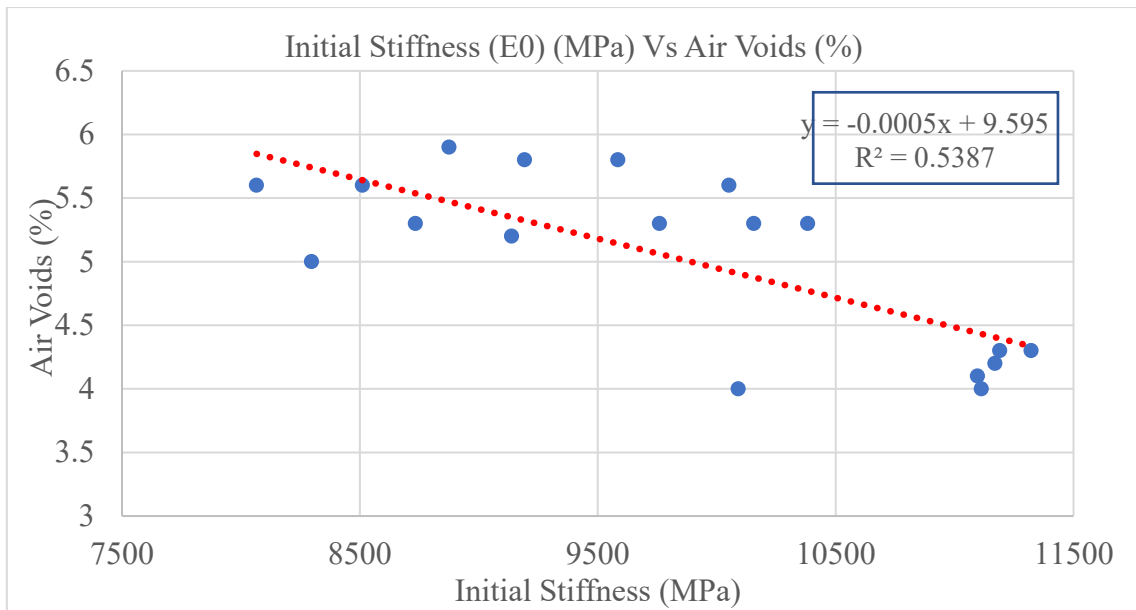


Figure 67 Graph showing the trend in Initial modulus variation w.r.t. air voids of beams - Binder

From the above Figure 67, it is observed that as the air voids increases the initial stiffness modulus decreases.

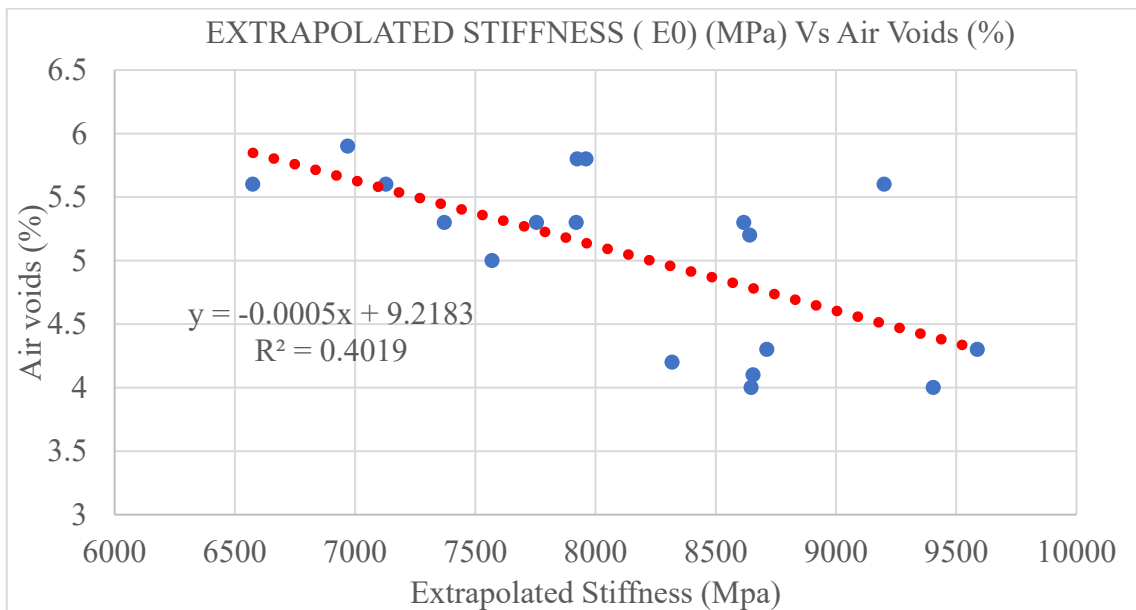


Figure 68 Graph showing the trend in Extrapolated modulus variation w.r.t. air voids of beams – Binder

**Base mixture:**

Below mentioned Table 28 are the initial modulus and extrapolated stiffness modulus results obtained from the testing with their respective strain level are represented separately. Also, the variation of the results are plotted in a graph. Histograms with the number of cycles are also represented.

*Table 28 Tables showing the Initial modulus and Extrapolated modulus of the beams - Base*

200 $\mu\text{m/m}$		
Beam ID	Initial stiffness E0 (MPa)	Extrapolated stiffness E00 (MPa)
4	4237	3028
6 R	5119	4200
10 C	5889	4636
11 R	5739	4363
13 C	7321	6093
17 R	7003	5620
Avg.	5884.67	4656.67
STD	650.14	614.037
C.V	11.05	13.186
140 $\mu\text{m/m}$		
Beam ID	Initial stiffness E0 (MPa)	Extrapolated stiffness E00 (MPa)
5	5845	5318
7 C	5399	3354
12 L	6629	4924
9 L	5420	4322
16 C	6541	4254
28 C	6057	4447
Avg.	5981.83	4436.5
STD	498.07	740.31
C.V	8.33	16.69
300 $\mu\text{m/m}$		
Beam ID	Initial stiffness E0 (MPa)	Extrapolated stiffness E00 (MPa)
3 R	5179	4093
19 C	5217	3883
24 L	4763	3599
26 R	4721	3997
29 R	5734	4454
Avg.	5122.8	4005.2
STD	205.65	202.43
C.V	4.01	5.054

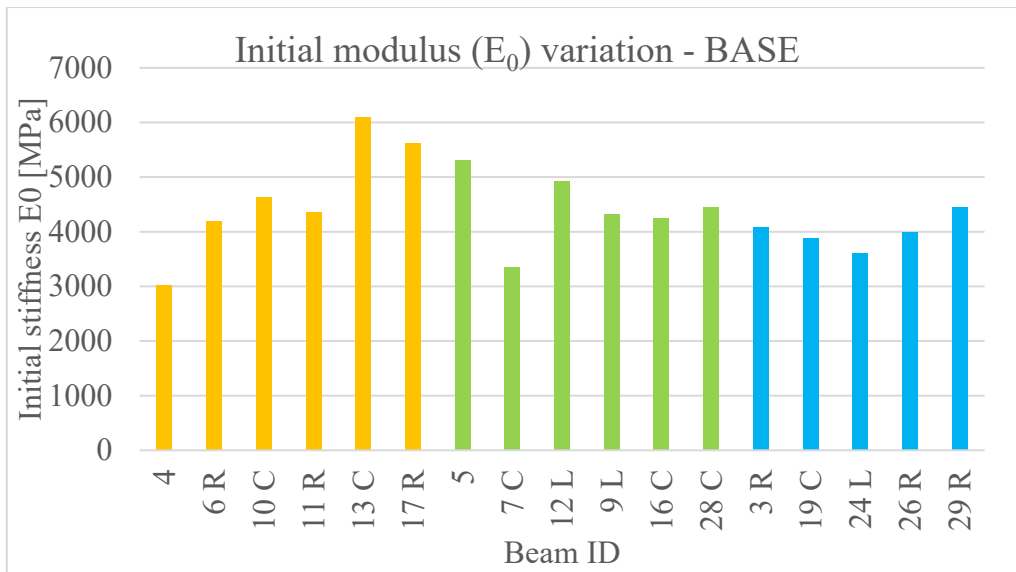


Figure 69 Plot showing the Initial modulus variation - Base

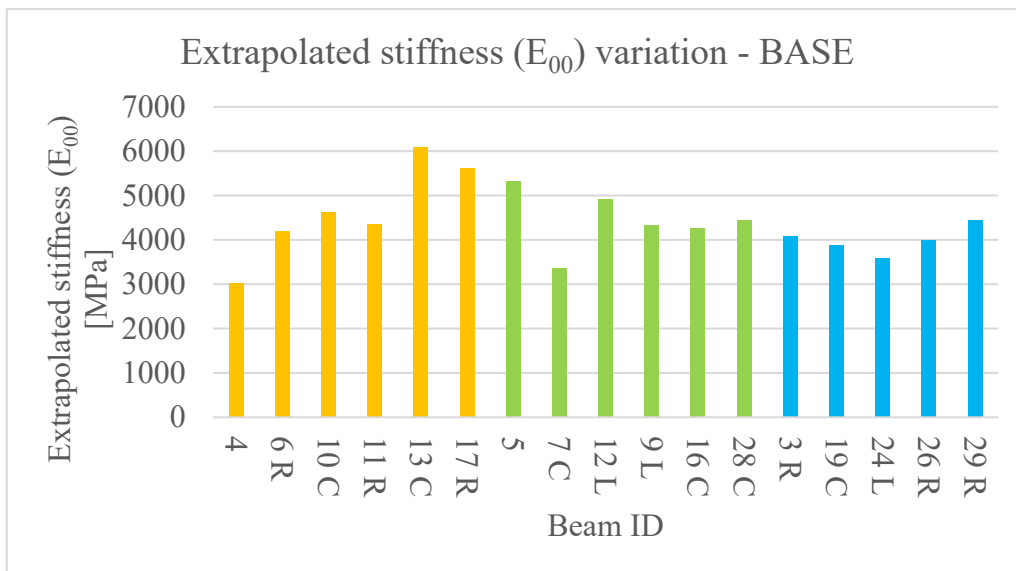


Figure 70 Plot showing the Extrapolated modulus variation - Base

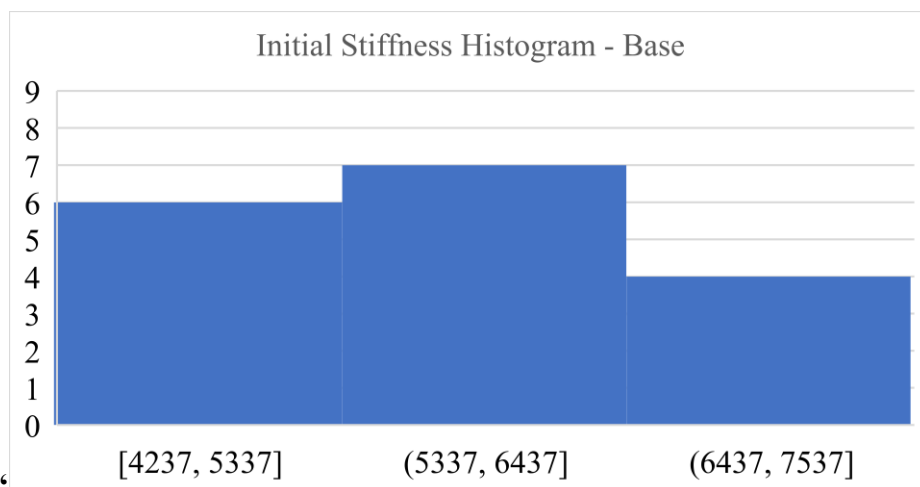


Figure 71 Initial stiffness Histogram - Base

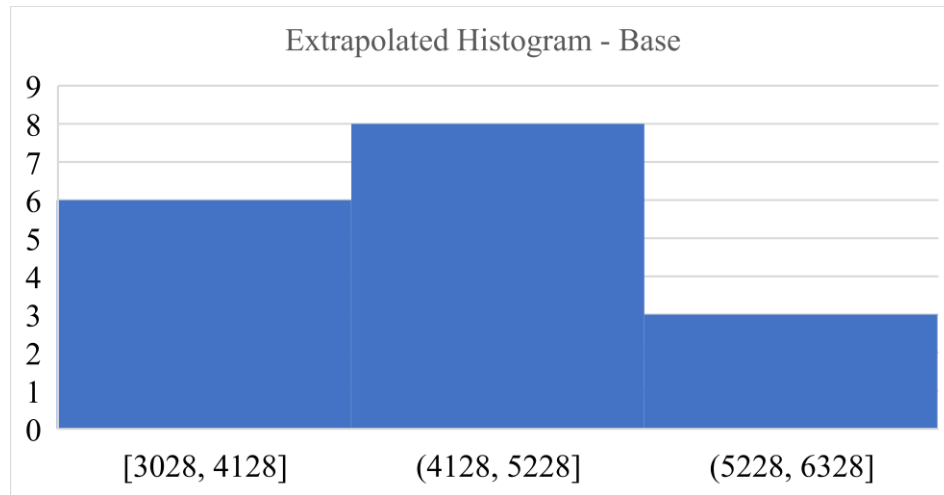


Figure 72 Extrapolated stiffness modulus Histogram - Base

From the above histogram, most of the beams shows that the Initial stiffness is in range of between 4000 MPa to 5300 MPa.

Table 29 Beams Initial stiffness and Extrapolated stiffness with their corresponding air voids - Base

Strain Level	Beam ID	Initial Stiffness (MPa)	Extrapolated Stiffness (E00) (MPa)	Air Voids (%)
200 $\mu\text{m/m}$	4	4237	3028	6.9
	6 R	5119	4200	5.2
	10 C	5889	4636	4.6
	11 R	5739	4363	5.1
	13 C	7321	6093	4.2
	17 R	7003	5620	5.4
140 $\mu\text{m/m}$	5	5845	5318	5.3
	7 C	5399	3354	5
	12 L	6629	4924	4.6
	9 L	5420	4322	5.2
	16 C	6541	4254	5.2
	28 C	6057	4447	5.4
300 $\mu\text{m/m}$	3 R	5179	4093	5.5
	19 C	5217	3883	5.5
	24 L	4763	3599	5.4
	26 R	4721	3997	5.3
	29 R	5734	4454	5.9

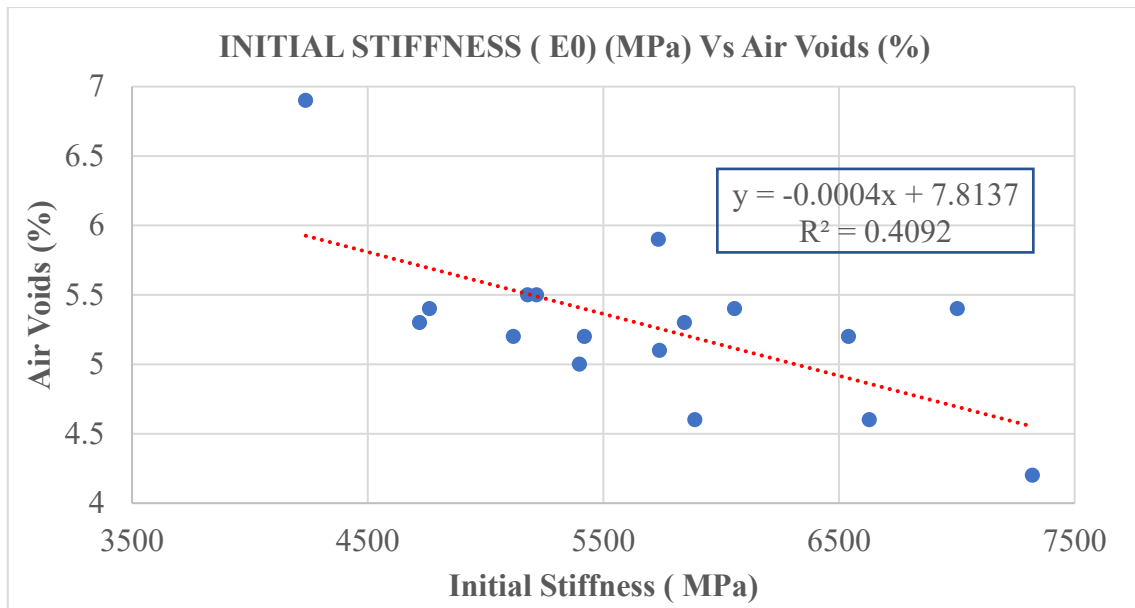


Figure 73 Graph showing the trend in Initial modulus variation w.r.t. air voids of beams - Base

Based on the results, it can be clearly concluded from the above histogram that there is a better consistency of the results in terms of the standard deviation. Most of the results shows that the initial stiffness is in range of between 7600 MPa to 8700 MPa.

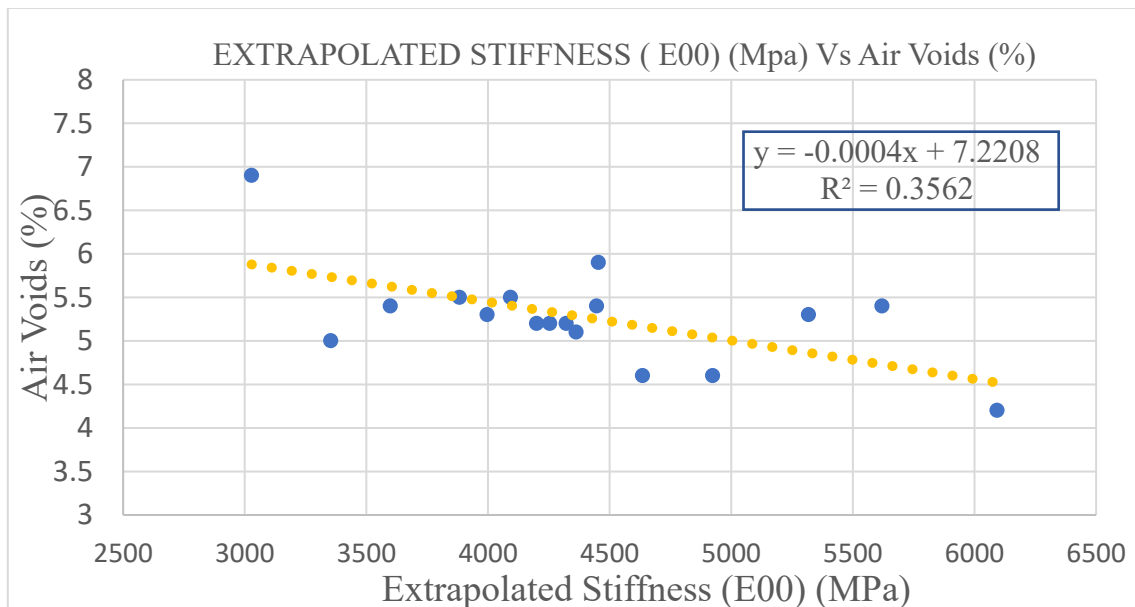


Figure 74 Graph showing the trend in Extrapolated modulus variation w.r.t. air voids of beams – Base

Based on the results, extrapolated stiffness vs Air voids graph, the data is much scattered for the Base mixtures when compared to the Binder mixture.

## 4.2 Fatigue failure analysis

### 4.2.1 Fatigue failure criterion 1: Reduction of initial modulus

This is the classical failure criterion which is in use to define the fatigue failure of bituminous mixtures, and it is defined as the point at which there is a 50% reduction in initial value of the modulus, which is taken at the 100<sup>th</sup> cycle, and the corresponding number of cycles is indicated as  $Nf_{50}$ .

This below plot Figure 75 shows typical test result with respect to this failure criterion, and the number of cycles for each test:

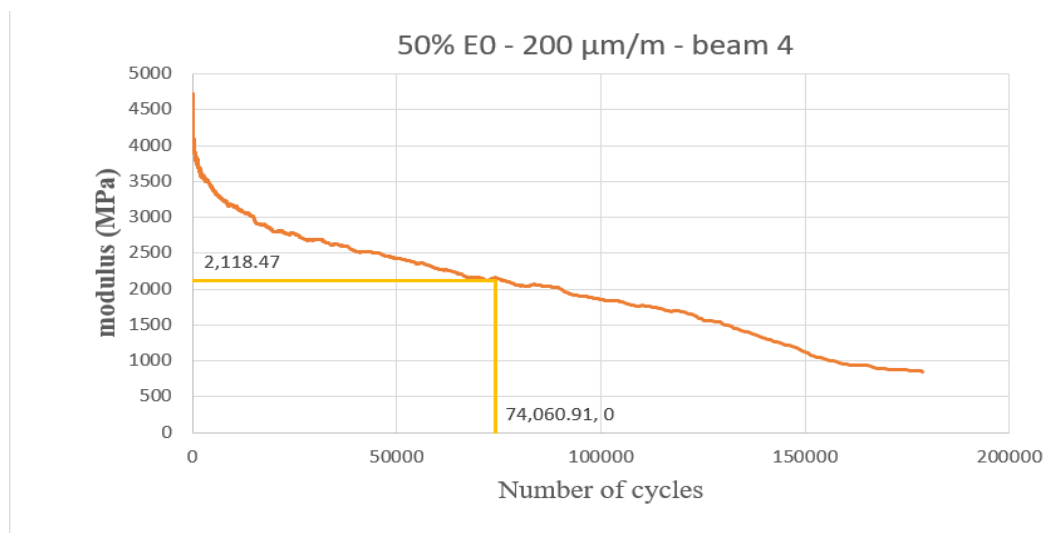


Figure 75 Typical graph of the 50 % reduction of initial modulus criterion

In this case initial modulus was 4236 MPa and the corresponding number of cycles following this criterion was 74061, tested on the Base mixture at 20 °C temperature.

The results of the two mixtures, binder and base are summarized in the following table:

## CHAPTER 4 RESULTS AND DISCUSSION

Table 30 Fatigue test results for all beams considering classical fatigue analysis

50 % E <sub>0</sub> of BINDER @10 °C			50 % E <sub>0</sub> OF BASE @ 20 °C		
Strain Level (µm/m)	Beam Id	Fatigue Life	Strain Level (µm/m)	Beam Id	Fatigue Life
300	13 L	9274	300	3 R	10703
	14 C	12484		19 C	14772
	18 R	9138		24 L	10492
	22 L	11470		26 R	9165
	24 R	7831		29 R	17557
	Average	10039		Average	12538
200	1 L	109556		200	4
	2 C	107822	6 R		46969
	5 C	88750	10 C		26425
	9 R	86768	11 R		53785
	10 L	48779	13 C		37100
	17 C	163003	17 R		28492
	Average	100779	Average		34747
	140	6 L	576791		140
7 L		926445	7 C	1069728	
11 C		1191942	12 L	230162	
12 R		1092367	9 L	701377	
Average		946886	16 C	418331	
			28 C	368798	
		Average	729812		

### 4.2.2 Fatigue failure criterion 2: Reduction of the Extrapolated Modulus

This method implies that the modulus would evolve linearly as the number of cycles with applied load increases over time

Modulus value ( $E_{00}$ ) which is obtained through linear extrapolation of the stage at which there is a linear reduction of the modulus (intermediate stage) when drawn versus the number of cycles. The number of cycles obtained at the 50 % reduction of this modulus is considered as the fatigue life of that specimen.

The length of the intermediate stage, which varies by each test, affects how this interval is defined, making it somewhat arbitrary.

In the Figure 76 below a typical test result graph after the analysis with respect to this failure criterion, and the number of cycles for each test:

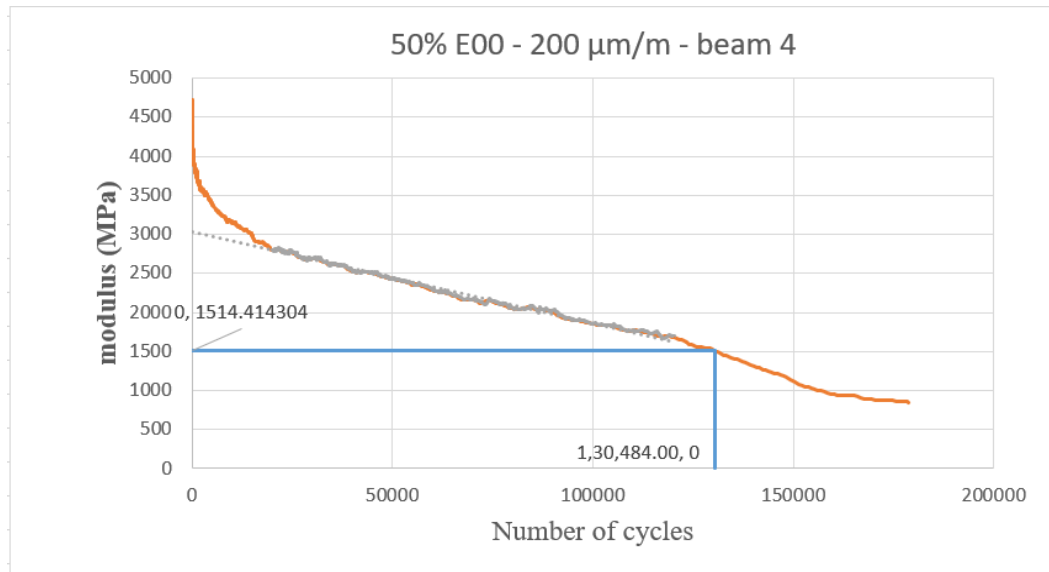


Figure 76 Typical graph showing the extrapolated stiffness reduction criterion

In this case the extrapolated stiffness was 3028 MPa and the corresponding number of cycles following this criterion was 130,484 tested on the Base mixture at 20 °C temperature.

Table 31 Fatigue test results for all beams considering 50 % E<sub>00</sub> analysis

50 % E <sub>00</sub> of BINDER @10 °C		
Strain Level (µm/M)	Beam Id	Fatigue Life
300	13 L	12162
	14 C	19276
	18 R	11795
	22 L	14566
	24 R	8297
	Average	13219
200	1 L	116592
	2 C	117791
	5 C	112490
	9 R	118935
	10 L	64072
	17 C	202613
	Average	122082
140	6 L	650629
	7 L	1267004
	11 C	1368079
	12 R	1203804
	Average	1122379

50 % E <sub>00</sub> of BASE @20 °C		
Strain Level (µm/M)	Beam Id	Fatigue Life
300	3 R	14934
	19 C	21054
	24 L	13082
	26 R	11007
	29 R	21962
	Average	16408
200	4	130484
	6 R	57324
	10 C	36448
	11 R	85114
	13 C	40272
	17 R	37584
Average	42907	
140	5	89468
	7 C	2311474
	12 L	268466
	9 L	1093677
	16 C	935464
	28 C	611881
Average	1446932	

### 4.2.3 Fatigue failure criterion 3: Peak in phase angle

If damage occurs during a fatigue test with cyclic loading, the observed phase angle often experiences a gradual climb, which is subsequently followed by a rapid decrease.

The cycle at which this abrupt decline occurs is described as fatigue life, or the number of cycles to failure  $N_f$ . Since this approach is dependent on the material's viscoelastic characteristic and this reduction signals a change in the material's internal regulating mechanism, it is thought to be more theoretical in nature.

The calculation of the peak phase angle is not clear and much difficult to obtain the results since the graph lot of variability in obtaining the peak value and in most of the cases the maximum value is at the end of the test. From this phase of the study, this failure criteria for is eliminated for any further comparisons.

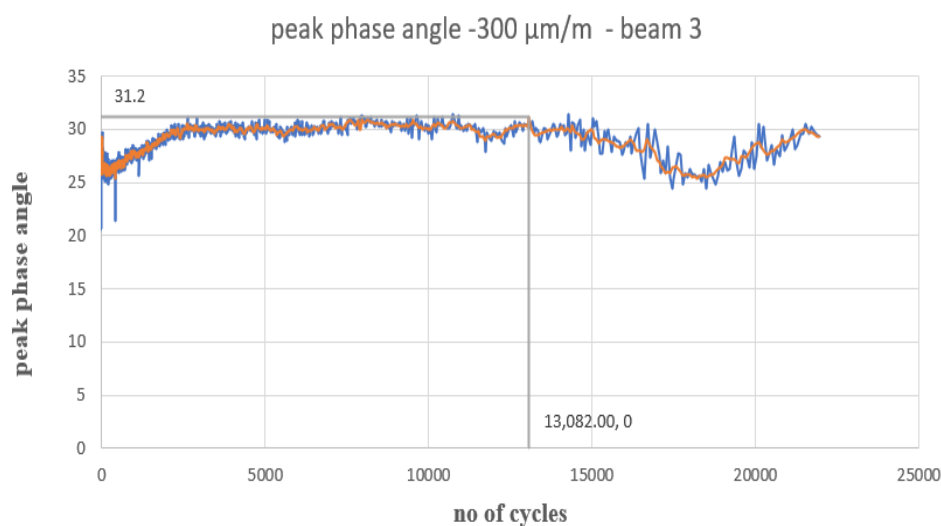


Figure 77 Typical graph showing the peak phase angle

### 4.2.4 Fatigue failure criterion 4: Energy ratio

If the results from the strain-controlled test were plotted, a standard graph might be produced. However, a further step of behaviour is observed. As the load in the controlled strain test decreases, a gradual crack spreads throughout the specimen at this latter stage. The  $N_1$  condition is much complicated to define for strain-controlled than to stress-controlled tests (This is because when the fracture spreads, the stress at the crack tip decreases, slowing the rate of crack propagation).

By using the same analysis for the controlled stress approach as was previously described, this issue might be solved. Hopman's analysis for stress-controlled testing may be applied, even

when the fatigue tests are conducted using strain-controlled tests. When plotting the product ( $N \times E$ ) versus  $N$  a noticeable peak was observed at failure  $N_1$ , as shown in the following example:

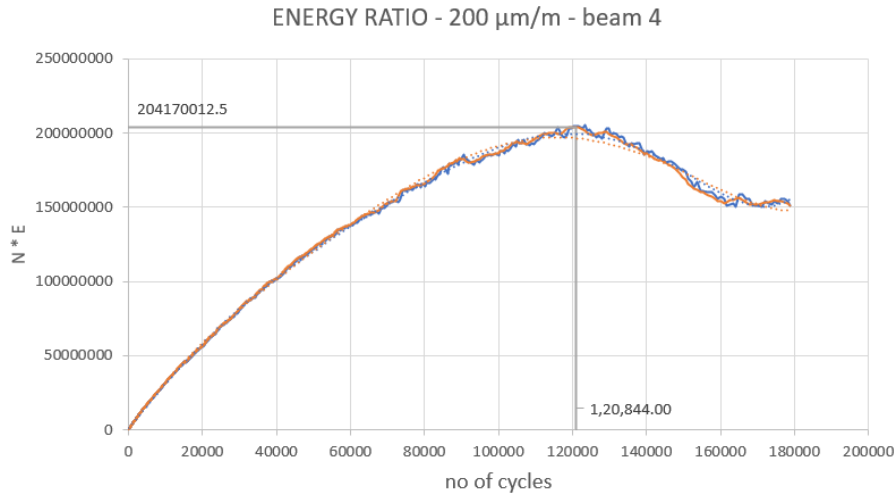


Figure 78 Typical graph showing the Energy ratio criterion

The results of the test of the both the mixtures are summarized in the following table:

Table 32 Fatigue test results for all beams considering Energy Ratio analysis

ENERGY RATIO of BINDER @10 °C			ENERGY RATIO @20 °C OF BASE		
Strain Level (μm/m)	Beam Id	Fatigue Life	Strain Level (μm/m)	Beam Id	Fatigue Life
300	13 L	12799	300	3 R	13722
	14 C	20655		19 C	18710
	18 R	13886		24 L	11256
	22 L	14353		26 R	10522
	24 R	7454		29 R	18029
	Average	13829.4		Average	14448
200	1 L	100077	200	4	119509
	2 C	101665		6 R	52571
	5 C	97802		10 C	33980
	9 R	110826		11 R	84115
	10 L	54270		13 C	31853
	17 C	197016		17 R	35444
Average	110276	Average	38462		
140	6 L	579386	140	5	87493
	7 L	209028		7 C	2060232
	11 C	1142215		12 L	234034
	12 R	1075641		9 L	1077495
	Average	751567.5		16 C	841578
			28 C	556387	
			Average	1326435	

### 4.2.5 Fatigue failure criterion 5: Dissipated Energy Ratio

A distinct method of determining the stage of fatigue damage at which the material undergoes a change from crack initiation to fracture propagation is provided by the graph showing the correlation between DER and the number of cycles in the stress-controlled mode.

The damage is minimal in the first section, and  $DER = n$ . (the dissipated energy is roughly equal for successive cycles). The dissipated energy ratio begins to deviate from the equality line when the percentage difference in dissipated energy between succeeding cycles increases significantly, which is regarded as the beginning of a fracture. The abrupt shift in DER, which may be connected to the point at which a crack starts to spread, is what defines the fatigue failure  $N_f$  point. This alteration is thought to be extremely material-specific and unrelated to the loading method.

As the example below in Figure 79, the failure point  $N_f$  for the strain-controlled test setup is represented by the intersection of two tangents. These two tangents are rather arbitrary since different samples exhibit different transitional phases.

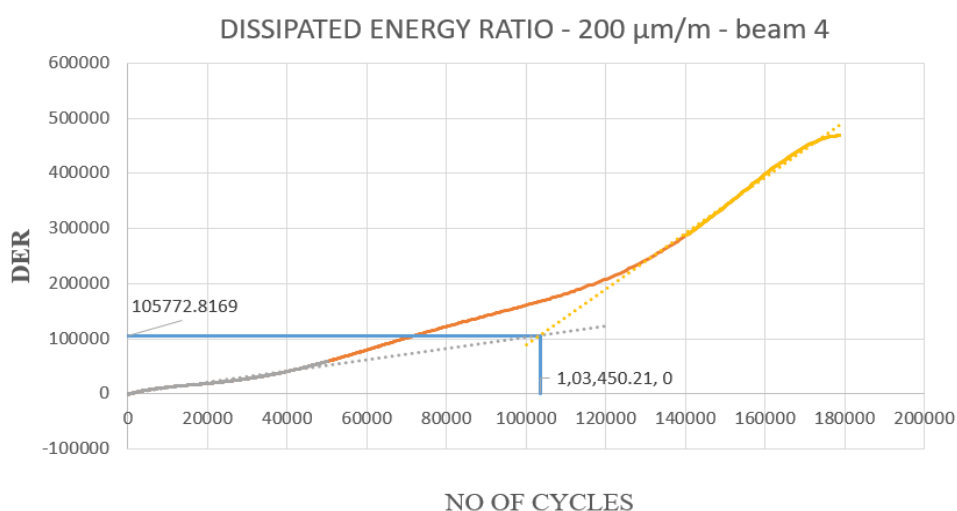


Figure 79 Typical graph showing the DER criterion

The interpretation of the second line is a function from of the termination stiffness, which is in our case was 20% of the initial stiffness ( $E_0$ ).

Table 33 Fatigue test results for all beams considering Dissipated Energy Ratio analysis

DISSIPATED ENERGY RATIO OF BINDER @10 °C		
Strain Level (µm/m)	Beam Id	Fatigue Life
300	13 L	11901
	14 C	21097
	18 R	10178

DISSIPATED ENERGY RATIO OF BASE @20 °C		
Strain Level (µm/m)	Beam Id	Fatigue Life
300	3 R	13034
	19 C	14502
	24 L	11122

	22 L	10411		26 R	12515
	24 R	7450		29 R	19518
	Average	12207.4		Average	14138
200	1 L	108082	200	4	103450
	2 C	80420		6 R	45091
	5 C	110012		10 C	42582
	9 R	100112		11 R	92402
	10 L	92525		13 C	40747
	17 C	175735		17 R	24011
	Average	111147.6667		Average	38108
140	6 L	803964	140	5	76320
	7 L	1518756		7 C	1906421
	11 C	1031908		12 L	269283
	12 R			9 L	863947
	Average	1118209.333		16 C	950146
			28 C	518066	
			Average	1240171	

### 4.3 Comparison of fatigue test results

From the statistical analysis in the previous section, the obtained data of the results showed a variability. To overcome further analysis has to be made in order to deal with the outliers in the data, this leads to obtain a reliable values which can be used later to compare the results and to conclude the observations.

Statistical parameters which are used to describe the data are the: average, standard deviation, and the coefficient of variation. For a better graphical visualization of the data, some bar charts, histograms, boxes, and Whisker plots are provided.

To construct the fatigue curve, statistical analysis is made to take out the outliers for each of the chosen failure criterion for both the mixtures used.

The number of cycles for each failure criterion for both the mixtures under a chosen strain levels are represented in the following tables:

Table 34 Fatigue results of the all the fatigue failure criteria in the Binder mixture tested at 300  $\mu$ s strain level and 10 °C

300 $\mu$ s	Beam 13 L	Beam 14 C	Beam 18 R	Beam 22 L	Beam 24 R	AVG	STD	C.V [%]
50% E0	9,274	12,484.00	9,138	11,470	7,831	9,428	1,307	13.9
50% E00	12,162	19,276.00	11,795	14,566	8,297	11,705	2,237	19.1
ER	12,799	20,655.00	13886	14,353	7,454	12,123	2,754	22.7
DER	11,901	21,097.00	10,178	10,411	7,450	9,985	1,606	16.1
Average	14,178.16							
E0 (MPa)	8066	9760	9585	8734	8297			
E00 (MPa)	6575	7755	7924	7372	7570			
Airvoids(%)	5.6	5.3	5.8	5.3	5.0			

## CHAPTER 4 RESULTS AND DISCUSSION

Table 35 Fatigue results of the all the fatigue failure criteria in the Binder mixture tested at 200  $\mu$ s strain level and 10 °C

200 $\mu$ s	Beam 1 L	Beam 2 C	Beam 5 C	Beam 9 R	Beam 10 L	Beam 17 C	AVG	STD	C.V [%]
50% E0	109,556	107,822	88,750	86,768	48,779	163,003	98,224	10506	10.7
50% E00	116,592	117,791	112,490	118,935	64,072	202,613	116,452	2433	2.1
ER	100,077	101,665	97,802	110,826	54,270	197,016	102,593	4948	4.8
DER	108,082	80,420	110,012	100,112	92,525	175,735	99,657	11710	11.8
Average	1,19,175.17								
E0 (MPa)	10091	11113	11170	10156	11322	8511			
E00 (MPa)	8648	9405	8319	7920	8713	7129			
Air voids (%)	4	4	4.2	5.3	4.3	5.6			

Table 36 Fatigue results of the all the fatigue failure criteria in the Binder mixture tested at 140  $\mu$ s strain level and 10 °C

140 $\mu$ s	Beam 6 L	Beam 7 L	Beam 8 C	beam 11 C	beam 12 R	Beam 15 R	AVG	STD	C.V [%]
50% E0	576,791	926,445	247,318	1,191,642	1,092,367	391,367	1,070,151	109,400	10.2
50% E00	650,629	1,267,004	253,773	1,368,079	1,203,804	406,340	1,279,629	67,657	5.3
ER	579,386	1,177,142	209,028	1,142,215	1,075,641	354,610	1,131,666	42,104	3.7
DER	576,808	1,518,756	164,179	1,031,908	-	-	1,275,332	243,424	19.1
Average	922,345								
E0 (MPa)	10383	8875	9138	11097	11190	10052			
E00 (MPa)	8617	6970	8642	8656	9588	9201			
Air voids (%)	5.3	5.9	5.2	4.1	4.3	5.6			

The above tables represent the fatigue cycles of the four-point bending test for the binder mixtures which is tested using the three strain levels and testing temperature is at 10 °C. Five failure criteria are considered to define the fatigue behaviour, to carry out the analysis based on the raw data obtained from the electronically generated system for their respective beams and thus values evaluated are shown in the tables.

Since, the fatigue results presents a high variability, taking this into consideration, statistical analysis is carried out to overcome the problem. Some of the beams are not considered to assess the fatigue behaviour which are shown in red due to their dissimilarity with the other beams tested at same strain level.

With the considered values the average, standard deviation and coefficient of variation are calculated. When the deleted beams are coefficient of variation is more than 25%, which is the limit set to decide the fatigue life of that particular beam

## CHAPTER 4 RESULTS AND DISCUSSION

*Table 37 Fatigue results of the all the fatigue failure criteria in the Base mixture tested at 300  $\mu$ s strain level and 20 °C*

300 $\mu$ s	Beam 3 R	Beam 19 C	Beam 24 L	Beam 26 R	Beam 29 R	AVG	STD	C.V [%]
50% E0	10703	14772	10492	9165	17557	10,120	681	6.7
50% E00	14934	21054	13082	11007	21962	13,008	1,604	12.3
ER	13722	18710	11256	10522	18029	11,833	1,369	11.6
DER	13034	14502	11122	12515	19518	12,224	807	6.6
AVGERAGE	15,588.72							
E0 (MPa)	5179	5217	4763	4721	5734			
E00 (MPa)	4093	3883	3599	3997	4454			
Airvoids (%)	5.5	5.5	5.4	5.3	5.9			

*Table 38 Fatigue results of the all the fatigue failure criteria in the Base mixture tested at 200  $\mu$ s strain level and 20 °C*

200 $\mu$ s	Beam 4	Beam 6 R	Beam 10 C	Beam 11 R	Beam 13 C	Beam 17 R	AVG	STD	C.V [%]
50% E0	74061	46969	26425	53785	37100	28492	34,747	8,113	23.3
50% E00	130484	57324	36448	85114	40272	37584	42,907	8,439	19.7
ER	119509	52571	33980	84115	31853	35444	38,462	8,245	21.4
DER	103450	45091	42582	92402	40747	24011	38,108	8,284	21.7
AVGERAGE	41,855.85								
E0 (MPa)	4237	5119	5889	5739	7321	7003			
E00 (MPa)	3028	4200	4636	4363	6093	5620			
Air voids (%)	6.9	5.2	4.6	5.1	4.2	5.4			

*Table 39 Fatigue results of the all the fatigue failure criteria in the Base mixture tested at 140  $\mu$ s strain level and 20 °C*

140 $\mu$ s	Beam 5	Beam 7 C	Beam 9 L	Beam 12 L	Beam 16 C	Beam 28 C	AVG	STD	C.V [%]
50% E0	81129	1069728	23012	701377	418331	368798	7,29,812	2,66,691	36.5
50% E00	89468	2311474	268466	1093677	935646	611881	14,46,932	6,14,718	42.5
ER	87493	2060232	234034	1077495	841578	556387	13,26,435	5,27,736	39.8
DER	76320	1906421	269283	863947	950146	518066	12,40,171	4,72,422	38.1
AVGERAGE	10,25,983.93								
E0 (MPa)	5845	5399	6629	5420	6541	6057			
E00 (MPa)	538	3354	4924	4322	4254	4447			
Air voids (%)	5.3	5	4.6	5.2	5.2	5.4			

Similar statistical analysis is carried out to eliminate the outliers of the results and the remaining are considered for the grand average. The above Tables 39,40,41 represent the fatigue cycles of the four-point bending test for the base mixture which is tested using the three strain levels and testing temperature is at 20 °C.

### 4.4 Fatigue Curves

The fatigue life can be depicted using the Wöhler curves, where the applied strain is plotted against the cycles until failure ( $N_f$ ). The fatigue curves are presented in Figure 80 and Figure 81 and the parameters of the fatigue curves are described in Table 40.

Investigating the Binder mixture tested at 10 °C, four fatigue curves that are obtained after performing the required analysis are represented in Figure 80 and the fatigue curves of the Base mixture tested at 20 °C are also represented (Figure 81).

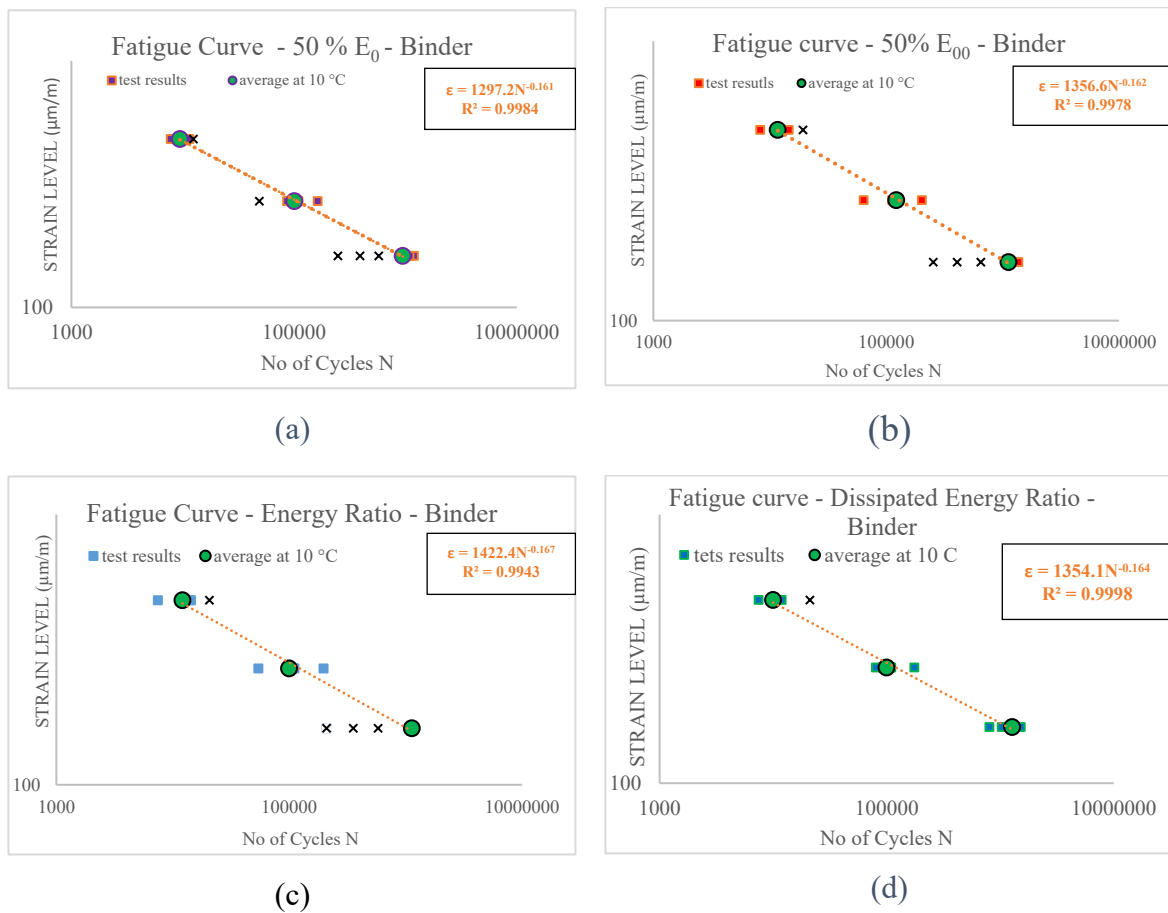


Figure 80 Fatigue curves of a Binder mixture (a) 50 %  $E_0$  (b) 50 %  $E_{00}$  (c) Energy Ratio (d) Dissipated Energy Ratio

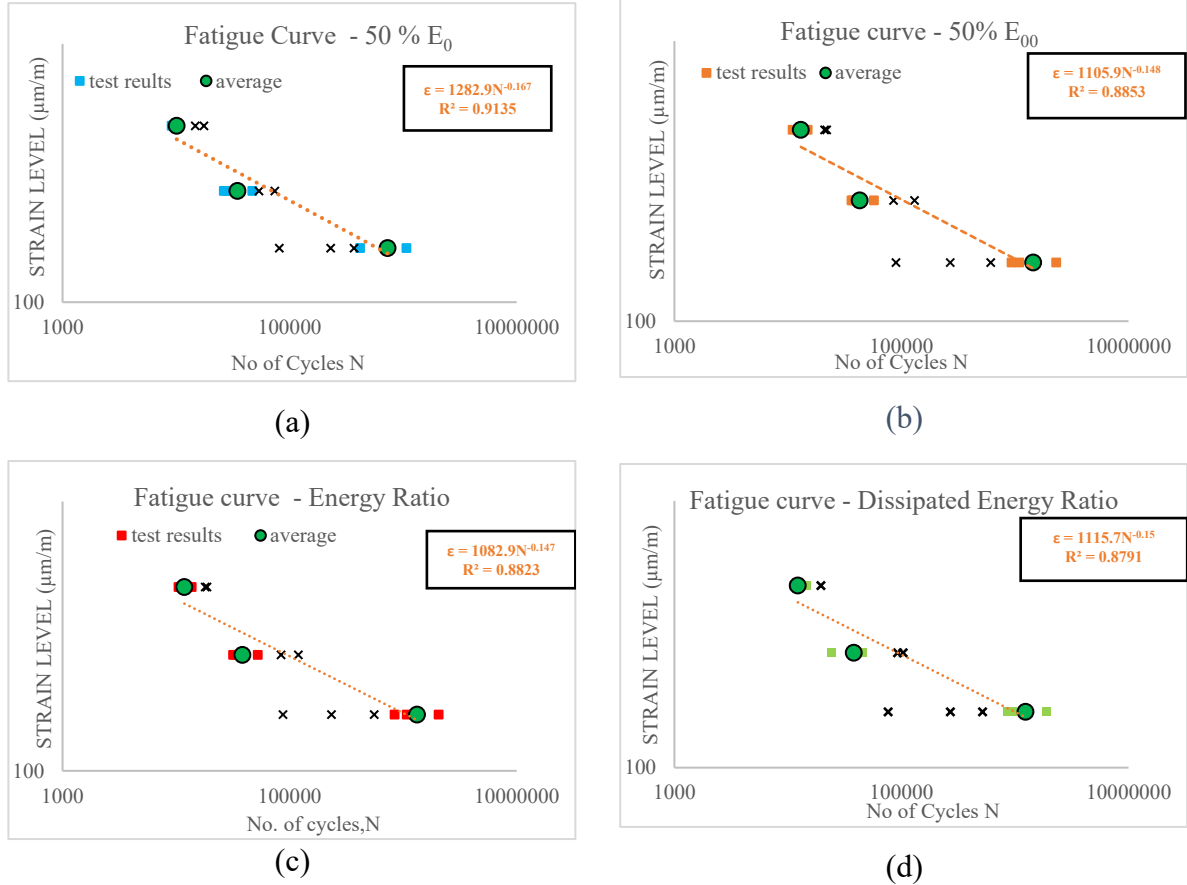


Figure 81 Fatigue curves of the Base mixture (a) 50 %  $E_0$  (b) 50 %  $E_{00}$  (c) Energy Ratio (d) Dissipated Energy Ratio

From the fatigue curve graphs the obtained equation using the power model fit is:

$$\epsilon_0 = u_1 \cdot N_f^{u_2}$$

To obtain the values of  $N_f$ , the above equation is manipulated and obtain the values of  $k_1$  and  $k_2$ , which is generally used to compare the results:

$$N_f^{u_2} = \frac{1}{u_1} \cdot \epsilon_0$$

$$N_f = \left(\frac{1}{u_2}\right)^{\frac{1}{u_2}} \cdot \epsilon_0^{\frac{1}{u_2}}$$

$$N_f = k_1 \cdot \epsilon_0^{k_2}$$

Therefore,  $k_1 = \left(\frac{1}{u_1}\right)^{\frac{1}{u_2}}$  ;  $k_2 = \frac{1}{u_2}$

## CHAPTER 4 RESULTS AND DISCUSSION

Table 40 Fatigue test parameters for the bituminous mixtures

$N_f = k_1 (\epsilon_0)^{k_2}$	Binder @ 10 °C				Base @ 20 °C			
Failure criterion	$k_1$	$k_2$	$R^2$ (%)	$\epsilon_6$ ( $\mu\text{m/m}$ )	$k_1$	$k_2$	$R^2$ (%)	$\epsilon_6$ ( $\mu\text{m/m}$ )
<b>50 % <math>E_0</math></b>	$2.2 \times 10^{19}$	-6.211	99.8	140	$4.1 \times 10^{18}$	-5.988	91.3	122
<b>50 % <math>E_{00}</math></b>	$2.2 \times 10^{19}$	-6.173	99.7	144	$3.7 \times 10^{20}$	-6.757	88.53	136
<b>ER</b>	$7.6 \times 10^{18}$	-5.988	99.4	142	$4.4 \times 10^{20}$	-6.803	88.2	134
<b>DER</b>	$1.2 \times 10^{19}$	-6.098	99.8	144	$2.1 \times 10^{20}$	-6.667	87.9	134

Below are some of the points that are highlighted about the results and fatigue curves of both the mixtures.

- For all the fatigue curves, results are fitted using the power law model and the equation is also represented in the figures.
- The 50% reduction in the initial stiffness modulus ( $E_0$ ) had the minimum fatigue life (number of cycles) irrespective of the strain level and the testing temperatures. This phase is characterized by a rapid decrease in stiffness due to the repetitive excitation. However, the decrease is not considered solely explained by fatigue damage. Heating and a third phenomenon (thixotropy or a local phenomenon) probably play important roles. The opinion regarding the important influence of parasitic phenomena is supported by observations that stiffness loss during cyclic loading is usually rapidly recoverable when the test is halted. This phase is considered dominated by the artefact (in the sense they are totally recoverable) effects.
- In the 50 % reduction in the extrapolated stiffness modulus ( $E_{00}$ ) failure criterion, the definition of the regression interval is different from one test to another, however this could be easily evaluated by fixing a high value for the coefficient of determination ( $R^2$ ), for example more than 0.95 (less than 5 % error), while making sure it is always extrapolating inside Phase II.
- Peak phase angle has yielded the most number of cycles and the variation is very high in the case of Binder mixture and very low fatigue resistance in the case of Base mixture, however the calculation of the number of cycles is not clearer due to the values obtained from the raw data.
- The definition of the transitional period can be seen clearly in the Energy ratio criterion because the obtained peak value indicates the transition between the crack initiation and crack propagation.

- The drawback of the Dissipated Energy ratio criterion is that the definition of the failure point is somehow subjective, since the intervals used to construct the intersection lines varies from each test to another. The error can be controlled simply by fixing a high value for the coefficient of determination ( $R^2$ ), for example more than 0.95 (less than 5 % error).
- The average number of cycles at each strain level (averaging the cycles for the six replicates for the five failure criteria), “50 % reduction in the extrapolated stiffness (E00)”, “Energy ratio”, and “Dissipated energy ratio” have the closest values.
- Outliers are excluded to make the correct judgement of the results.
- The combined fatigue curves of all the considered fatigue criterion are represented in the graphs below for both mixtures tested at their respective temperatures to see the better comparison between the failure criteria.

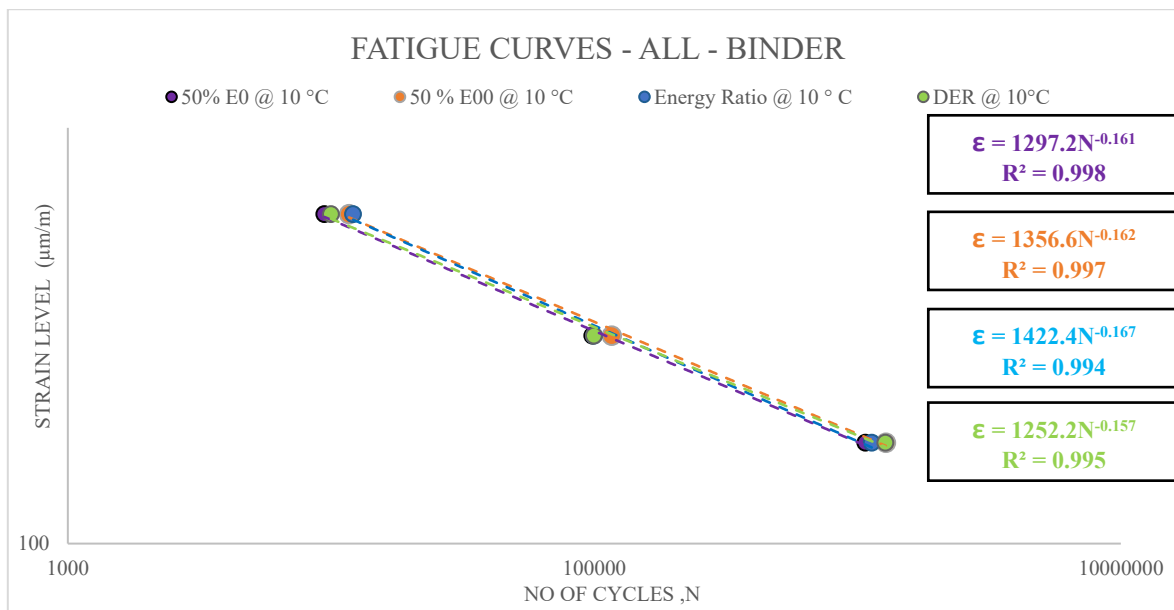


Figure 82 Fatigue curves - ALL - Binder @ 10 °C

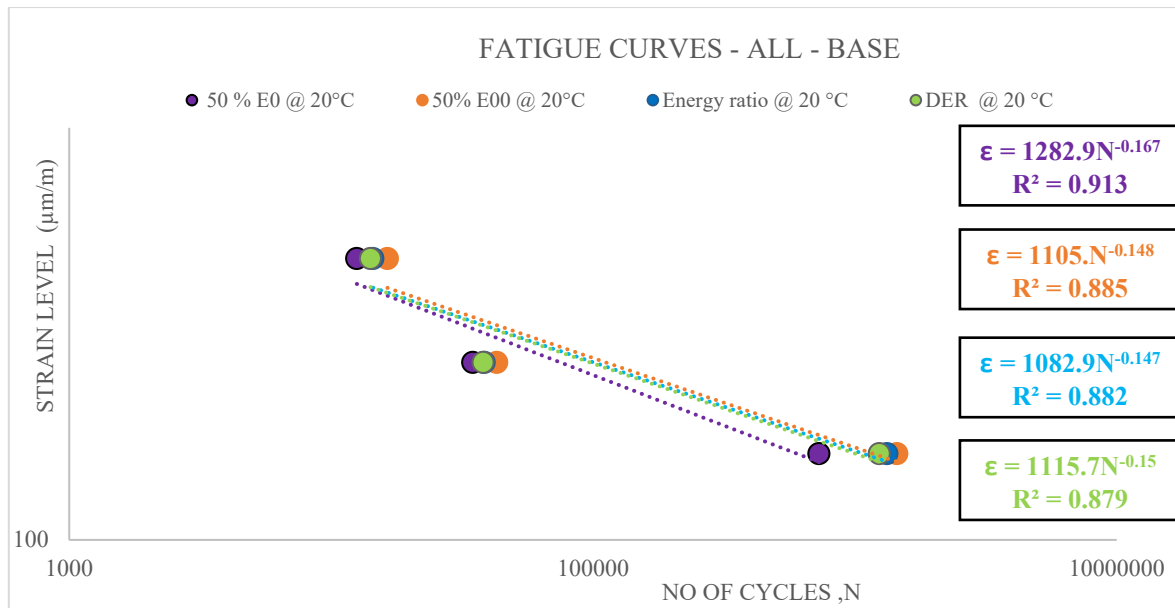


Figure 83 Fatigue curves - ALL - Base @ 20 °C

### 4.5 Comparing the effect of temperatures on fatigue life

As per the objective of this study, the results of the Binder mixture tested at temperatures 10 ° C and 20 ° C were compared which are presented in the following graphs.

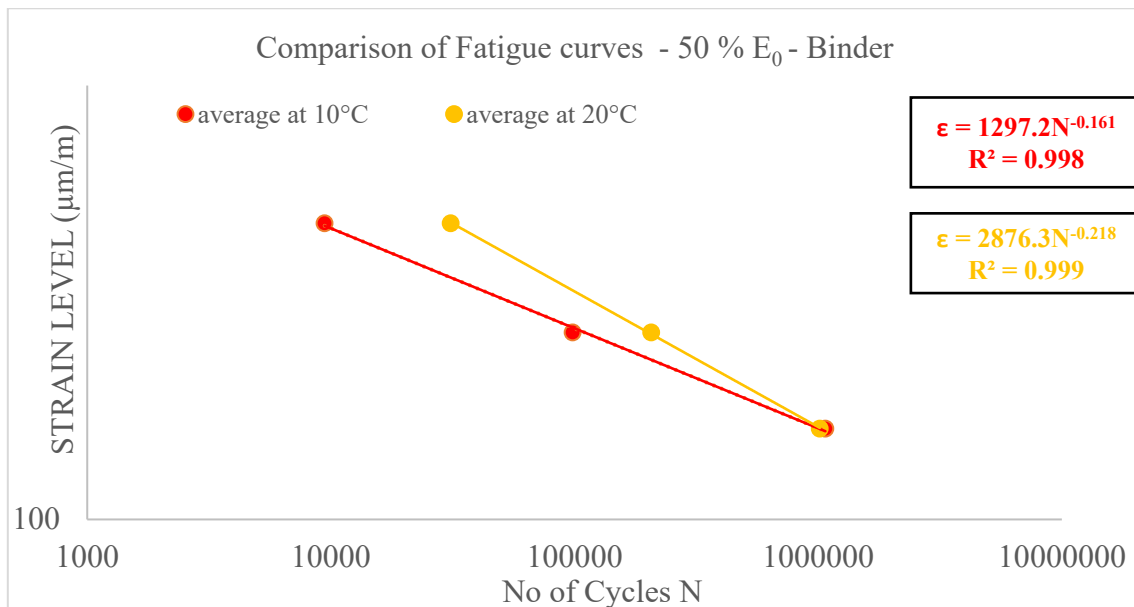


Figure 84 Comparison of the fatigue curves at different temperature - 50 % E<sub>0</sub> - Binder

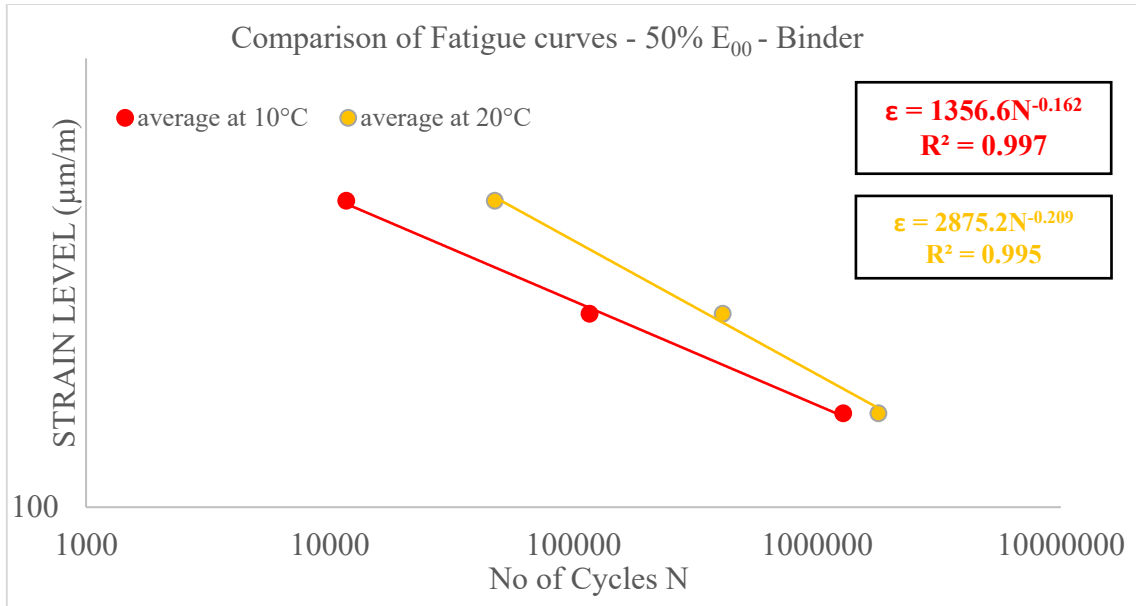


Figure 85 Comparison of the fatigue curves at different temperature - 50 % E00 - Binder

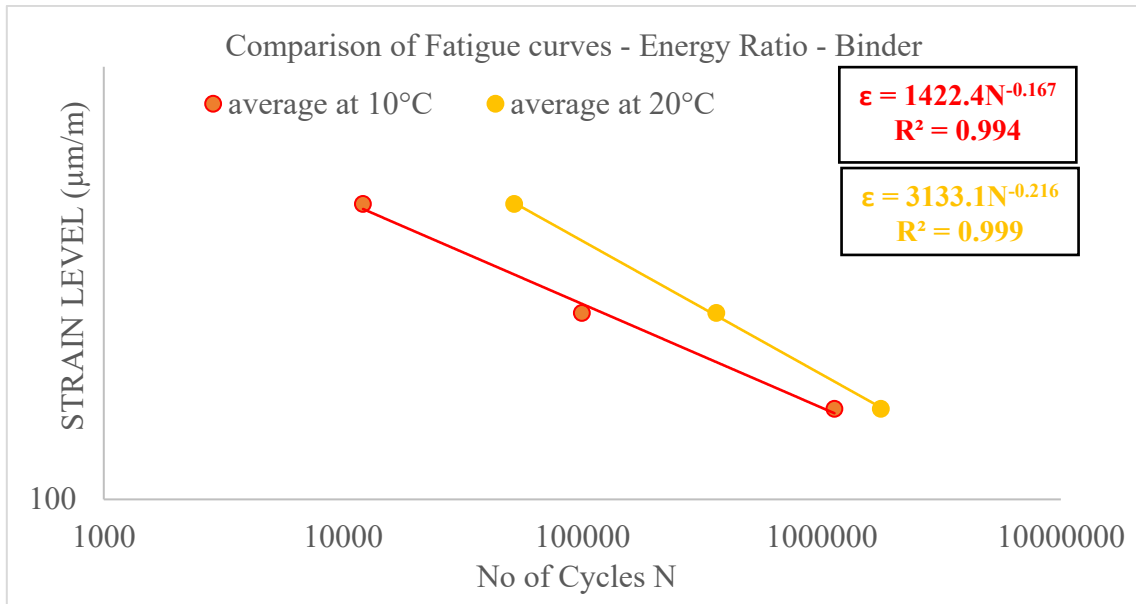


Figure 86 Comparison of the fatigue curves at different temperature - Energy Ratio - Binder

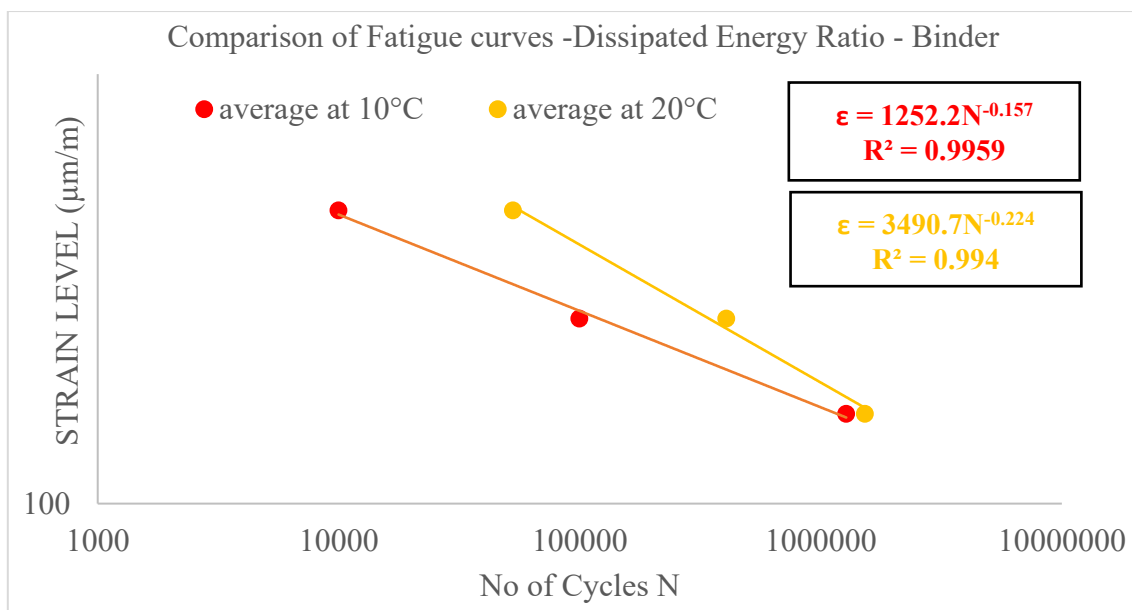


Figure 87 Comparison of the fatigue curves at different temperature - DER – Binder

For both types of mixtures, the fatigue life  $N_{f50}$  of the mixture drops roughly linearly with the increase of strain level on the double logarithmic basis. The temperature also has an apparent effect on fatigue life, the increasing temperature causes an increase in fatigue life.

Table 41 Temperature effect on fatigue life parameter for Binder mixture

$N_f = k_1(\epsilon_0)^{k_2}$	Binder @ 20 °C			Binder @ 10 °C		
	$k_1$	$k_2$	$\epsilon_6$ (µm/m)	$k_1$	$k_2$	$\epsilon_6$ (µm/m)
50 % $E_0$	$7.3 \times 10^{15}$	-4.587	141	$2.2 \times 10^{19}$	-6.211	140
50 % $E_{00}$	$3.5 \times 10^{16}$	-4.785	161	$2.2 \times 10^{19}$	-6.173	144
ER	$1.5 \times 10^{16}$	-4.630	159	$7.6 \times 10^{18}$	-5.988	142
DER	$6.6 \times 10^{15}$	-4.464	157	$1.2 \times 10^{19}$	-6.098	144

The Binder mixture tested at the 20 °C exhibited more fatigue life compared to the 10 °C irrespective of their fatigue criteria, a similar trend is obtained for the previous research study by Cheng et al., [76] as well. s

The difference in the strain level between the two mixtures are very less and it is around 10 µm/m. Plots at high temperature (20 °C) are different from the lower temperature 10 °C, implying that the effects of the strain levels on the fatigue life become more notable at higher temperatures.

At lower strain level (140  $\mu\text{m/m}$ ), this mixture tested at both temperatures have the same fatigue life, but at the higher strain levels (300  $\mu\text{m/m}$  and 200  $\mu\text{m/m}$ ), the fatigue performance of the mixture is distinct.

For the peak phase angle criteria, the results at the temperature 20 °C are not reliable since the fatigue life at the lower strain level are not clear, the comparison might not be possible.

The fitted equations imply that both temperature and strain/stress levels have apparent influences on the fatigue life of asphalt mixture.

The  $\epsilon_6$  parameter represents the strain level at which the fatigue life is  $10^6$  cycles and is widely used as a fatigue resistance parameter. A higher  $\epsilon_6$  indicates a higher fatigue life. For this study the Binder mixture at 20 ° C exhibited the highest fatigue resistance when compared to the same mixture at lower temperature (10 °C) (see Table 41 ). At the  $\epsilon_6$  point the difference in the strain level between the two temperatures clearly explains the effect of temperature on the fatigue life of asphalt mixtures.

Since the values of the reduction in initial modulus was effected by so many factors , it is not considered for the final determination of the fatigue life.

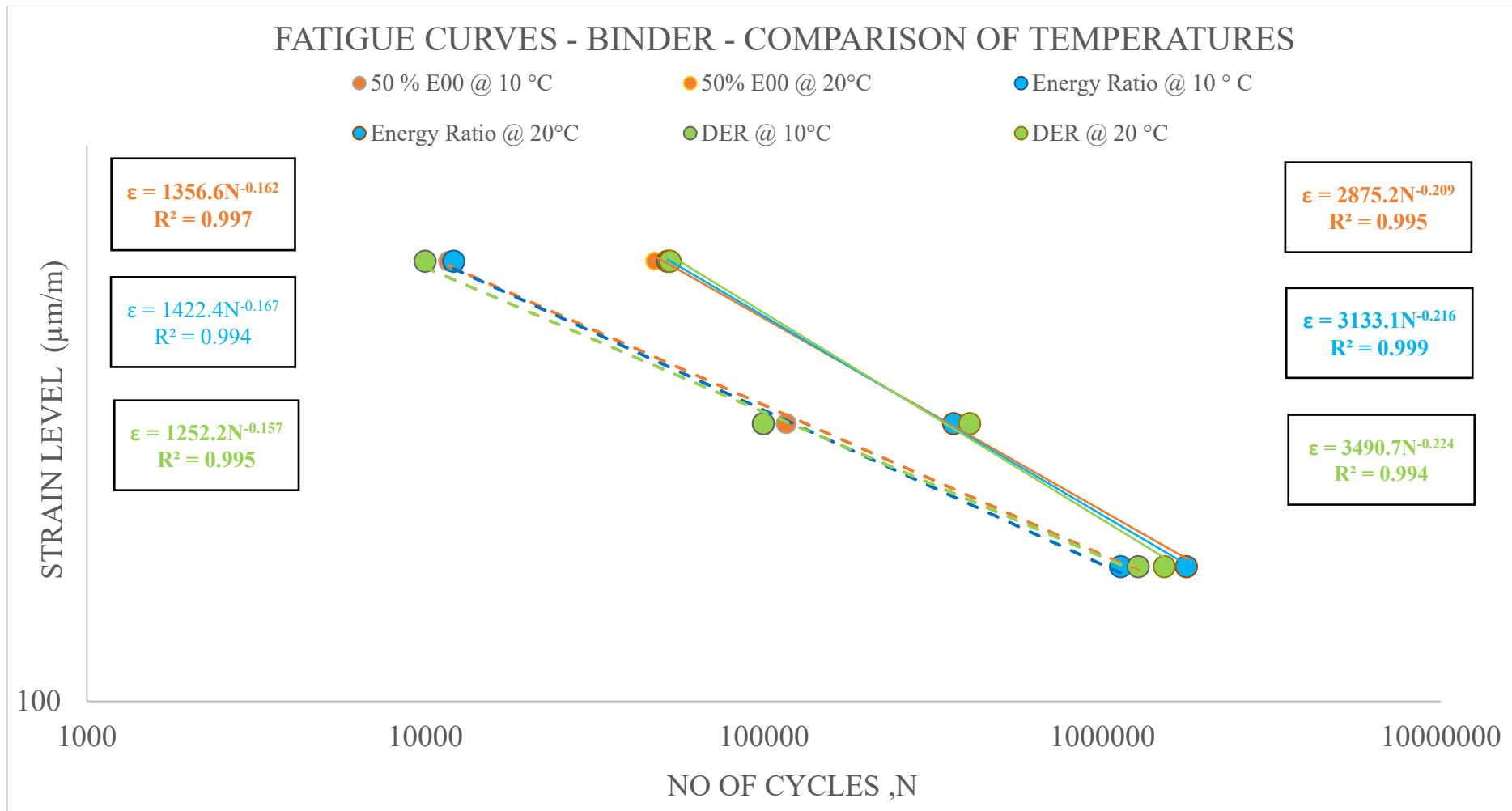


Figure 88 Fatigue curves showing the comparison of temperatures tested with the same mixture (Binder)

4.6 Comparing the effect of mixture type on fatigue life

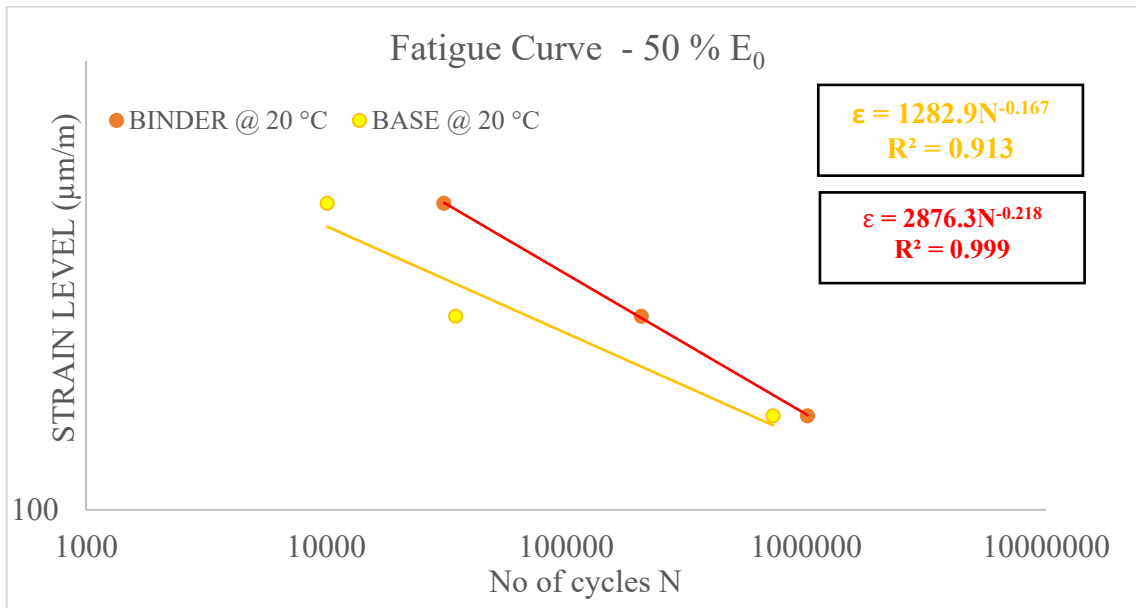


Figure 89 Comparing the effect of mixture on fatigue behaviour – 50% E<sub>0</sub>

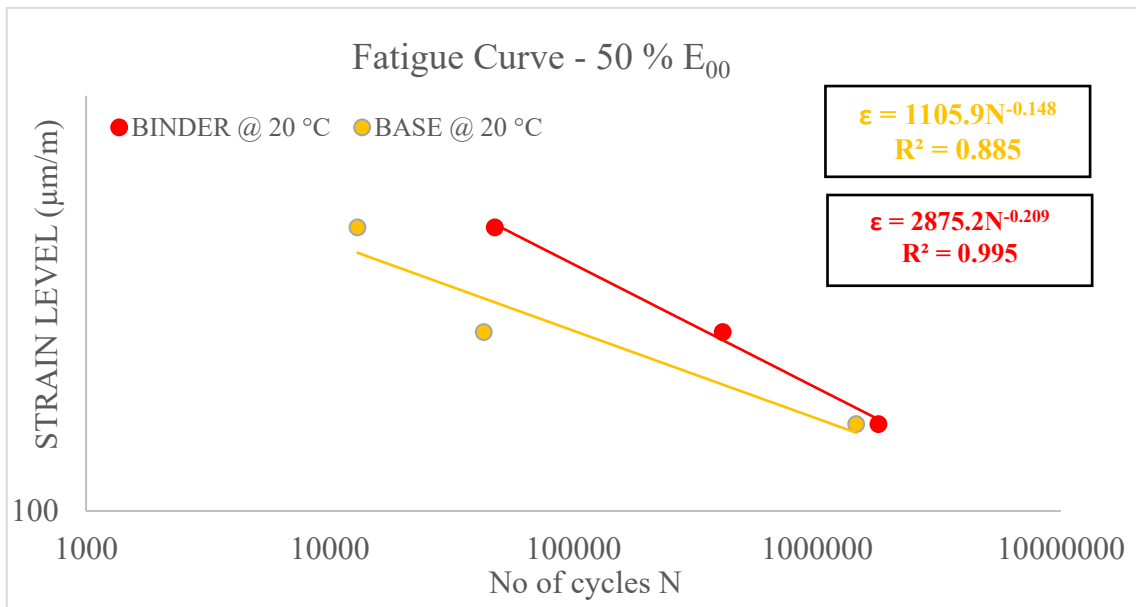


Figure 90 Comparing the effect of mixture on fatigue behaviour – 50% E<sub>00</sub>

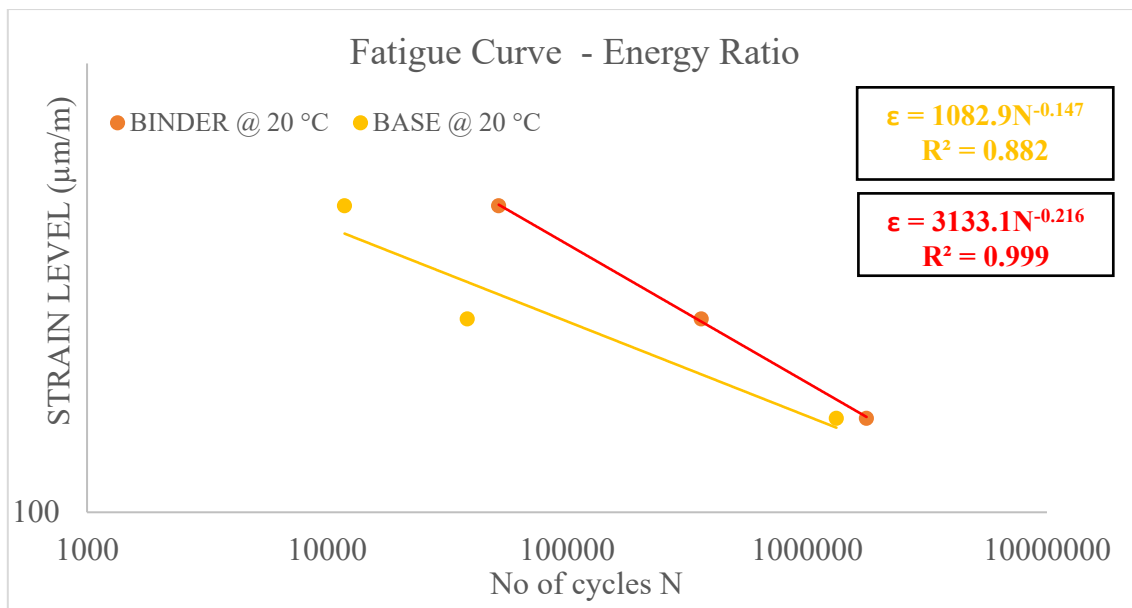


Figure 91 Comparing the effect of mixture on fatigue behaviour – Energy Ratio

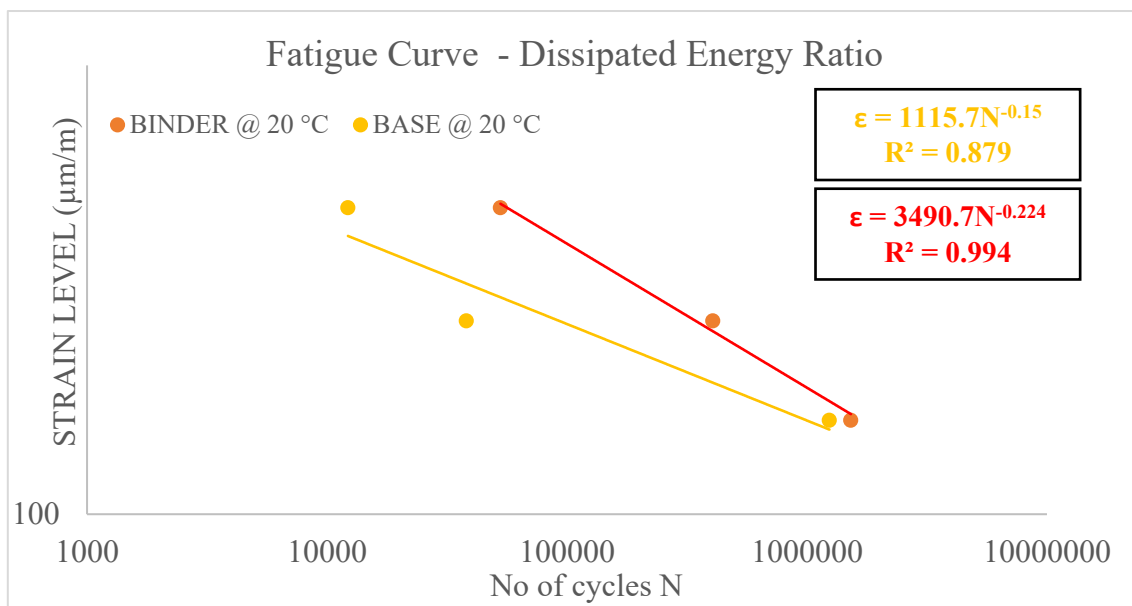


Figure 92 Comparing the effect of mixture on fatigue behaviour – DER

The effect of mixture type on the fatigue behaviour is also the objective of this study, following that, the above Figures 100-104.

For the two mixtures considered the classical, reduction of 50 % initial modulus show the least fatigue life. The other failure criteria peak phase angle is not reliable for both the mixtures due to the high variation in the results since it should not be considered for the assessing of fatigue life.

Table 42 Gradation effect on Fatigue life of asphalt mixtures

$N_f = k_1 (\epsilon_0)^{k_2}$	Binder @ 20 °C			Base @ 20 °C		
	$k_1$	$k_2$	$\epsilon_6$ ( $\mu\text{m/m}$ )	$k_1$	$k_2$	$\epsilon_6$ ( $\mu\text{m/m}$ )
<b>50 % E<sub>0</sub></b>	$7.3 \times 10^{15}$	-4.587	141	$4.1 \times 10^{18}$	-5.988	122
<b>50 % E<sub>00</sub></b>	$3.5 \times 10^{16}$	-4.785	161	$3.7 \times 10^{20}$	-6.757	136
<b>ER</b>	$1.5 \times 10^{16}$	-4.630	159	$4.4 \times 10^{20}$	-6.803	134
<b>DER</b>	$6.6 \times 10^{15}$	-4.464	157	$2.1 \times 10^{20}$	-6.667	134

The reduction in the extrapolated modulus, 50 % E<sub>00</sub>, Energy Ratio and the Dissipated Energy Ratio (DER) exhibits the closest values. The  $\epsilon_6$  parameter represents the strain level at which the fatigue life is  $10^6$  cycles and is widely used as a fatigue resistance parameter. A higher  $\epsilon_6$  indicates a higher fatigue life. For this study the Binder mixture exhibited the highest fatigue resistance. The Base mixture showed the lowest fatigue life. At  $\epsilon_6$  point, the difference in strain level between the two mixtures was only 22  $\mu\text{m/m}$ . This points out the significance of the gradation in assessing the fatigue performance of the asphalt mixtures.

Due to the presence of the high air voids and the lower binder content when compared to the Binder mixture, the effect of the gradation is noticeable.

Highlighting the effect of gradation below Figure 93 is drawn to compare among the five failure criteria for the both the mixtures is represented.

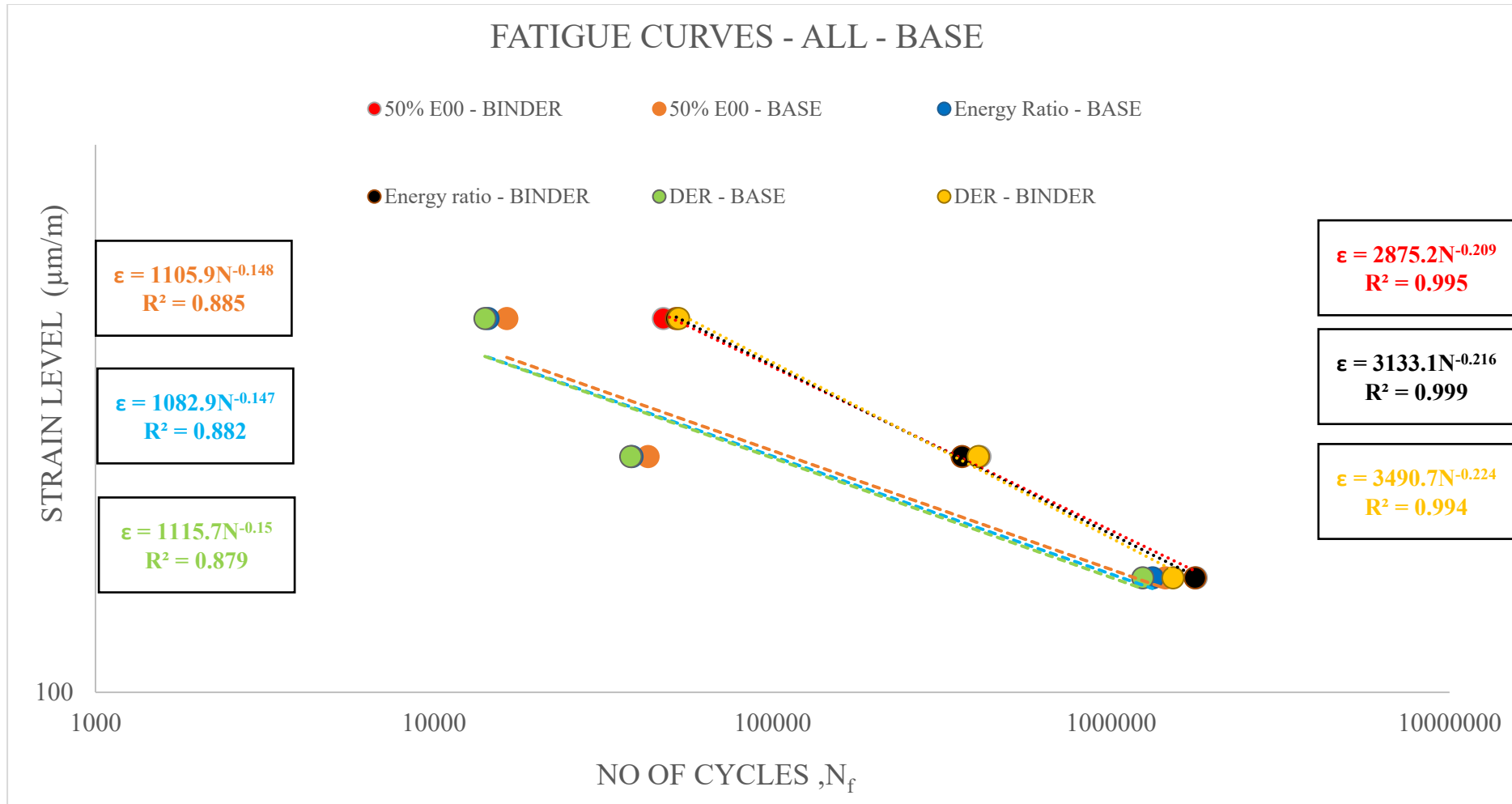


Figure 93 Fatigue curves showing the Comparison of mixtures tested at same temperature

**5 CHAPTER 5 CONCLUSION AND  
RECOMMENDATIONS**

### 5.1 Conclusions

This last chapter includes the conclusions of this study which is explained in the previous section. Some recommendations will also be provided, along with the future works for further extension of this study.

- The characterization of the fatigue resistance of bituminous mixtures was carried out in accordance with the BS EN 12697-24-2018 using the four-point bending test. Two mixtures are chosen to study the effect of temperature and effect of the gradation on fatigue behaviour of the asphalt mixtures.
- A minimum of six beams have been tested adopting a minimum of three strain levels, at 10 °C and 20 °C for binder and base mixtures respectively, with a reference frequency of 10 Hz, in strain-controlled testing configuration.
- Five different failure criteria have been analysed, and they are: 50 % reduction in the initial stiffness ( $E_0$ ), 50 % reduction in the extrapolated stiffness ( $E_{00}$ ), Peak in the phase angle, Energy ratio, and Dissipated energy ration.
- The two failure criteria which exhibits the lowest fatigue life in both the mixtures are the classical 50% reduction of initial stiffness modulus and Peak Phase angle. The other considered failure criteria show the maximum fatigue life, and the values are nearer and are consistent in both the mixtures.
- This study aims to assess the effect of temperature using the Binder mixture, the temperatures used are 10 °C and 20 °C. From results obtained after required analysis shows that the binder mixtures exhibit the high fatigue life as the temperature increases in the 4PB test configuration, which is confirming the previous studies made by the other researchers.
- In the other hand, this study also aims to evaluate the effect of gradation using the two mixtures which is tested at two temperatures, using the previous results on binder mixture tested at 20 °C and the results of the base mixtures which is tested at 20 °C the comparison is made possible.
- Binder mixtures yields the higher fatigue life when compared to the Base mixture, which is agreeable since the base mixtures have the high air void content and the low binder content which might possible to lessen the fatigue life of the asphalt mixtures.
- For both the mixtures, the significant difference is observed only at the higher strain level but at the lower strain level the number of cycles doesn't differ much.

- As the statistical analysis is concerned, the beams obtained from the roller compacted slabs after cutting are tested for the air void content and the comparison was made to see the variation in all the beams.
- The beams which are positioned centre of the slabs always has the higher compaction which leads to the lower air voids content for both the mixture, while it is not clear whether about the sides of the slabs since they are always switching their roles.
- The initial modulus and the extrapolated stiffness modulus are inversely proportional to the air void content. It is also observed that, values are much scattered in the base mixtures when compared to the binder mixture.

## 5.2 Recommendations and future work

- The effect on temperature must be further investigated to characterise the fatigue resistance in bituminous mixtures using the other tests like Indirect tensile fatigue test.

## Bibliography

- [1] H. di Benedetto, C. De, L. Roche, H. Baaj, A. Pronk, and R. Lundström, “Fatigue of bituminous mixtures,” 2004.
- [2] Y. Nashaat, A. Kareem, and S. Chandra, “Review of Studies on Fatigue Behavior of Bituminous Concrete Sustainable asphalt mixtures View project Development of Performance Parameters for Two-lane Roads under Mixed Traffic Condition View project Review of Studies on Fatigue Behavior of Bituminous Concrete,” 2012. [Online]. Available: <https://www.researchgate.net/publication/270508306>
- [3] H. Cheng, J. Liu, L. Sun, L. Liu, and Y. Zhang, “Fatigue behaviours of asphalt mixture at different temperatures in four-point bending and indirect tensile fatigue tests,” *Constr Build Mater*, vol. 273, Mar. 2021, doi: 10.1016/j.conbuildmat.2020.121675.
- [4] F. Hugo and A. E. Martin, *Significant findings from full-scale accelerated pavement testing*, vol. 325. Transportation Research Board, 2004.
- [5] Y. Yan, R. Roque, D. Hernando, and S. Chun, “Cracking performance characterisation of asphalt mixtures containing reclaimed asphalt pavement with hybrid binder,” *Road Materials and Pavement Design*, vol. 20, no. 2, pp. 347–366, Feb. 2019, doi: 10.1080/14680629.2017.1393002.
- [6] J. Deacon, A. Tayebali, J. Coplantz, F. Finn, and C. Monismith, “Fatigue Response of Asphalt-Aggregate Mixes, Part III—Mix Design and Analysis,” *Strategic Highway Research Program Report: No. SHRP-A*, vol. 404, 1994.
- [7] R. West *et al.*, “Phase IV NCAT pavement test track findings: Draft report,” 2012.
- [8] M. L. Hines, C. de La Roche, and P. Chaverot, “Evaluation of fatigue behavior of hot mix asphalt with the LCPC nantes test track and SHRP testing tools,” *Journal of the Association of Asphalt Paving Technologists*, vol. 67, 1998.
- [9] M. Pasetto and N. Baldo, “Fatigue Characterization of Asphalt Rubber Mixtures with Steel Slags,” in *7th RILEM International Conference on Cracking in Pavements*, 2012, pp. 729–737.
- [10] M. Pasetto and N. Baldo, “Fatigue Performance of Asphalt Concretes with RAP Aggregates and Steel Slags,” in *7th RILEM International Conference on Cracking in Pavements*, 2012, pp. 719–727.
- [11] “False Failure in Flexural Fatigue Tests”.

- [12] R. Guo and J. A. Prozzi, "Predicting in-service fatigue life of flexible pavements based on accelerated pavement testing," Ann Arbor, 2007. [Online]. Available: <https://www.proquest.com/dissertations-theses/predicting-service-fatigue-life-flexible/docview/304794646/se-2?accountid=28840>
- [13] A. ASTM, "D7460-10, Standard Test Method for Determining Fatigue Failure of Compacted Asphalt Concrete Subjected to Repeated Flexural Bending, ASTM, Philadelphia, PA, 2014."
- [14] C. Standard, "Standard test methods of bitumen and bituminous mixtures for highway engineering," *JTG E20; Ministry of Transport of the People's Republic of China: Beijing, China*, 2011.
- [15] T. Aashto, "321-07,(2007) Determining the fatigue life of compacted hot mix asphalt subjected to repeated flexural bending," *American Association of State Highways and Transportation Officials, Washington, DC, USA*.
- [16] B.-W. Tsai, *High-temperature fatigue and fatigue damage process of aggregate-asphalt mixes*. University of California, Berkeley, 2001.
- [17] S. C. S. R. Tangella, J. Craus, J. A. Deacon, and C. L. Monismith, "Summary report on fatigue response of asphalt mixtures," 1990.
- [18] R. Lundstrom, H. di Benedetto, and U. Isacsson, "Influence of asphalt mixture stiffness on fatigue failure," *Journal of materials in civil engineering*, vol. 16, no. 6, pp. 516–525, 2004.
- [19] H. U. Bahia, H. Zhai, K. Onnetti, and S. Kose, "Non-linear viscoelastic and fatigue properties of asphalt binders," *Journal of the Association of Asphalt Paving Technologists*, vol. 68, 1999.
- [20] H. di Benedetto, Q. T. Nguyen, and C. Sauzéat, "Nonlinearity, Heating, Fatigue and Thixotropy during Cyclic Loading of Asphalt Mixtures," *Road Materials and Pavement Design*, vol. 12, no. 1, pp. 129–158, Jan. 2011, doi: 10.1080/14680629.2011.9690356.
- [21] J. M. Read, "FATIGUE CRACKING OF BITUMINOUS PAVING MIXTURES," 1996.
- [22] F. Moreno-Navarro and M. C. Rubio-Gámez, "A review of fatigue damage in bituminous mixtures: Understanding the phenomenon from a new perspective," *Construction and Building Materials*, vol. 113. Elsevier Ltd, pp. 927–938, Jun. 15, 2016. doi: 10.1016/j.conbuildmat.2016.03.126.

- [23] E. R. Brown, P. S. Kandhal, and J. Zhang, “Performance testing for hot mix asphalt,” *NCAT report*, vol. 1, no. 05, 2001.
- [24] *BSI Standards Publication Bituminous mixtures-Test methods*. 2018.
- [25] *Bituminous mixtures-Test methods*. 2019.
- [26] S. Kocak and M. E. Kutay, “Effect of devulcanized rubber modification on the performance grade, fatigue cracking resistance, and rutting resistance of asphalt binders,” *Journal of Materials in Civil Engineering*, vol. 33, no. 9, p. 04021248, 2021.
- [27] J. L. O. L. Júnior, L. F. A. L. Babadopulos, and J. B. Soares, “Moisture-induced damage resistance, stiffness and fatigue life of asphalt mixtures with different aggregate-binder adhesion properties,” *Constr Build Mater*, vol. 216, pp. 166–175, 2019.
- [28] B. R. Clark, L. Piacere, and C. Gallage, “Effects of recycled asphalt pavement on the stiffness and fatigue performance of multigrade bitumen asphalt,” *Journal of Materials in Civil Engineering*, vol. 30, no. 2, p. 04017278, 2018.
- [29] B. W. Al-Mistarehi, T. S. Khadaywi, and A. K. Hussein, “Investigating the effects on creep and fatigue behavior of asphalt mixtures with recycled materials as fillers,” *Journal of King Saud University-Engineering Sciences*, vol. 33, no. 5, pp. 355–363, 2021.
- [30] J. G. Bastidas-Martínez, H. A. Rondón-Quintana, and M. Muniz de Farias, “Behavior of asphalt mastics containing different materials as filler,” *Canadian Journal of Civil Engineering*, vol. 48, no. 4, pp. 347–355, 2021.
- [31] D. Wang, W. Linbing, D. Christian, and G. Zhou, “Fatigue properties of asphalt materials at low in-service temperatures,” *Journal of Materials in Civil Engineering*, vol. 25, no. 9, pp. 1220–1227, 2013.
- [32] F. Zhou, W. Mogawer, H. Li, A. Andriescu, and A. Copeland, “Evaluation of fatigue tests for characterizing asphalt binders,” *Journal of Materials in Civil Engineering*, vol. 25, no. 5, pp. 610–617, 2013.
- [33] C. Liu, S. Lv, X. Peng, J. Zheng, and M. Yu, “Analysis and comparison of different impacts of aging and loading frequency on fatigue characterization of asphalt concrete,” *Journal of Materials in Civil Engineering*, vol. 32, no. 9, p. 04020240, 2020.
- [34] H. di Benedetto, C. de La Roche, H. Baaj, A. Pronk, and R. Lundstrom, “Fatigue of bituminous mixtures: different approaches and RILEM group contribution,” in *Sixth International RILEM Symposium on Performance Testing and Evaluation of Bituminous Materials*, 2003, pp. 15–38.

- [35] J. A. Epps and C. L. Monismith, *Fatigue of Asphalt Concrete Mixtures--Summary of Existing Information*. ASTM International, 1972.
- [36] M. Muniz de Farias, F. Quiñonez Sinisterra, and H. A. Rondón Quintana, "Behavior of a hot mix asphalt made with recycled concrete aggregate and crumb rubber," *Canadian Journal of Civil Engineering*, vol. 46, no. 6, pp. 544–551, 2019.
- [37] H. A. Rondón-Quintana, J. C. Ruge-Cárdenas, J. G. Bastidas-Martínez, M. Y. Velandia-Castelblanco, and M. Muniz de Farias, "Use of thermally treated bentonite as filler in hot mix asphalt," *J. Mater. Civ. Eng.*, vol. 32, no. 5, p. 04020070, 2020.
- [38] M. A. Elseifi, G. W. Flintsch, and I. L. Al-Qadi, "Quantitative effect of elastomeric modification on binder performance at intermediate and high temperatures," *Journal of Materials in Civil Engineering*, vol. 15, no. 1, pp. 32–40, 2003.
- [39] G. Dondi, M. Pettinari, C. Sangiorgi, and S. E. Zoorob, "Traditional and Dissipated Energy approaches to compare the 2PB and 4PB flexural methodologies on a Warm Mix Asphalt," *Constr Build Mater*, vol. 47, pp. 833–839, 2013.
- [40] K. A. Ghuzlan and S. H. Carpenter, "Fatigue damage analysis in asphalt concrete mixtures using the dissipated energy approach," *Canadian Journal of Civil Engineering*, vol. 33, no. 7, pp. 890–901, 2006.
- [41] S. C. S. R. Tangella, J. Craus, J. A. Deacon, and C. L. Monismith, "Summary report on fatigue response of asphalt mixtures," 1990.
- [42] S. H. Carpenter and S. Shen, "Dissipated energy approach to study hot-mix asphalt healing in fatigue," *Transp Res Rec*, vol. 1970, no. 1, pp. 178–185, 2006.
- [43] G. Liu, Y. Jia, T. Yang, H. Du, J. Zhang, and Y. Zhao, "Fatigue performance evaluation of asphalt mixtures based on energy-controlled loading mode," *Constr Build Mater*, vol. 157, pp. 348–356, 2017.
- [44] T.-W. Hsu and K.-H. Tseng, "Effect of rest periods on fatigue response of asphalt concrete mixtures," *J Transp Eng*, vol. 122, no. 4, pp. 316–322, 1996.
- [45] H. A. Rondón-Quintana, W. D. Fernández-Gómez, and J. A. Hernández-Noguera, "Influence of subgrade and unbound granular layers stiffness on fatigue life of hot mix asphalts-HMA," *TecnoLógicas*, no. 31, pp. 53–72, 2013.
- [46] F. Finn, C. L. Saraf, R. Kulkarni, K. Nair, W. Smith, and A. Abdullah, *Development of pavement structural subsystems*, no. 291. 1986.
- [47] A. Institute, *Research and Development of the Asphalt Institute's Thickness Design Manual*. Asphalt Institute, 1982.

- [48] F. P. Bonnaure, A. Huibers, and A. Boonders, “A laboratory investigation of the influence of rest periods on the fatigue characteristics of bituminous mixes (with discussion),” in *Association of Asphalt Paving Technologists Proceedings*, 1982, vol. 51.
- [49] C. L. Monismith, J. A. Epps, and F. N. Finn, “Improved asphalt mix design (with discussion),” in *Association of Asphalt Paving Technologists Proc*, 1985, vol. 54.
- [50] P. S. Pell and K. E. Cooper, “The effect of testing and mix variables on the fatigue performance of bituminous materials,” *Journal of the Association of Asphalt Paving Technologists*, vol. 44, pp. 1–37, 1975.
- [51] G. M. Rowe, “Performance of asphalt mixtures in the trapezoidal fatigue test (with discussion),” *Journal of the Association of Asphalt Paving Technologists*, vol. 62, 1993.
- [52] B. Eckmann, “Exxon Research in Pavement Design-Moebius Software: A Case Study Reduction of Creep through Polymer Modification,” *Proc. Assoc. Asphalt Paving Technologist*, vol. 58, pp. 337–361, 1989.
- [53] G. M. Rowe and M. G. Bouldin, “IMPROVED TECHNIQUES TO EVALUATE THE FATIGUE RESISTANCE OF ASPHALTIC MIXTURES,” 2000. [Online]. Available: <https://www.researchgate.net/publication/304115473>
- [54] J. Zhang, M. Sabouri, M. N. Guddati, and Y. R. Kim, “Development of a failure criterion for asphalt mixtures under fatigue loading,” *Road Materials and Pavement Design*, vol. 14, no. sup2, pp. 1–15, Aug. 2013, doi: 10.1080/14680629.2013.812843.
- [55] J. Zhang, M. Sabouri, M. N. Guddati, and Y. R. Kim, “Development of a failure criterion for asphalt mixtures under fatigue loading,” *Road Materials and Pavement Design*, vol. 14, no. sup2, pp. 1–15, 2013.
- [56] S. Mangiafico, C. Sauzeat, H. di Benedetto, S. Pouget, F. Olard, and L. Planque, “Quantification of biasing effects during fatigue tests on asphalt mixes: non-linearity, self-heating and thixotropy,” *Road Materials and Pavement Design*, vol. 16, no. sup2, pp. 73–99, 2015.
- [57] K. P. Biligiri, K. Kaloush, and J. Uzan, “Evaluation of asphalt mixtures’ viscoelastic properties using phase angle relationships,” *International Journal of Pavement Engineering*, vol. 11, no. 2, pp. 143–152, Apr. 2010, doi: 10.1080/10298430903033354.
- [58] R. A. Reese, “Properties of aged asphalt binder related to asphalt concrete fatigue life,” *Journal of the association of asphalt paving technologists*, vol. 66, 1997.

- [59] J. Zhang, “Development of Failure Criteria for Asphalt Concrete Mixtures under Fatigue Loading.,” 2012.
- [60] P. C. Hopman, P. Kunst, and A. C. Pronk, “A renewed interpretation method for fatigue measurements-verification of Miner’s rule,” in *Proceedings of The 4th Eurobitume Symposium, Madrid*, 1989, pp. 557–561.
- [61] G. M. , Rowe, “Performance of Asphalt Mixtures in the Trapezoidal Fatigue Test,” *Association of Asphalt Paving Technologist*, 1993.
- [62] G. Rowe and M. G. Bouldin, “Improved techniques to evaluate the fatigue resistance of asphaltic mixtures,” pp. 754–763, Jan. 2000.
- [63] A. Subhy, D. lo Presti, and G. Airey, “New simplified approach for obtaining a reliable plateau value in fatigue analysis of bituminous materials,” *Eng Fail Anal*, vol. 79, pp. 263–273, 2017.
- [64] T. D. Gillespie, *Effects of heavy-vehicle characteristics on pavement response and performance*, vol. 353. Transportation Research Board, 1993.
- [65] M. J. Brennan and F. Clancy, “A new initiative in measuring the fatigue performance of bituminous materials,” in *International Conference on Asphalt Pavements, 7th, 1992, Nottingham, United Kingdom*, 1992, vol. 2.
- [66] L. Francken and J. Verstraeten, “Methods for predicting moduli and fatigue laws of bituminous road mixes under repeated bending,” 1974.
- [67] J. Myre, “Fatigue of asphalt materials for Norwegian conditions,” in *Seventh International Conference on Asphalt Pavements*, 1992, vol. 3.
- [68] J. Myre, “Fatigue of asphalt materials for Norwegian conditions,” in *Seventh International Conference on Asphalt Pavements*, 1992, vol. 3.
- [69] A. A. Tayebali, J. A. Deacon, and C. L. Monismith, “DEVELOPMENT AND EVALUATION OF SURROGATE FATIGUE MODELS FOR SHRP A-003A ABRIDGED MIX DESIGN PROCEDURE (WITH DISCUSSION),” *Journal of the Association of Asphalt Paving Technologists*, vol. 64, 1995.
- [70] D. Bodin, G. Pijaudier-Cabot, C. de La Roche, J.-M. Piau, and A. Chabot, “Continuum damage approach to asphalt concrete fatigue modelling,” *Journal of Engineering Mechanics-ASCE*, vol. 130, no. 6, pp. 700–708, 2004.
- [71] D. A. Anderson, Y. M. le Hir, M. O. Marasteanu, J.-P. Planche, D. Martin, and G. Gauthier, “Evaluation of fatigue criteria for asphalt binders,” *Transp Res Rec*, vol. 1766, no. 1, pp. 48–56, 2001.

- [72] S. C. S. R. Tangella, J. Craus, J. A. Deacon, and C. L. Monismith, “Summary report on fatigue response of asphalt mixtures,” 1990.
- [73] T. W. Kennedy *et al.*, “Superior performing asphalt pavements (Superpave): The product of the SHRP asphalt research program,” 1994.
- [74] H. M. R. D. Silva, J. R. M. Oliveira, and L. G. Picado-Santos, “Influence of temperature on the fatigue life of flexible pavements,” in *3rd European Pavement and Asset Management Conference*, 2008, vol. 1075, pp. 1–10.
- [75] J. Zhu, “Evaluation and critical damage position for fatigue behavior of asphalt pavement considering the full temperature profile.” Shanghai: Tongji University, 2016.
- [76] H. Cheng, J. Liu, L. Sun, L. Liu, and Y. Zhang, “Fatigue behaviours of asphalt mixture at different temperatures in four-point bending and indirect tensile fatigue tests,” *Constr Build Mater*, vol. 273, Mar. 2021, doi: 10.1016/j.conbuildmat.2020.121675.
- [77] British Standards Institution, *Bituminous mixtures. Test methods. Part 39, Binder content by ignition*.
- [78] *BSI Standards Publication*. 2012.
- [79] *BSI Standards Publication Bituminous mixtures-Test methods*. 2019.
- [80] British Standards Institution, *Bituminous mixtures. Test methods. Part 6, Determination of bulk density of bituminous specimens*.
- [81] *BSI Standards Publication Bituminous mixtures-Test methods*. 2019.
- [82] BSI Group and European Committee for Standardization., *Bituminous mixtures - Test method. Part 33: Specimen prepared by roller compactor*.
- [83] British Standards Institution, *Bituminous mixtures. Test methods. Part 29, Determination of the dimensions of a bituminous specimen*.
- [84] *BSI Standards Publication Tests for mechanical and physical properties of aggregates Part 6: Determination of particle density and water absorption*. 2013.

